Titre: Title:	Assessing the Energy Flexibility Potential of Residential Photovoltaic Panel with Battery Systems in Cold Climate
Auteur: Author:	Behzad Barzegar Bafrouei
Date:	2021
Type:	Mémoire ou thèse / Dissertation or Thesis
Référence: Citation:	Barzegar Bafrouei, B. (2021). Assessing the Energy Flexibility Potential of Residential Photovoltaic Panel with Battery Systems in Cold Climate [Ph.D. thesis, Polytechnique Montréal]. PolyPublie. https://publications.polymtl.ca/9998/

POLYTECHNIQUE MONTRÉAL

affiliée à l'Université de Montréal

Assessing the energy flexibility potential of residential photovoltaic panel with battery systems in cold climate

BEHZAD BARZEGAR BAFROUEI

Département de génie mécanique

Thèse présentée en vue de l'obtention du diplôme de *Philosophiæ Doctor*

Génie mécanique

Décembre 2021

POLYTECHNIQUE MONTRÉAL

affiliée à l'Université de Montréal

Cette thèse intitulée:

Assessing the energy flexibility potential of residential photovoltaic panel with battery systems in cold climate

présentée par **Behzad BARZEGAR BAFROUEI**

en vue de l'obtention du diplôme de *Philosophiæ Doctor*

a été dûment acceptée par le jury d'examen constitué de :

Hanane DAGDOUGUI, présidente

Michaël KUMMERT, membre et directeur de recherche

Massimo CIMMINO, membre

Ahmed DAOUD, membre externe

ACKNOWLEDGEMENTS

My special thanks of gratitude go to my supervisor Prof. Michaël Kummert who gave me the golden opportunity to do this wonderful project. I am really grateful for your guidance, encouragement, suggestions and invaluable time throughout the different steps of my PhD study. Any attempt can't be satisfactorily completed without your support, positive feedback and kind personality. It was a great privilege and honor to work and study under your supervision.

I would like to thank my past and present fellow lab mates and friends. Thank you for your help on the technical and nontechnical issues I have encountered. You made my PhD journey and the time away from home more enjoyable.

Finally, I am really grateful to my parents and brother for your love, prayers, caring and always being there, actually or virtually. Last but not least, my deepest gratitude to my caring, loving, and supportive wife. Your encouragement when the times got rough are much appreciated and duly noted.

RÉSUMÉ

Le secteur résidentiel représente une partie importante de la consommation énergétique et des émissions de gaz à effet de serre (GES) dans le monde, et il est la cible de nombreux programmes visant à réduire ces émissions. Les systèmes photovoltaïques (PV) résidentiels sont ainsi devenus financièrement intéressants pour les propriétaires dans de nombreuses régions du monde, y compris dans certaines provinces canadiennes, en raison de programmes incitatifs généreux et de la baisse du prix des modules PV.

Cependant, la pénétration croissante des systèmes PV pose des problèmes aux gestionnaires des réseaux électriques, ce qui a conduit les distributeurs d'électricité à sévèrement réduire ou supprimer les programmes incitatifs. Dans le même temps, l'attention s'est portée non plus sur l'objectif de générer une quantité maximale d'énergie, mais sur l'objectif de répondre aux besoins en puissance du réseau, c'est-à-dire d'offrir à celui-ci une flexibilité énergétique.

L'addition de stockage électrique aux systèmes PV résidentiels permet de délivrer cette flexibilité. Cette thèse étudie les systèmes résidentiels PV+Batterie dans le contexte canadien par des études en modélisation utilisant le logiciel TRNSYS, un outil de simulation des systèmes énergétiques basés sur une approche par composants.

D'abord, une librairie de modèles est développée dans TRNSYS, afin d'améliorer la représentation des différentes technologies de batteries, la prise en compte de la dégradation des performances, et les effets de la température sur les performances. Les modèles développés sont comparés à des résultats expérimentaux pour confirmer leur validité.

Ensuite, un modèle archétypal est développé, comprenant une résidence typique canadienne avec un système de chauffage, ventilation et conditionnement d'air et un système d'eau chaude tout-électrique, et un système PV+Batterie. Le modèle utilise des profils de consommation mesurés pour les besoins reliés aux occupants (eau chaude, appareils électriques, éclairage).

Le modèle développé est utilisé pour évaluer la flexibilité offerte par les systèmes PV+Batterie en utilisant des indices de performance (*key performance indices, KPI*) annuels tels que l'autoconsommation. Des indices dynamiques sont ensuite utilisés pour caractériser la flexibilité offerte par différentes stratégies de contrôle.

Une analyse économique est réalisée en utilisant deux structures tarifaires typiques au Canada : un tarif basé sur le moment de l'utilisation (en utilisant l'Ontario comme exemple) et un tarif constant avec des crédits ou pénalités pendant des évènements de gestion de la demande de pointe (en utilisant les tarifs volontaires récemment introduits au Québec comme exemples). Une analyse de la valeur nette actualisée est réalisée, et le coût d'investissement pour disposer d'une puissance pendant les évènements de gestion de la demande est comparé à des alternatives.

Les résultats montrent que, même si les systèmes PV+Batterie ne sont pas rentables dans les conditions actuelles du marché sans avoir recours à des incitatifs généreux ou sans compter sur une baisse significative du coût des batteries, ils représentent un atout intéressant pour les distributeurs d'électricité dans leur adaptation aux futurs réseaux décarbonisés qui auront à gérer un parc de bâtiments ayant électrifié les besoins en chauffage et en eau chaude.

ABSTRACT

The residential sector represents a significant share of worldwide energy consumption and greenhouse gases emissions; it is targeted by numerous programs aiming at reducing these emissions. Generous incentive programs and a notable price drop have made residential photovoltaic (PV) systems financially interesting for homeowners in many regions of the world, including some provinces in Canada.

However, the increasing penetration rate of PV generation poses significant challenges to the grid, and as utilities were reducing or canceling the generous feed-in tariffs, the focus of distributed generation systems has changed from generating more energy to responding better to power needs, i.e. providing energy flexibility to the grid.

Adding electrical storage in the form of batteries to a residential PV system allows to deliver this flexibility. This thesis assesses PV+Battery systems in the residential context in Canada through modelling studies performed in TRNSYS, a component-based energy simulation tool.

First, a library of battery models is developed and integrated in the software tool to improve the modelling capabilities regarding the accurate representation of battery technologies, capacity degradation, and temperature effects. The library models are compared to experimental data to confirm their validity.

Then, an archetypal model is developed including a validated model of a typical Canadian single-family home, an all-electric heating, ventilation and air-conditioning (HVAC) system, and PV+Battery system components. The model uses selected measured profiles for occupant-driven loads such as domestic hot water and appliances.

The developed model is used to assess the flexibility offered by residential PV+Battery systems using yearly Key Performance Indices (KPIs) such as self-consumption to assess system sizing. Dynamic KPIs are then used to assess the flexibility offered by different designs and control strategies.

An economic analysis is performed using two typical rate structures for Canada: a time-of-use rate structure (using Ontario as an example), and a flat-rate structure with flexibility incentives or price signals (using the recently introduced voluntary program in Québec as an example). A net present

value analysis is performed, and the cost of flexible power generation offered by PV+Battery systems is compared to alternatives.

The results show that, although they are not profitable without feed-in tariffs or further decreases of battery prices, PV+Battery systems can represent significant assets for utilities in their adaptation to a decarbonized building sector relying on the electrification of heating and hot water production.

TABLE OF CONTENTS

LIST OF TABLES

LIST OF FIGURES

LIST OF SYMBOLS AND ABBREVIATIONS

Symbols

A, B	Amplitude of correction [-]
C_1	Battery capacitor in RC branch [F]
C_1	Battery capacity in 1 hours discharge rate [Ah]
C_{10}	Battery capacity in 10 hours discharge rate [Ah]
C_{100}	Battery capacity in 100 hours discharge rate [Ah]
C_p	Battery specific heat [J/g °C]
$C_{n_{ref}}$	Capacity for discharge in (usually 10) hours [Ah]
cf	Correction factor [-]
C_n	Capacity for discharge in n hours [Ah]
$C_1 - C_5$	Regression coefficient [-]
$C_{N,0}$	Nominal capacity of new battery [Ah]
$C_{initial}$	Battery initial capacity [Ah]
E_a	Activation energy [kJ/mol]
f_i	Correction factor [-]
h	Global heat transfer coefficient [W/m^{2}K]
I_{zp}	Diode current [A]
I_q	Battery current in normal operating condition [A]
I_{gas}	Battery current in gassing [A]
I_{sd}	Self-discharge current [A]
$I_{sd,ref}$	Reference self-discharge current [A]
I_{bat}	Battery in/out current [A]

k	Peukert coefficient [-]
k_{cal}	Calendar correction factor [-]
k_{zp}	Diode constant [-]
m	Battery mass [kg]
m_c , m_d	Cell type parameter [-]
P_{Load}	Demand load power [W]
$P_{battery}$	Battery power [W]
P_{grid}	Power to the electricity grid [W]
$\dot{Q}_{loss,Bat}$	Battery heat loss [J]
q_1	Available battery charge [Ah]
q_2	Battery bound charge [Ah]
Q_c , Q_d	Charge and discharge parameter [-]
$R_{int,qc}$	Internal resistance in full charge [Ω]
$R_{int,qd}$	Internal resistance in full discharge [Ω]
R_{int}	Battery internal resistance [Ω]
R_0	Battery equivalent series resistance [Ω]
R_1	Battery resistance in RC branch [Ω]
R_2	Battery resistance in RC branch [Ω]
T_{ref}	Reference temperature [°C]
T	Battery temperature [°C]
$V_{OC,base}$	Battery open circuit voltage at 0 state of charge and reference temperature [V]
V_R	Battery ideal voltage [V]

V_{oc}	Battery open circuit voltage [V]
V_{Bat}	Battery terminal voltage [V]
V_{pol}	Polarization voltage [V]
X_C	Ratio between current and capacity [1/h]
η_c	Columbic efficiency [-]
ζ	Cycle load [-]
α, β	Experimental coefficient (for battery voltage model) [-]

Abbreviations

BEM	Building Energy Modelling
BPS	Building Performance Simulation
CAPEX	CAPital EXpenditure
CDF	Cumulative Distribution Frequency
CC	Constant current
CV	Constant voltage
DHW	Domestic Hot Water
DR	Demand Response
DHW	Domestic Hot Water
DOD	Depth of Discharge
EV	Electric Vehicle
ECM	Equivalent Circuit Model
FIT	Feed-In Tariff
HVAC	Heating, Ventilating and Air-Conditioning
KPI	Key Performance Indicator
LFP	Lithium Iron Phosphate battery

LTO	Lithium Titanate battery
LMO	Lithium Manganese Oxide
NCA	Lithium Nickel Cobalt Aluminium Oxide battery
NCM	Lithium Nickel Manganese Cobalt Oxide battery
NPV	Net Present Value
PV	Photovoltaic
PV+Battery	System including photovoltaic panels and battery energy storage
SOH	State of Health
SOC	State of Charge
SOW	State of Wear
SAM	System Advisor Model
TRNSYS	TRaNsient Energy SYstem Simulation (modelling software tool)
TOU	Time of Use

CHAPTER 1 INTRODUCTION

This chapter presents the context and the motivation for this PhD thesis, and then provides an overview of the thesis organization and the contributions in each chapter. Photovoltaic (PV) systems have first been introduced in residential buildings to provide on-site renewable energy generation and help decarbonize the electricity supply. The trend towards "net zero" energy buildings, which generate as much electricity as they consume, has resulted in large disturbances in the electric grids in some parts of the world, leading to the realization that energy flexibility (the ability to adapt a building energy generation and demand) is a key aspect in decarbonizing the building sector: space and water heating can be effectively decarbonized by switching to electricity, but peak demands must be mitigated to maintain and increase the resilience of the grid. Thermal storage (in the building structure or dedicated storage tanks) plays a large role in energy flexibility, but the recent trends in battery energy storage technologies has reduced costs and renewed interest for residential Photovoltaic systems including battery energy storage, denoted as PV+Battery in this thesis. The goal of the presented research is to assess the technoeconomic potential of PV+Battery systems for residential buildings in the cold climate region (e.g. Canadian context). The methodology consists in improving the available modelling tools, developing residential archetypes (e.g. system size, load and etc.), assessing the energy flexibility of PV+Battery systems through Key Performance Indicators (KPIs), and assessing the economic potential of these systems.

1.1 Context and motivations

According to the International Energy Agency (IEA, 2021), residential buildings accounted for 21 % of the final energy consumption in 2019. Their share decreased slightly over the past 55 year (from 24 % in 1965), but their absolute consumption has increased continuously and is predicted to keep rising. According to the World Resources Institute, these residential buildings account for 15 % of energy-related greenhouse gas emissions (WRI, 2020). This makes residential buildings one of the main targets in decarbonization efforts throughout the world, and in particular in Canada.

Decarbonization in buildings relies mainly on electrification of space heating and hot water production to replace fossil fuels, together with a transition towards cleaner electricity sources. Using the electricity as the primary source of energy in building sector (e.g. heating, cooling, lighting and appliances) leads to considerable peak demands during certain times of the day, with

typical "morning and evening peaks" in winter and "later afternoon peaks" in summer. Electric grids have to meet these peak demands while coping with intermittent renewable resources, increasing the challenge to match demand and supply.

Instead of contributing to the supply and demand matching problem, buildings have the potential to become an asset to electric grid by offering *energy flexibility*. Annex 67, an international collaboration project within the International Energy Agency Energy in Buildings and Communities programme (IEA-EBC), "Energy Flexibility of a building is the ability to manage its demand and generation according to local climate conditions, user needs and grid requirements." (Jensen, Madsen, et al., 2017). Enabling flexibility requires adapted control strategies capable of using on-site energy storage (both electrical and thermal) and managing on-site generation devices such as photovoltaic (PV) systems.

PV systems were initially integrated to buildings with an objective of contributing renewable energy to the generation mix and helping decarbonize the electric grid. Combined with improvements in energy efficiency, this led to the target of "net-zero energy buildings" (Pless & Torcellini, 2010). This was encouraged by generous Feed-In Tariff (FIT) programs offering long-term contracts to residential prosumers to purchase their electricity excess well above the market price. As an example, the Ontario FIT went from 42 ¢/kWh in 2006 to 80 ¢/kWh in 2009. However, most programs were downscaled or supressed after their introduction (for example, the Ontario FIT was between 19 ¢/kWh and 31 ¢/kWh in 2017).

When the share of integrated non-dispatchable (renewable energy) generators in the grid increases, the procedure of balancing supply and demand becomes more challenging. In particular, in the case of PV, the daily production peak (roughly centered on solar noon for favorable orientation) often creates a pronounced drop in the net system load, which is then followed the afternoon/early evening peak. The ramp rate leading to that peak increases with PV penetration, leading to the so-called "duck curve" problem, because the shape of the load curve resembles that of a duck belly. This high ramp rate increases the risk of failure in power plant facilities. In order to increase the value of PV generation for grid operators, it is necessary to offer *flexibility* by reshaping the net demand profile, as discussed above. This can also increase the value of PV generation for the building owner, as most utilities have already adopted or are planning to adopt time-varying electricity rates that impose a penalty on demand at peak times and lower the price of electricity

when demand is low and/or renewable generation is high. In the case of building-integrated PV systems, flexibility can be achieved by leveraging thermal and electrical storage. The potential of utilizing thermal mass through advanced control strategies is for example investigated in (K. Zhang, 2018).

Electrical storage through building-integrated batteries is another option to achieve flexibility of the net demand profile in residential buildings. Grid-tied photovoltaic systems with battery storage, referred to as PV+battery systems in this thesis, have recently gained in popularity because they offer some resilience in case of grid power failure. Prices have declined with the introduction of new technologies and manufacturers, and their economics can be greatly improved if their storage capacity can also be used to respond to variable pricing of electricity imports and exports.

The overall goal of the work presented in this thesis is to assess the benefits of PV+Battery systems in typical residential buildings in the Canadian context. From the utility perspective, the potential of these systems to offer energy flexibility to the grid will be quantified. From the building owner's perspective, the economic impact of these systems on the electricity bills under different pricing schemes will be assessed.

1.2 Thesis organization and contributions

1.2.1 Chapter 1: Introduction

This chapter has presented the context and motivations for this research. The rest of the chapter presents the organization and contribution of the other chapters of this thesis.

1.2.2 Chapter 2: A new TRNSYS library for battery storage

Assessing energy flexibility of PV+Battery systems requires to perform detailed simulation studies. Building Performance Simulation (BPS) tools (also referred to as Building Energy Modelling, BEM) have historically focused on thermal modelling of the building envelope and Heating, Ventilating and Air-Conditioning (HVAC) systems. Photovoltaic systems were introduced more recently, and battery energy storage is often considered using very simple models. TRNSYS was selected for this work (Klein, S.A. et al, 2017). The software includes state-of-the-art models for buildings and PV panels, but does not currently have models for modern lithium-ion (Li-ion)

batteries. The included lead-acid battery models also neglect the impact of temperature on battery performance, and ignores some aspects like self-discharge and capacity degradation.

Chapter 2 presents the author's contribution to BPS in the form of a library of components implementing state-of-the-art models for generic, lead-acid and Li-ion batteries.

1.2.3 Chapter 3: Residential archetype

The size of the PV system that can be integrated to a residential building is limited by roof area, and single-detached houses offer the highest potential from that perspective. That type of housing also represents 64 % of the residential floor area in Canada (NRCan-OEE, 2021). This thesis focuses on that type of building, and Chapter 3 presents the archetypal house model that was created to enable simulation studies. A typical single-detached house is modelled in TRNSYS and is combined with different electricity demand profiles for appliances and lighting to create archetypes that will be used in assessing the energy flexibility and economic potential of PV+Battery systems. Electricity rate structures are also discussed.

1.2.4 Chapter 4: Energy flexibility

PV systems have historically contributed to decarbonize the grid but also to exacerbate the problems related to peak demand and rapid changes in the building sector electricity demand. On-site battery storage is currently being introduced to provide resilience towards power outages, but managing the on-site storage also offers a great potential to provide energy flexibility. Chapter 4 defines this concept and the Key Performance Indicators (KPIs) used to assess flexibility. The developed archetypes are then used to assess the flexibility of PV+Battery systems and provide design and operation guidelines.

1.2.5 Chapter 5: Economic assessment

The price of PV modules has decreased significantly over the last decade, and the technology is sometimes competitive with purchasing electricity from the grid in some regions. However, the high feed-in tariffs that were introduced between 1990 and 2010 in several countries in the world have been adjusted and, in some cases, discontinued due to supply and demand matching problems of PV systems. In Chapter 5, The current situation in Canada is assessed and the potential of

managing on-site battery storage to reduce the electricity bills of residential customers is investigated using two typical rate structures for Canada (Ontario and Québec).

1.2.6 Chapter 6: Discussions and conclusions

This thesis concludes with a summary of contributions to the literature and to the implementation of PV+Battery systems in Canada, a discussion of some limitations and recommendations for future work.

CHAPTER 2 A NEW TRNSYS LIBRARY FOR BATTERY STORAGE

Electrical energy storage is a key enabling technology to match intermittent renewable energy sources with the dynamic energy demand of buildings. Various forms of storage exist, but batteries dominate the market in small-scale (residential) and large-scale (utility) applications (Rahman et al., 2020). In a PV+Battery system, they represent the main "mass" in the system, and they also represent the priciest component. So modelling their dynamic behaviour is an important aspect of modelling buildings with integrated renewable energy systems.

Building Performance Simulation (BPS) tools such as EnergyPlus (https://energyplus.net/), ESP-r (http://www.esru.strath.ac.uk/Courseware/ESP-r/tour/), and TRNSYS (http://www.trnsys.com) were historically developed with a focus on thermal heat transfer. Electrical systems, and batteries in particular, have been introduced more recently.

The next section presents some general information on batteries, discussing the main technologies (or chemistries) and presenting some general definitions that will be useful in the chapter. It is followed by a literature review of existing battery models in selected BPS tools and in more generic energy system simulation tools. Then, the objectives of our work regarding battery modelling are described, before presenting the methodology and results.

2.1 Battery characteristics and general definitions

2.1.1 Battery chemistries

A battery "chemistry" refers to its chemical composition, i.e. the nature of the two electrodes (anode and cathode) and the nature of the electrolyte. This thesis will consider two main types of batteries: lead-acid (or Pb-Acid) batteries, and Lithium-ion (Li-ion) batteries. Among all type of secondary (rechargeable) batteries (lead-acid, Li-ion and Nickel cadmium (Ni-Cd), Nickel metal Hydride (NiMH), etc.), these two chemistries are the most widely used (Albright et al., 2012). Some key characteristics of these two chemistries are summarized in Table 2.1 (Albright et al., 2012; Reddy & Linden, 2010).

Table 2.1: Comparison of typical characteristics for lead-acid and Li-ion chemistries

Characteristic	**Lead-acid batteries**	**Lithium-ion batteries**
Nominal voltage [V]	2	2.3 – 3.7
Operating temperature [°C]	-20 to 40 (1)	-20 to 50 (2)
Energy density [Wh/L]	50 – 90	150 – 700
Specific energy [Wh/kg]	10 – 40	100 – 300
Specific power [W/kg]	150 – 200	250 – 350
Cycle life	500 – 1200 @ 50 % DOD (3)	1000 – 10000 @ 80 % DOD
Self-discharge [%/month]	3 – 20	0.5 – 5
Cycle efficiency [%]	50 – 90	80 – 95

(1) Starter, light and ignition batteries (used in conventional cars) have a larger range, -40 °C to 50 °C
(2) Many Lithium-ion batteries can be discharged under 0 °C but cannot be charged below 0 °C
(3) DOD stands for depth of discharge, this will be discussed later in the chapter

2.1.1.1 **Lead-acid batteries** (Reddy & Linden, 2010)

The lead-acid chemistry is a very mature technology (it as invented in 1859) and it has been used in a wide range of applications (e.g. uninterruptible power supply, power quality, start and ignition). The large power to weight ratio due to high surge capabilities, the relatively low cost, and an acceptable cycle efficiency, are the main characteristics of lead-acid battery. However, the existing limitations including low energy density (energy to weight and volume), short functional life span and necessity of regular maintenance are the major drawbacks of employing the lead-acid battery in stationary energy systems for demand management.

In lead-acid batteries, the active material of the positive and negative electrodes are lead dioxide (PbO_2) and metallic lead (Pb) respectively, which are immersed in sulfuric acid as the electrolyte.

The chemical reaction in lead-acid battery electrodes, over the discharge phase are provided in the following equations and the corresponding reaction reverses during charge process:

$$\text{(negative electrode)} \quad Pb + SO_4^{2-} \xrightarrow{Discharge} PbSO_4 + 2e^- \tag{2.1}$$

$$\text{(positive electrode)} \quad PbO_2 + 4H^+ + SO_4^{2-} \xrightarrow{Discharge} PbSO_4 + 2H_2O \tag{2.2}$$

$$\text{(Total cell)} \quad PbO_2 + Pb + 2H_2SO_4 \xrightarrow{Discharge} PbSO_4 + 2H_2O \tag{2.3}$$

The nominal voltage of lead-acid cells ranges from $2.05\ V$ to $2.15\ V$ (depending on the electrolyte density), and the number of cells connected in series defines the terminal voltage of the battery. Lead-acid batteries can be classified in two broad families depending on the state of the electrolyte. Flooded batteries have a liquid electrolyte that submerges the electrodes. They are the original type, and typically require maintenance to add water to the electrolyte to replace the amount that has been electrolyzed through a phenomenon known as gassing. Valve-Regulated lead-acid (VLRA) batteries are not open to the environment, they are sometimes designed as "hermetic" or "sealed" but a safety valve allows gases to escape if pressure differences become too high. In VRLA batteries, the electrolyte can be immobilized as a gel ("Gel" batteries) or in a highly porous glass microfiber separator (Absorbed Glass Mat, AGM batteries). Gel and AGM batteries are generally considered to be maintenance-free as there is no need for (and no possibility to) add water to the electrolyte. AGM and gel batteries typically have lower self-discharge rates than flooded batteries, and longer lifetimes. Flooded batteries are the least expensive ones and have a higher energy density, but a lower power density. Gelled batteries typically have a higher internal resistance, and are better adapted to SLI (Starter, Light and Ignition) applications.

2.1.1.2 **Lithium-ion batteries** (Buchmann, 2011; Reddy & Linden, 2010)

Lithium-ion (**Li-ion**) batteries are much more recent than lead-acid batteries; the first commercially available battery was developed by Sony in 1991, i.e. more than 130 years after the lead-acid battery was invented. In Li-ion batteries, the active material is lithium, and the lithium ions (Li^+) move between the positive and the negative electrode. The battery performance (e.g. voltage range, lifecycle and energy density) is highly dependent on its internal chemistry (cathode, anode and electrolyte material) – but all chemistries have higher energy and power densities and better cycle life than lead-acid batteries.

The anode (negative electrode in a battery) is generally made of graphite (porous carbon) for all chemistries. Several different materials are used for the cathode (positive electrode), including cobalt, nickel, manganese, iron phosphate, and aluminum. The cathode chemistry is reflected in the commonly accepted chemistry name.

In **Lithium Cobalt Oxide (LCO)** batteries, the anode active material is graphite carbon, and the cathode consists of cobalt oxide which has a layer structure. This was the design of the original Sony battery, and it is still in use today. The high energy to weight/volume ratio is the major advantage of this battery class, which makes it an appropriate option for portable electronic devices. This battery has relatively low cycle and calendar life in comparison to another LIBs chemistry. Other issues with the employed cathode material, are the low thermal stability (high susceptibility to thermal runaway) and failure in delivering the current at high discharge rates. These limitations and the high cost of cobalt have reduced the market share of this technology for larger battery sizes such as PV+Battery systems.

Phosphate has been employed as cathode in LIB for the first time in 1996 to form the **lithium iron phosphate (LFP).** This type of LIB provides a high current while showing a good thermal stability as well as long cycle life. It is also more tolerant to over-charge and over-discharge, but it exhibits higher self-discharge rate. LFP batteries have a slightly lower nominal voltage than other LIBs, which results in a specific energy 20% lower than the average value. But the open-circuit voltage is very stable, changing by less than 100 mV when the battery state of charge changes from 0.9 to 0.1 (Buchmann, 2011).

The **lithium nickel cobalt aluminum oxide (NCA)** chemistry dates back to 1999 when it was introduced for particular applications such as medical devices. This class was developed as a variation of the lithium nickel oxide cathodes, where cobalt and aluminum were added to provide stability. NCA batteries have a high energy density and specific power, as well as an extended functional life cycle. On the other side, high production cost and safety issues are the main drawbacks for this class of LIBs.

Lithium **nickel manganese cobalt (NMC)** was introduced as a variation of LCO, with similar voltage and energy/power density, but reduced cost since the amount of cobalt is reduced. Nickel is associated with high specific energy, manganese with low internal resistance. The cathode

materials (nickel, manganese and cobalt) can be mixed with various proportion while two more frequently used ratios are 1-1-1 and 5-2-3 respectively (Buchmann, 2011). Employing the corresponding blend decrease the share of cobalt content in cathode which reduces the cost of raw material significantly. This LIB offers high rate of energy density and long cycle life in a reasonably low price which makes it an appropriate option for both stationary and mobile applications ranging from hybrid system to electrical vehicles.

In **lithium titanate oxide (LTO)** batteries, the graphite in the anode has been replaced with titanate. The cathode material usually is comprised of lithium manganese oxide (LMO) or NMC. The possibility for fast charging and the capability to supply a high current (up to full discharge in 6 minutes) make it a suitable choice for powertrain and UPS applications. Moreover, the high thermal stability of LTO enhances the energy storage efficiency at extreme high or low temperature while offering excellent performance characteristics (e.g. the capacity remains at 80% of the nominal capacity at −30°C) (Buchmann, 2011). LTO is at the high end of the cost range within LIB technologies, but it offers a long cycle life (10000 cycle at 80% DOD), making it a viable option (Hesse et al., 2017). One disadvantage of this chemistry is its lower nominal voltage resulting in lower specific energy in comparison to other LIBs.

The three-dimensional spinel structure in **lithium manganese oxide (LMO)** batteries plays a pivotal role to facilitate ion transfer between electrodes. This improvement in the ion flow between cathode and anode leads to a lower internal resistance. The current-carrying capacity, high safety standard along with enhanced thermal stability are the main advantages of LMO batteries, with the abundance, low cost, and relative environmental friendliness of manganese. This chemistry delivers shorter cycle life than others, but it is employed in a wide range of applications including electrical vehicles, power tools and medical devices.

The main operating parameters corresponding to different Li-ion battery chemistry classes are shown in Table 2.2.

Table 2.2 Main parameters of commonly use Li-ion chemistry class (Hesse et al., 2017; Xu et al., 2010)

Li-ion chemistry	Nominal voltage (V)	Voltage range (V)	Cycle life	Application
Lithium Cobalt Oxide (LCO)	3.6	3 - 4.2	500 - 1000	mobile, laptop, camera
Lithium Manganese Oxide (LMO)	3.7	3 – 4.2	300 - 700	medical device electric power train Power tools
Lithium Nickel Manganese Cobalt (NMC)	3.6	2.7 - 4.15	>5000	E-bike, Electrical vehicle stationary
Lithium Iron Phosphate (LFP)	3.2	2 – 3.6	>6000	stationary and portable (high load current and endurance)
Lithium Titanate Oxide (LTO)	2.3	1.5 – 2.7	10000	UPS, solar street light, electric powertrain
Lithium Nickel Cobalt Aluminium Oxide (NCA)	3.6	3 – 4.2	>2000	Medical instruments, Electric powertrain

The most commonly used technologies for stationary applications (e.g. PV+Battery systems) and at this time are NMC, LFP and NCA. NMC have dominated the market both for electrical vehicles (EV) and stationary applications, while NCA were used for high-end EVs and LFP for some stationary applications. But NMC is expected to lose some ground to LFP and other technologies (LMO, LTO) according to a market report by Wood Mackenzie cited by NREL (Guittet et al., 2021).

2.1.2 General definitions

This section presents some common definitions which will be used when discussing the battery models (Buchman, 2001).

Battery cell, module, and pack

A battery **cell** is the basic unit of a battery. For typical chemistries, it consists of one anode, one cathode, and a volume of electrolyte, enclosed in a solid case. The rated voltage of a cell is fixed by the battery chemistry, it is generally around 2 V for a lead-acid battery and between 2.3 V and 3.7 V for a Li-ion battery. The cell capacity depends on its size, but is generally in the order of a few Ah for building applications (see below for a definition of battery capacity). A battery **module** is an assembly of cells that can be purchased as a single unit. Cells are connected in series and/or parallel to reach the desired voltage and capacity – typically, several cells are connected in series to reach a usable voltage of 12 V, 24 V, etc. Finally, a battery pack is assembled by connecting several modules in series and/or parallel to reach the desired system voltage (which can be in the order of several hundred volts) and capacity. For building applications, the distinction between modules and packs is sometimes blurred, with "modules" weighing as much as 100 kg and having an energy capacity in the order of 10 kWh. In that case, the pack typically refers to a unit that includes the battery module, a dedicated controller, and associated electronics.

Voltage and current

The battery voltage (V_{Bat}), expressed in volts (V), is the useful voltage difference at the battery terminals. The battery current (I_{Bat}), expressed in amperes (A), is the current entering or leaving the battery. The convention is to use a positive current when the battery is charged.

Capacity

The battery capacity represents the electrical charge that can be stored in the battery. Instead of being expressed in coulombs, capacity is typically expressed in ampere-hours, (1 Ah = 3600 C). The capacity is closely related to the amount of energy that can be stored in the battery, which is obtained by multiplying the capacity by the voltage (1 Ah · 1 V = 1 Wh = 3600 J). Sometimes, the term "capacity" will refer to the energy value, using the nominal voltage of the battery. For example, a lead-acid battery having 6 cells in series (rated voltage = 12 V) and a capacity of 100 Ah will be referred to as a 1.2 kWh battery.

The capacity of a battery depends on various factors (e.g. temperature), and is largely influenced by the current that is drawn from the battery – i.e. by the speed at which it is discharged. It is common to compare batteries by using a standard period for the discharge, typically 10 h. the

capacity in those conditions is expressed as C_{10}, and represents the amount of Ah that can be drawn from the battery when it is fully discharged in 10 hours (in other words, when the discharge current is equal to 1/10th of the capacity). Other values can be used, e.g. C_{100} (for lead-acid batteries) or C_1 (for Lithium-ion batteries).

Note that when talking about the rate of discharge of a battery, a similar – but different – notation is sometimes used, where $1C$ means that the battery is discharged at a rate of "1 capacity (per hour)", i.e. with a current equal to the capacity in Ah divided by 1 h. In that case, the battery capacity is assumed to be known (at it can be, for example, the C_{10} value) but the same battery is discharged at different rates corresponding to $1C$, $0.1C$, etc. known as the **C-rate**. The "proper" rate to verify C_{10} would be $0.1C$.

State of charge

The state of charge (SOC) of a battery is the ratio between its charge at a given point in time and its nominal charge, i.e. the ratio between its charge and the nominal capacity (for example C_{10}). Since the battery voltage varies depending on operating conditions, and since the energy stored in the battery is obtained by multiplying the charge by the voltage, the state of charge is not strictly equal to the ratio between the energy in the battery at a given point in time and the energy in the battery when fully charged in rated conditions. For simple models that do not model the battery voltage (i.e. assume it is constant), however, the SOC is the same as a "ratio of energy".

Depth of discharge

The depth of discharge DOD can have two meanings. Sometimes, it is just considered as $1 - SOC$, i.e. it represents the "discharge state" of the battery. But the main use of DOD is to indicate the magnitude of a discharge cycle: it represents the ratio between a discharge-charge cycle magnitude and the battery capacity. So a battery charged at $SOC = 0.9$ that would be discharged to an $SOC = 0.3$ and then charged back to $SOC = 0.9$ would accomplish a cycle with a $DOD = 0.6$, calculated as the max SOC minus the min SOC during the cycle.

Self-discharge rate

The battery self-discharge rate is the amount of charge which is lost per unit time when the battery is idle. Self-discharge is related to chemical reaction within the battery cells, and depends on the

battery chemistry, the battery type, and external factors such as temperature. The rate of self-discharge is typically expressed in percent per unit of time, e.g, %/month, where the % refer to the charge at the beginning of the period. So a fully charged battery with a self-discharge rate of 5 %/month stored without any load would have an SOC of 95 % at the end of the first month, and an SOC of 77.4 % after 5 months $(1 - 0.95^5)$.

State of health

The state of health of a battery (SOH) describes the evolution of a performance indicator over time. The SOH is expressed in percent of the initial value (of the selected performance indicator). A typical indicator chosen to monitor battery life is the capacity C, so that the SOH would be defined as the ratio between the capacity at a point in time and the initial capacity (for a new battery), $SOH = C(t)/C_{initial}$. But the SOH can also be based on the battery voltage, or the internal resistance, or a combination of factors. The end of the useful life of a battery is reached when the SOH reaches a given threshold which is defined as the minimum acceptable performance. Keeping the example of the battery capacity, one could decide that the battery will not be able to fulfil its role if its capacity is below 80 % of the design (initial) value. In that case, the minimum acceptable SOH would be 80 % and the battery would have to be replaced when the SOH reaches that limit.

Note: some tools (e.g. PVSYST, see below) refer to the state of wear of a battery (SOW) instead of the state of health. The state of wear accounts for the same performance degradation as the SOH, but uses a different scale: the SOW goes from 100 % (new battery) to 0 % when the battery is deemed to be unusable. If the remaining capacity is used to assess wear/health, and if the use case imposes that the battery should at least have 80 % of its rated capacity, the SOH at the end of the useful life would be 80 %, but it would be defined as a SOW of zero.

Battery efficiency

The energy efficiency of a battery is expressed as the ratio of the useful energy extracted from the battery over the energy transferred to the battery over a given period. This efficiency is affected by different types of losses:

- A battery affected by **self-discharge** loses charge over time, the energy stored is decreased, and the loss in charge is equivalent to a loss in energy when multiplied by the voltage.

- The **coulombic efficiency** (or **current efficiency**) expresses the ratio between the current recovered from the battery during discharge and the current injected into the battery during charge. The losses are due to electrochemical processes, and this efficiency is typically very high, except in the case of "gassing" in lead-acid batteries (see below).
- The **ohmic (in)efficiency** is normally the main factor affecting battery efficiency as can be shown in Figure 2.1, the series resistance (R_{int} or $R_0 + R_1$ in the figure) will dissipate power through ohmic losses both when the battery is charged ($I_{Bat} > 0$) and when it is discharged ($I_{Bat} < 0$). The power dissipated as heat is equal to $R_{int} \cdot I_{Bat}^2$, so in charging mode the ohmic efficiency will be $V_{OC}/(V_{OC} + R_{int}\, I_{Bat})$ and in discharging mode it will be $1 - R_{int} I_{Bat}/V_{OC}$. In both cases the ohmic efficiency depends on battery internal parameters (V_{OC} and R_{int}) **and** on the (dis)charging current.
- Finally, the battery voltage can depend on the battery temperature (typically, the voltage decreases for colder temperatures). If a battery is charged and discharged at different temperatures, the same current going in and out will be associated to a different voltage, hence to a different power, resulting in an apparent **temperature efficiency**. This effect is normally calculated automatically by the models that account for battery temperature. In theory, it could result in an efficiency higher than one, but since this effect is notably smaller than the other losses, the overall battery efficiency is always lower than one.

2.2 Literature review: battery models

Modelling techniques employed to represent batteries can be classified in three main categories: electrochemical (chemistry-based), empirical, and electrical (circuit-based). These approaches are briefly discussed in the next section.

2.2.1 Battery modelling approaches

2.2.1.1 Electrochemical model

The electrochemical model describes the chemical processes taking place inside the battery with high details. All physiochemical reactions (e.g. intercalation, diffusion, etc.) occurring within the

battery cell are defined throughout the series of complex time-varying differential equations. The physics basis of all corresponding models is adapted from the porous electrode theory, which was developed, by Newman and Tiedeman in 1974 (Newman & Tiedemann, 1974). This modelling approach is mainly used for battery design, since it has potential to accurately estimate the macroscopic (e.g. current and voltage) and microscopic (e.g. electrolyte and solid concentration) variables during charge and discharge regimes.

This modelling approach is associated with a high complexity, leading to a high computational cost and requiring in-depth knowledge in the field of electrochemistry to interpret and identify the required parameters, which makes this technique less appropriate for energy engineering system design and simulation tools.

2.2.1.2 Empirical (mathematical) model

In this modelling approach, collected experimental data is used to estimate the battery behaviour under various operating conditions. Empirical models (e.g. Shepherd (Shepherd, 1965a) and Nernst (Fang et al., 2014) typically employ few equations to describe the relationships between certain battery parameters (e.g. voltage-current). In the majority of empirical models, the battery terminal voltage is defined as a function of battery state of charge and input/output current. The simplicity and low number of required inputs for the empirical model are notable advantages for modelling real-time energy systems. But empirical model parameters depend on the represented battery module, even if they have the same chemistry, which necessitates performing detailed experiments for each module individually. Using average or "representative" parameters greatly decreases the accuracy of the model (Fotouhi et al., 2016; C. Zhang et al., 2014). In addition, experiments cannot reproduce all the dynamic loading conditions, so steady-state performance is typically measured, which limits the applicability of the resulting model.

2.2.1.3 Electrical equivalent circuit model

The Equivalent Circuit Model (ECM) (Thakkar, 2021) is comprised of a network of voltage source, resistors and capacitors which are used to simulate the dynamic behaviour of the battery. The diagram in Figure 2.1 illustrates the schematic of the first order ECM where V_{oc} (voltage source) represents the open circuit voltage (V_{OC}) of the battery. The voltage difference at the battery

terminals, V_{Bat}, which is the useful voltage, will be different form V_{oc} as soon as an electrical current I_{bat} will flow through the battery (current is positive in the direction of the arrow when the battery is discharging). The ohmic resistor R_0 represents the equivalent series resistance. It explains that the voltage at the battery terminals will drop when it is under load (positive current) and increase when the battery is charged (negative current), which is known as the polarization phenomenon. The RC branch consisting of resistance R_1 and capacitor C_1 describes a dynamic behaviour of the polarization: when (dis)charged, the voltage at the battery terminal will show a transient behaviour (similar to an exponential curve), and when allowed to rest, the battery will not return immediately to V_{oc}. The schematic in Figure 2.1 shows a single RC cell, corresponding to a first-order ECM model, but additional RC cells can be added to represent a more complex short- and long-term transient response of the battery voltage during charge and discharge. Conversely, the (R_1, C_1) cell can be removed to obtain a simplified steady-state model.

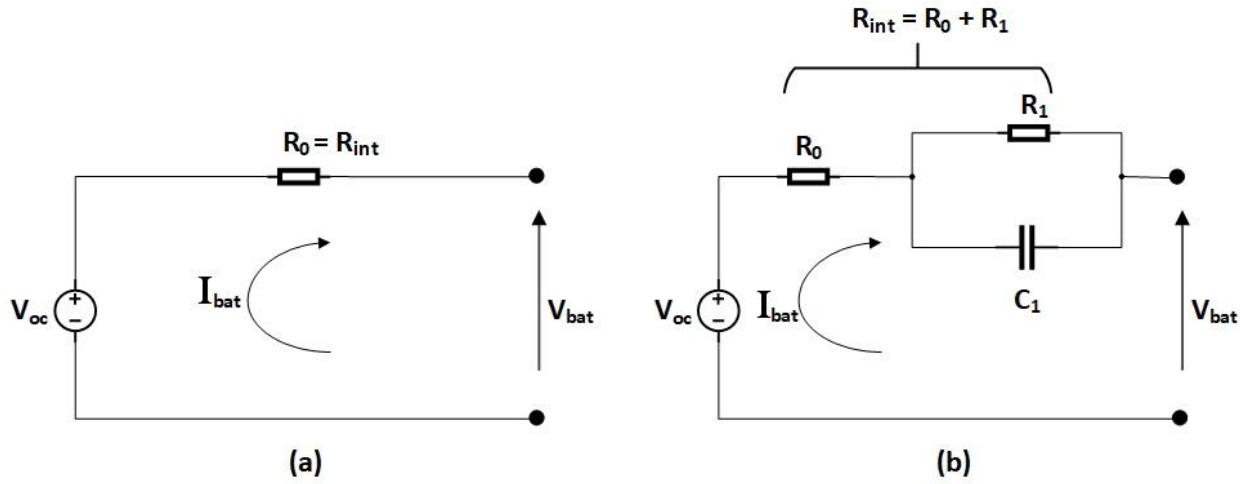

Figure 2.1 Schematic diagram of a steady-state (a) and a 1st order (b) ECM

All the parameters of the ECM (V_{oc}, R_0, R_1 and C_1) are multivariable functions of the battery state of charge, temperature and charge/discharge current/power, so identifying their value (or the equations defining their value) requires testing the modelled battery. The battery chemistry, type of application, and required precision are the main deciding factors in selecting the appropriate structure and order of the ECM.

Note that I_{Bat} is defined positively as the battery is discharged. This convention will be used when all models. Defining the internal resistance R_{int} as R_0 (steady-state model) or $(R_0 + R_1)$ (first-order model), the steady-state battery voltage is related to the open-circuit voltage by:

$$V_{Bat} = V_{OC} - R_{int}\, I_{Bat} \quad \text{(in steady state)} \tag{2.4}$$

The voltage across the equivalent internal resistance is often referred to as the "polarization voltage" V_{pol}:

$$V_{pol} = R_{int}\, I_{Bat} \quad \text{(in steady state)} \tag{2.5}$$

2.2.1.4 Battery modelling approach comparison

Table 2.3 shows an overview of the advantages and disadvantages of the three modeling approaches discussed above.

Table 2.3 Advantages and limitations of battery modelling methods

Method	Electrochemical	Mathematical	ECM
Advantage	High accuracy	Simplicity Ease of implementing	Reliable for any loading and operating condition Acceptable level of accuracy and simplicity
Limitation	Complexity and high computational cost Expert level knowledge of electrochemistry is required	inaccurate for dynamic loading	complex parameters identification procedure

2.2.2 Battery models implementation in energy systems simulation tools

This review of battery models implemented in energy systems simulation tools starts with 2 software programs dedicated to PV and PV+Battery systems, PVSYST (https://www.pvsyst.com/, version 7.2) and PV*SOL (https://pvsol.software/, version 2021 Release 2). Then, we present the battery model implemented in the System Advisor Model (SAM) (https://sam.nrel.gov/, version

2020.11.29), a techno-economic tool designed to facilitate decision-making for renewable energy systems. SAM can model a large variety of systems, from high concentration solar thermal systems to marine energy systems, and it addresses PV and PV+Battery systems with a great level of detail – its battery model is often referenced by other simulation tools. Finally, we review the models available in two BPS tools, EnergyPlus (https://energyplus.net/, version 8.2.0) and TRNSYS (http://www.trnsys.com/, version 18), and we conclude with an overview of the features of all models and the desired capabilities for the developed TRNSYS component models.

The model comparison focuses on the employed methodologies to estimate the battery voltage, capacity and state of charge, as well as battery degradation under dynamic loading conditions (charge-discharge cycles) and temperature effects. The complexity level, required input parameters, and supported battery chemistries are also compared.

2.2.2.1 PVSYST

PVSYST (https://www.pvsyst.com/) uses a simple steady-state ECM Figure 2.1 to investigate the relation between battery terminal voltage (V_{Bat}) and current (I_{Bat}).

Note: PVSYST documentation uses a different convention for the sign of I_{Bat}. The equations below have been adapted to our convention ($I_{Bat} > 0$ when discharging, as shown in Figure 2.1).

through the following equation:

$$V_{Bat} = V_{OC}(SOC\,, T) - R_{Int}(T)\, I_{Bat} \tag{2.6}$$

Where V_{OC} is the open circuit voltage and varies as a function of battery SOC and temperature (T). R_{Int} denotes the internal resistance, it can vary with temperature T, but this is only implemented in the Li-ion model, not in the lead-acid model. The level of detail varies for the two battery technologies that are considered, lead-acid and Lithium-ion.

2.2.2.1.1 Lead-acid model

ECM parameters V_{OC} and R_{int}

For lead-acid batteries, R_{int} is assumed to be constant and is obtained from datasheets. Typical values for generic batteries result in a voltage drop between 0.015 V and 0.040 V per cell when

discharging at 0.1C, i.e. with a current equal to $C_{10}/10$ (the suggested default value is 0.040 V). For example, a 6-cell battery (12 V nominal voltage) with a C_{10} value of 100 Ah would have an internal resistance R_{int} between 9 mΩ and 24 mΩ.

V_{OC} is assumed to be a bilinear function of SOC and T:

$$V_{OC} = V_{OC,base} + \alpha\, SOC + \beta\,(T - T_{ref}) \tag{2.7}$$

Where T_{ref} is a reference temperature (usually 20 °C), $V_{OC,base}$ is the open-circuit voltage at $SOC = 0$ and $T = T_{ref}$. α and β are constant coefficients obtained from manufacturer data. Default battery models in the software have α values equal to 180 mV per cell (when SOC is expressed from 0 to 1) and β values between -4 and -6 mV/°C (per cell).

The model includes an empirical correction to account for deep discharge. The voltage is assumed to drop following a quadratic curve for $SOC < 0.3$, modifying equation (2.7). Since $V_{OC,base}$ is not used, the user inputs the value of V_{OC} at reference temperature and an $SOC = 0.5$ instead of $V_{OC,base}$. The default battery models use $V_{OC} = 2.045$ V per cell at reference temperature.

The model also includes a "gassing" effect to account for over-charging losses: part of the battery current (I_{Bat}) does not participate in the useful chemical reaction (useful current I_q), but instead electrolyzes water in the battery electrolyte, forming H_2 and O_2 gases. This gassing current I_{gas} contributes to an energy loss equal to $V_{Bat} \cdot I_{gas}$. Empirical curves are used to calculate the gassing current as a function of SOC and the charging current. When the battery is fully charged, any further positive current will entirely consist of gassing current (no useful charging current), which should be avoided by the battery controller.

Battery efficiency

The coulombic efficiency is assumed to be constant, with a suggested value of 97 % for lead-acid batteries. This efficiency value is applied to the charging current. Note that this does not include the effect of the gassing current described above (the gassing current is subtracted from the battery current to obtain the charging current). Ohmic and temperature effects are taken into account by the voltage model (see above).

Self-discharge at reference temperature (20 °C) is obtained from data sheets. Default models use values between 2 %/month and 5 %/month. The self-discharge current is corrected as a function of temperature according to a predefined profile (no correction below 20 °C, increasing losses for higher temperatures). The curve is only provided as a drawing in the documentation but the correction above 20 °C can be approximated by $I_{sd}/I_{sd,ref} = 1 + 0.0045 \cdot \left(T - T_{ref}\right)^2$, where I_{sd} is the self-discharge current.

Battery capacity and state of charge

The nominal capacity of the battery is described by the value C_{10}. The actual capacity in operation is affected by the discharge rate; it typically increases quickly for discharge times between 10 h and 50 h, and then plateaus for longer discharge times. PVSYST fits a curve based on various C_{nn} values provided in data sheets. Alternatively, the Peukert law can be used to correct the capacity value:

$$\frac{C_n}{C_{n_{ref}}} = \left(\frac{n}{n_{ref}}\right)^{k-1} \tag{2.8}$$

Where C_n is the capacity for a discharge time n (in hours), and $C_{n_{ref}}$ is the capacity for a discharge time n_{ref} (in hours, this would be 10 hours if C_{10} is known). The Peukert coefficient k is between 1.12 and 1.13 for lead-acid batteries.

The capacity is also affected by temperature: for lead-acid batteries, the capacity increases strongly with temperature, but datasheets rarely provide that information, so PVSYST uses a default correction curve for $C_{10}(T)/C_{10}\left(T_{ref}\right)$. The coefficient is 1 at 20 °C, and it ranges from 0.4 at -20 °C to 1.2 at 50 °C. It should be noted that battery life is severely (and negatively) affected by temperature, so operating at high temperature is not a viable option, in spite of the positive impact on capacity.

The state of charge SOC is calculated from the current charge (balance of charging/discharging current) and the calculated capacity (depending on current and temperature).

Battery state of health

Battery ageing is modelled in PVSYST as a combination of two effects: static ageing and operating ageing. Both effects are used to calculate a "state of wear" (SOW), which is different from the "state of health" (SOH) discussed above. In particular, the state of wear has no impact on any battery parameter (voltage, capacity, etc.) in the calculations. It is just used as an indicator of the remaining battery life, so that the economic analysis can account for renewing the batteries when they reach an $SOW = 0$. The static ageing is just represented by a lifetime in years (e.g. 10 years), and the SOH is decremented accordingly (i.e. for a lifetime of 10 years, the SOW would be decremented by 1/87600 every hour). The lifetime is affected by temperature, and it is assumed that above 25 °C, the lifetime decreases by a factor of 2 for each increase of 10 °C. The dynamic ageing is represented by a total number of "equivalent full cycles" that the battery can perform, and how much of that amount has been used. For example, assuming a battery can perform 1500 full cycles with a DOD of 1 (from $SOC = 1$ to $SOC = 0$ and back to $SOC = 1$), an equivalent ageing would be obtained by performing 15000 cycles with a DOD of 0.1 (e.g. between $SOC = 0.8$ and $SOC = 0.7$). In practice, however, cycles with a larger DOD are more damaging to the battery than cycles with a smaller DOD, so that the number of lifetime cycles multiplied by the DOD is not a constant value. PVSYST applies a correction to ageing to account for that effect, so that in the above example, the battery could perform 15000 cycles with $DOD = 0.1$, but less than 1500 full cycles. The correction is based on manufacturer data or can be modeled as a linear correction in percent. Keeping the same example, with a linear correction factor of 50 %, the battery could perform 15000 cycles with a $DOD = 0.1$ (an equivalent number of full cycles of 1500), but with a $DOD = 0.9$, the total equivalent number of full cycles would not remain at 1500 but would be decreased by 50 % of the DOD increase, i.e. it would become $1500 \cdot \big(1 - 0.5 \cdot (0.9 - 0.1)\big) = 900$ equivalent full cycles – meaning that the battery could perform 1000 cycles with a DOD of 0.9. PVSYST combines static ageing with dynamic ageing by computing both at each time step and selecting the minimum of the two calculated SOW values.

2.2.2.1.2 Lithium-ion model

ECM parameters V_{OC} and R_{int}

For Li-ion batteries, R_{int} varies with temperature and SOC. The typical reference value provided in the software results in a voltage drop of 15.5 mV per cell when discharging at 0.1C, i.e. with a current equal to $C_{10}/10$. For example, a 4-cell battery (12.8 V nominal voltage) with a C_{10} value of 100 Ah would have an internal resistance $R_{int} = 6$ mΩ. The variation with temperature is expressed as:

$$R_{int}(T) = R_{int}(T_{ref}) \cdot e^{\frac{E_a}{8.315}\left(\frac{1}{273.15+T} - \frac{1}{273.15+T_{ref}}\right)} \quad (2.9)$$

Where E_a is the activation energy (in kJ/mol), which depends on the particular battery chemistry. (default values in PVSYST are between 20 and 30 kJ/mol). T and T_{ref} must be expressed in °C.

The variation of R_{int} with SOC is an empirical factor representing the increase of the voltage (caused by an increase in the internal resistance) which is observed at the end of the charge process in Li-ion batteries. The correction is applied at the end of the charge and at the beginning of the discharge; it is expressed as:

$$cf = 1 + A\, e^{-B\,(1-SOC)} \quad (2.10)$$

Where cf is a correction factor, and A and B are parameters that control respectively the amplitude of the correction and the range over which it is applied. The default values in PVSYST are $A = 14$ and $B = 44$.

The open-circuit voltage V_{OC} is assumed to be independent of temperature, it is calculated as a function of SOC:

$$V_{OC} = V_{OC,SOC=0.5} + \alpha\,(SOC - 0.5) \quad (2.11)$$

Where $V_{OC,SOC=0.5}$ is the open voltage at $SOC = 0.5$. It is technology-dependent, around 3.3 V for LFP and 3.7 V for NMC and NCA. α is a linear correction factor with default values of 0.15 V for LFP and 0.78 V for NMC and NCA. As for lead-acid batteries, the model also includes a correction

for deep-discharge, which is fitted to data sheets. That correction reduces V_{OC} for $SOC < 0.1$, and its effect is a reduction by 0.2 to 0.3 V at $SOC = 0$ for default performance curves.

Battery efficiency

The coulombic efficiency is assumed to be constant, with a suggested value of 96 % for Li-ion batteries. This efficiency value is applied to the charging current. Ohmic effects are taken into account by the voltage model (see above).

Self-discharge at reference temperature (20 °C) is obtained from data sheets. Default models use values around 5 %/month. The self-discharge current is corrected as a function of temperature according to a predefined profile (no correction below 20 °C, increasing losses for higher temperatures). The curve is only provided as a drawing in the documentation but the correction above 20 °C can be approximated by $I_{sd}/I_{sd,ref} = 1 + 0.01 \cdot \left(T - T_{ref}\right)^2$, where I_{sd} is the self-discharge current.

Battery capacity and state of charge

The nominal capacity of the battery is described by the value C_{10}. As for lead-acid batteries, the capacity in operation is affected by the discharge rate. The model adopts the same correction using the Peukert coefficient, shown in equation (2.8). The Peukert coefficient k is around 1.02 for Li-ion batteries.

The capacity is also affected by temperature. The capacity increases slightly with temperature, and PVSYST uses discharge curves from data sheets to estimate a correction curve for $C_{10}(T)/C_{10}\left(T_{ref}\right)$. In default curves, the coefficient is 1 at 20 °C, and it ranges from 0.58 at -30 °C to 1.02 at 50 °C. Manufacturers typically specify minimum temperatures for charging and discharging which severely restrict this range however, with default values at -20 °C for discharging and 0 °C for charging. As for lead-acid batteries, it should be noted that battery life is severely (and negatively) affected by temperature, so operating at high temperature is not a viable option, in spite of the positive impact on capacity.

The state of charge SOC is calculated from the current charge (balance of charging/discharging current) and the calculated capacity (depending on current and temperature).

Battery state of health

Battery ageing is modelled in the same manner as for lead-acid batteries.

2.2.2.2 PV*SOL

PV*SOL (https://pvsol.software/) uses a curve-based model that does not rely on the ECM model structure described above, and can be categorized as an empirical model. The model seems to have been developed for lead-acid batteries, and the adaptations for Li-ion batteries are not always documented. No corrections to account for temperature effects are documented.

2.2.2.2.1 Discharge

The discharge behavior is modelled by approximation functions fitted to discharge curves provided in manufacturers data sheets. These curves represent the voltage evolution versus the SOC for different current values (or different discharge rates, e.g. 0.5C, 2C, etc.). The model fits these curves and then interpolates a performance map to obtain the voltage from SOC and current. If power is imposed, the current is calculated iteratively.

2.2.2.2.2 Charge

PV*SOL implements a charging strategy adapted to lead-acid batteries known as IUoU, which is a succession of three phases: constant current (I), constant over-voltage (Uo), and constant voltage (U).

The model used to calculate the battery voltage during these charging phases is only documented for lead-acid batteries. Three stages of charging (Bulk, Absorption and Float) are simulated independently. The equation used to calculate the voltage during bulk charging is based on a curve fit of manufacturer data sheets. This equation formulates the variation of bulk voltage (V_B) as a function of SOC and C-rate (Which defines the charge current):

$$V_B(SOC, X_C) = V_R(SOC) + V_K + SOC^2(0.35 + 0.15X_C) \quad (2.12)$$

Where V_R denotes the Battery idle voltage and V_k identify the voltage drop due to the occurrence of crystallization. The acronym X_C stands for C-rate, the ratio between the charge current and the battery capacity in Ah. The second phase of charge starts when the battery voltage reaches a certain

setpoint and the battery voltage remains constant over this stage. The voltage threshold as well as duration corresponding to the absorption stage depends on battery design and can be set by the user (based on battery data sheet). The charge cycle ends with a float stage when the battery voltage drops (usually to $2.23 - 3\ V$) to keep the battery from overcharging consequences. The voltage model in charging mode is not documented for Li-ion batteries.

2.2.2.2.3 Capacity

The battery capacity is modelled by a curve similar to the Peukert coefficient used in equation (2.8), but it is entered as data points taken in a data sheet.

2.2.2.2.4 State of health

The battery state of health (SOH) represents the remaining capacity, and it is assumed that the battery has reached its end of life when $SOH = 0.8$ (80 % of initial capacity). According to the documentation, PV*SOL performs yearly simulations and extrapolates the lifetime from the SOH degradation over the first year of operation, so the reduced capacity is not used in the simulation but is just used as an indicator of battery replacement for economic analyses.

Similarly to PVSYST, the software does not only count the number of equivalent full cycles, but adds a penalty for deeper discharge cycles. A parameter called the cycle load (ζ) is defined to calculate the capacity loss percentage during battery operation. This parameter varies between zero and one, it is determined by dividing the weighted sum of discharged capacity (referencing the cycle range) to maximum potential capacity of battery (at standard cycle range):

$$\zeta = \frac{\sum_{i=0}^{Now}(f_i(DOD_i)I_i t_i}{C_{Totall}} \tag{2.13}$$

Where C_{Totall} indicate the battery life cycle in term of potential usable capacity (Ah) at standard depth of discharge (DOD) and f_i is the correction factor, assigned to each discharge cycle range. The reachable capacity ($C_{Available}$) can be estimated by the following equation:

$$C_{Available} = C_{N,0}(1 - 0.2\zeta) \tag{2.14}$$

The $C_{N,0}$denote the amount of nominal capacity in Ah for the new battery at start of the simulation. The battery SOH is simply

$$SOH = 1 - \zeta \tag{2.15}$$

The battery is assumed to be replaced when SOH reaches 0.8, and ζ is reset to zero.

2.2.2.3 System Advisor Model (SAM)

The SAM software (https://sam.nrel.gov/) uses a steady-state ECM to represent batteries. Some parts of the model are common to lead-acid and Li-ion technologies: the battery voltage (V_{Bat}) model, the thermal model, and most of the battery degradation model. They are combined to technology-specific capacity models.

2.2.2.3.1 ECM parameters V_{OC} and R_{int}

The battery voltage model is based on a generic electrochemical model suggested by Tremblay (Tremblay & Dessaint, 2009):

$$V_{OC} = V_0 - K\left(\frac{C}{C - \int I_{Bat}\, dt}\right) + A\, e^{-B \int I_{Bat}\, dt} \tag{2.16}$$

Where V_0 is a battery constant voltage, K is the battery polarization voltage, which depends on the battery capacity C (in Ah) and the history of charge/discharge (integral of current over time). The polarization voltage accounts for the dependence of V_{OC} versus SOC. A and B are respectively the amplitude (in V) and the inverse of the time constant (in $(Ah)^{-1}$) of an exponential correction term.

The internal resistance R_{int} is assumed to be constant. All parameters in equation (2.16) and the value of R_{int} are obtained from discharge curves provided by manufacturers. According to (DiOrio et al., 2015), SAM uses typical values for different chemistries, which are not documented but can be found in the original reference (Tremblay et al., 2007).

Neither V_{OC} nor R_{int} are assumed to vary with temperature; R_{int} is simply a constant value, and V_{OC} varies with the state of charge and current as shown in equation (2.16).

2.2.2.3.2 Thermal model

SAM models the battery as a lumped capacitance which exchanges heat with the environment through a global heat transfer coefficient representing convection and longwave radiation (no shortwave radiation is assumed):

$$m\, c_p \frac{dT_{Bat}}{dt} = h\, A\, (T_{Bat} - T_{room}) + R_{int}\, I_{Bat}^2 \tag{2.17}$$

Where T_{Bat} is the battery (lumped, or bulk average) temperature, T_{room} is the room temperature (assumed to be constant in SAM), h is the global heat transfer coefficient, A is the surface area of the battery, m is its mass, and c_p the average specific heat of the battery. Default values suggested in SAM are $c_p = 1500$ J/K and $h = 7.5$ W m^{-2} K^{-1}, and the default constant room temperature is 25 °C.

Temperature has an effect on capacity and (for Li-ion chemistries only) on lifetime.

2.2.2.3.3 State of health

SAM uses the battery capacity as an indicator of health, so SOH is defined as the ratio between the current capacity and the initial capacity. SOH is affected by two effects: static ageing, which affects the remaining capacity depending on elapsed time (and optionally temperature), and dynamic ageing, which affects the remaining capacity depending on the number of charge/discharge cycles and their depth-of-charge. Two main options are available to model degradation in SAM, lookup tables or simple equations (applicable to all technologies), and a very specific model for Li-ion batteries.

Calendar and cycle degradation lookup tables / equations

Calendar degradation can be modelled using a similar approach, by entering a 2-column table (time and remaining capacity or using regression curves accounting for temperature and SOC. The suggested equations for Li-ion batteries are

$$q = q_0 - k_{cal}\sqrt{t} \tag{2.18}$$

$$k_{cal} = a\, e^{b\left(\frac{1}{T+273.15} - \frac{1}{296}\right)}\, e^{\left(\frac{SOC}{T+273.15} - \frac{1}{296}\right)} \tag{2.19}$$

With q_0 and q the initial and remaining normalized capacity (it is suggested that $q_0 = 1.02$), t the time in days, and k_{cal} a calendar correction factor. Proposed values for parameters in the k_{cal} equations are $a = 0.00266$ day$^{-0.5}$, $b = -7280$ K, $c = 930$ K.

The first option to model cycle degradation in SAM uses a 3-column lookup table specifying the DOD, the number of cycles, and the remaining capacity. In its original default form (DiOrio et al., 2015), the table provided for 3 capacity levels at 20 % and 80 % DOD, but the table was extrapolated from only one set of values. These tables are combined with a bookkeeping algorithm known as a "Rainflow algorithm", which allows to count the number of cycles and weigh their impact by the average DOD even for incomplete cycles. The conventional Rainflow algorithm was proposed for the first time by Matsuishi and Endo in 1968 (Matsuichi & Endo, 1968) to analyze the irregular loading and cycles. This method is mainly developed for fatigue analyse of mechanical parts under fluctuated stress and tension load. The name refers to the similarity of this technique with the falling water from the edge of pagoda roof under the rain. This technique converts the time dependent data series to the extreme points which is merely comprised of deeps and valleys. The simplified data then be interpreted through 3 or 4 points method (Samavatian et al., 2018), where the full and micro cycles are counted for any formed closed loop. The length and mean values corresponding to each cycle are the output parameters which are determined by the Rainflow technique. This procedure continues until the end of data series for all extracted extreme points. Most algorithms require to know the whole series of data points before applying the algorithm, so they are not usable for online calculations – they cannot be used at each time step of a running simulation (Gundogdu et al., 2018). Downing & Socie (Downing & Socie, 1982b) originally proposed an algorithm suited for online calculations, which is referenced in SAM although no details are provided on the implementation.

Detailed degradation model for specific Li-ion technologies

SAM implements empirical curves for selected specific Li-ion chemistries. The Li-ion NMC model is based on (Smith et al., 2017). The curves express SOH (associated to capacity) as a function of temperature, SOC, DOD, calendar time, and number of cycles. They rely on a large number of empirical parameters, and SAM uses values based on testing 11 cells and presented in (Mishra et al., 2020). Other Li-ion chemistries are under development and can be treated with separate

calendar and cycle degradation lookup tables. The online calculation of the number of cycles uses the Rainflow algorithm (see above).

One particular aspect in SAM is that the calculated capacity taking ageing into account is applied immediately in the simulation (i.e. for the next time step) – if the remaining capacity is less than the current charge (which would result in an $SOC > 1$), the SOC is reset to 1.

2.2.2.3.4 Capacity

The impact of temperature on capacity is modelled with a user-selectable curve. The default curve ranges from 60 % at -10 °C to 100 % at 25 °C and saturates at 100 % above that temperature. For Li-ion batteries, this is the only correction affecting capacity.

For lead-acid batteries, SAM uses the Kinetic battery model (KiBaM) (Manwell, F James. McGowan, 1994), which was developed to represent the fact that – in lead-acid batteries – part of the charge is chemically bounded and must become available before being released.

The KiBaM represents the relationships between bound and available capacity using the concept of two connected "tanks" to determine the amount of energy which can be store or drawn over each time step. The first tank represents the available energy that can be instantly converted to electricity and sent to the load. The second tank contains bound energy which can only supply electrons to the first tank. In order to describe the distributed energy through this tank system, two parameters need to be identified for each battery model. The capacity ratio of available energy tank to combined size of both tanks (C) and the conductance constant (K) which determines the conversion rate between bound and available energy. Assuming that the current remains constant over the time step (Δt), the available (q_1) and bound (q_2) charge can be calculated using the following two equations:

$$q_1 = q_{1,0}e^{-k\Delta t} + \frac{(q_0 kc - I)(1 - e^{-k\Delta t})}{k} - \frac{Ic(k\Delta t - 1 + e^{-k\Delta t})}{k} \qquad (2.20)$$

$$q_2 = q_{2,0}e^{-k\Delta t} + q_0(1-c)(1 - e^{-k\Delta t}) - \frac{I(1-c)(k\Delta t - 1 + e^{-k\Delta t})}{k} \qquad (2.21)$$

where $q_{1,0}$, $q_{2,0}$ and q_0 indicates the values at the beginning of the time step, respectively, of the available (q_1), bound (q_2), and total ($q = q_1 + q_2$) energy. k is a rate constant (h^{-1}) and c is the capacity ratio (-). Those two coefficients must be calculated from manufacturer data, using different capacity values at different C-rates, e.g. C_{10} and C_{20}. The concept of this correction is similar to the Peukert correction used e.g. in PVSYST: if the battery is discharged faster, the capacity will be reduced, because some energy is bound and cannot be discharged quickly enough.

For lead-acid batteries, the same k and c coefficients can be used to calculate the maximum charging and discharging current.

2.2.2.4 EnergyPlus

EnergyPlus (https://energyplus.net/) proposes three models for simulating the electrical storage systems: simple energy balance, Kinetic battery model (KiBaM) (Manwell, F James. McGowan, 1994) and Lithium-ion Nickel Manganese Cobalt (NMC) model (DiOrio et al., 2015).

2.2.2.4.1 Simple energy balance

The simple model (known as ElectricLoadCenter:Storage:Simple) works as an energy bucket to store and release quantities of electrical energy, regardless of storage technology. The maximum allowed charge-discharge rate as well as state of charge (SOC) thresholds can be set by the user to control the power dispatch to/from storage unit. This model estimates the energy losses based on user-defined constant values for charge and discharge cycles efficiencies. Additionally, the system operation can be scheduled manually to restrict access to the storage device over the certain periods. The capacity is user-specified and constant, and self-discharge is not modelled.

2.2.2.4.2 Kinetic Battery Model

This model is known under a generic name (ElectricLoadCenter:Storage:Battery) in EnergyPlus, presumably because it was the first battery model implemented – but it only applies to lead-acid batteries.

Capacity

The KiBaM capacity model is similar to the implementation in SAM (see section 2.2.2.3.4), but there is no correction for temperature.

Voltage

The terminal voltage (V_{Bat}) is modeled with a steady-state ECM. The internal resistance is assumed to be constant. The open-circuit voltage V_{OC} is expressed as 2 functions of SOC, one for charging and one for discharging:

$$V_{OC,charge} = E_{0,c} + A_c X_c + \frac{C_c X_c}{D_c - X_c} \quad (2.22)$$

$$V_{OC,discharge} = E_{0,d} + A_d X_d + \frac{C_d X_d}{D_d - X_d} \quad (2.23)$$

A, C and D are constant parameters where charge and discharge mode denoted by c and d subscripts respectively. $E_{0,c}$ and $E_{0,d}$ represent V_{OC} for a fully charged and fully discharged battery, respectively. X_c is the normalized capacity at a given charging current, $X_c = q_0/q_{max}(I_{Bat})$, and X_d is the normalized capacity at a given discharging current, $X_d = (q_{max} - q_0)/q_{max}(I_{Bat})$.

These model parameters need to be identified through curve fitting technique based on the chare-discharge profile (V_{OCV} versus SOC) at different current rates.

State of health

The model estimates the battery life in terms of potential maximum number of cycles until failure (C_f) as a function of cycle range (R) through the following double exponential decay equation:

$$C_F = C_1 + C_2 e^{C_3 R} + C_4 e^{C_5 R} \quad (2.24)$$

Where R indicates the cycle range (in term of fractional SOC and $C_1 - C_5$ are the regression coefficients which need to be obtained from detailed experiments. The default values provided in the EnergyPlus documentation are:

$$C_F = 1380 + 6834\, e^{-8.75\, R} + 6747\, e^{-6.22\, R} \quad (2.25)$$

That equation is applied to a specified number of ranges (10, by default) to obtain a series of $C_{F,i}$ values where i denotes the "bin" number for a given range. A Rainflow counting method (Downing

& Socie, 1982a) is then applied to count the equivalent number of cycles, and those cycles are sorted into the defined bins of cycle range. The degradation D is then calculated by:

$$D = \sum_{i=1} (N_i \frac{1}{C_{F,i}}) \quad (2.26)$$

Where N_i is the number of completed cycles in bin i. D is equivalent to a state of wear (SOW) and varies between zero and one to indicate the proportion of remaining battery life (0 = new, 1 = end-of-life). This SOW can be used as an indicator for economics but has no impact on the battery capacity during the simulation.

2.2.2.4.3 Lithium-ion (NMC) model

The model implemented for Li-ion batteries in EnergyPlus (known as ElectricLoadCenter:Storage:LiIonNMCBattery) is limited to one specific chemistry, Nickel Manganese Cobalt oxide (NMC). The model is directly imported form the SAM library and is identical to the one described in 2.2.2.3 with the detailed degradation model for NMC described in section 2.2.2.3.3. Some of the degradation model parameters can be changed from their default values in EnergyPlus but they are not documented.

2.2.2.5 TRNSYS

TRNSYS (Klein, 2017) has two component models representing batteries in its electrical library. TRNSYS component models are known as "Types" associated to a number, and the battery models are Type 47 (Simple Lead Acid Battery) and Type 185 (Advanced lead-acid battery with gassing current effects). Component models often provide several "modes" of operations, providing different internal models or different inputs/outputs. Both battery models in TRNSYS can use the battery power (P_{Bat}) or current (I_{Bat}) as inputs. Type 47 also includes a technology-independent mode that performs a simple energy balance similar to the equivalent model in EnergyPlus described in section 2.2.2.4.1. Besides that mode, all the models in TRNSYS address the lead-acid chemistry, and there is no dedicated model for Li-ion batteries. In the following sections, operation modes relying on different internal models are treated independently.

2.2.2.5.1 Type 47 – Simple energy balance mode

This model performs a simple energy balance and performs as an "Energy bucket". The capacity is assumed to be constant, and there is no temperature dependency in the model. A user-defined constant efficiency is used for charging, but there is no equivalent in discharge mode. There are no provisions for SOH degradation or self-discharge.

2.2.2.5.2 Type 47 – Lead-acid battery mode

The lead-acid battery model implemented in Type 47 is based on the work of Shepherd (Shepherd, 1965). The Shepherd model is a steady-state ECM where the open-circuit voltage is corrected to different SOC values. R_{int} is assumed to be constant.

Note: Type 47 documentation uses a different convention for the sign of I_{Bat}. The equations below have been adapted to our convention ($I_{Bat} > 0$ when discharging, as shown in Figure 2.1).

The equation used to calculate the battery voltage V_{Bat} as a function of I_{Bat} and SOC has the same form but different parameters in charging and discharging modes:

Charging $$V_{Bat} = V_{OC,qc} - g_c(1 - SOC) - R_{int,qc}\ I_{Bat}\left(1 + \frac{m_c\,(1 - SOC)}{Q_c/C}\right) \quad (2.27)$$

Discharging $$V_{Bat} = V_{OC,qd} - g_d(1 - SOC) - R_{int,qd}\ I_{Bat}\left(1 + \frac{m_d\,(1 - SOC)}{Q_d/C}\right) \quad (2.28)$$

Where C is the rated capacity of a single cell. All parameters are fixed to default values for a single cell, which are listed below with their definition (parameter with a c subscript are used in the charging equation, and with a d subscript in the discharging equation):

- Open-circuit voltage at full charge: $V_{OC,qc} = 2.25$ V, $V_{OC,qd} = 2.10$ V
- Linear dependency in SOC: $g_c = g_d = 0.08$ V
- Internal resistance at full charge: $R_{int,qc} = 3/C$, $R_{int,qd} = 0.5/C$ (C in Ah to get R in Ω)
- Cell-type parameters: $m_c = 0.864$, $m_d = 1$
- Charge parameters: $Q_c = -0.035\ C$, $Q_d = C/0.85$

The documentation does not specify which particular lead-acid battery type was used to select those parameters.

Optionally, the model can use a correction proposed by Hyman (Hyman, 1979) to improve the model accuracy at low current values. The correction replaces $V_{OC,qc}$ and $V_{OC,qd}$ in the equations above by $V_{OC} + V_{zp}$ in charge mode, and $V_{OC} - V_{zp}$ in discharge mode. In this model, V_{OC} is defined as $\left(V_{OC,qc} + V_{OC,qd}\right)/2$. V_{zp} is a correction voltage calculated as:

$$V_{zp} = \frac{1}{k_{zp}} \ln\left(\frac{|I_{Bat}|}{I_{zp}} + 1\right) \tag{2.29}$$

k_{zp} is a constant (set to 29.3) and I_{zp} can be seen as a diode current (set to 2.5 A).

The model does not account for self-discharge or temperature effects, but a constant user-defined charging efficiency is implemented (it is applied to I_{Bat} in charging mode).

2.2.2.5.3 Type 185 – Advanced lead-acid battery with gassing current effects

As its name implies, Type 185 implements a detailed model of lead-acid batteries which accounts for gassing current.

Note: Type 185 documentation uses a different convention for the sign of I_{Bat}. The equations below have been adapted to our convention ($I_{Bat} > 0$ when discharging, as shown in Figure 2.1).

As discussed in section 2.2.2.1 (PVSYST lead-acid model), gassing current does not contribute to battery charging and results in significant losses (as well as battery degradation). The gassing current I_{gas} is calculated as:

$$I_{gas} = I_{10}\ g_0\ e^{\left(\frac{V_{Bat}}{g_1} - \frac{g_2}{T_{Bat}+273.15}\right)} \tag{2.30}$$

Where I_{10} is the discharge current corresponding to a 10 h discharge (i.e. corresponding to 0.1C), and g_0, g_1, g_2 are constants to be identified from manufacturer data or tests. The power dissipated by gassing is simply $P_{Bat} = V_{Bat}\ I_{gas}$. The effective charging/discharging current (I_q) is then different from the total battery current (I_{Bat}):

$$I_q = I_{Bat} + I_{gas} \tag{2.31}$$

As for any steady-state ECM, the battery voltage is expressed by:

$$V_{Bat} = V_{OC} - R_{int}\, I_{Bat} \tag{2.32}$$

The open-circuit voltage is expressed as a function of SOC:

$$V_{OC} = V_{OC,0} + V_{OC,1}\, SOC \tag{2.33}$$

Where $V_{OC,0}$ and $V_{OC,1}$ are parameters to be identified from manufacturer data or tests.

In Type 185, the impact of R_{int} is modelled through an empirical relationship, and the polarization voltage ($V_{pol} = R_{int}\, I_{Bat}$) is expressed differently during charge and discharge:

$$V_{pol,ch} = V_{ch}\, a_{ch} \left(1 - \mathrm{e}^{-\frac{|I_q|/I_{10}}{b_{ch}}} + c_{ch} \frac{|I|}{I_{10}}\right) \tag{2.34}$$

$$V_{pol,dch} = V_{dch}\, f_{dch}\, g_{dch} \tag{2.35}$$

V_{ch}, V_{dch}, f_{dch}, g_{dch} are empirical constants to be identified from manufacturer data or tests, and a_{ch}, b_{ch}, c_{ch} are empirical functions of SOC. They are not documented but can be found in Type 185 source code.

Type 185 does not account for temperature effects or self-discharge. Its main weakness is that it relies on many parameters that must be identified from performance data. Besides the data that are commonly available from manufacturers or easily identified from charge/discharge curves, some parameters (g_0, g_1, g_2, V_{ch}, V_{dch}, f_{dch}, g_{dch}) require detailed test data which are not typically available without performing dedicated experiments on a particular battery.

2.2.2.6 Comparison building performance simulation software battery model

The battery models implemented in building performance simulation software discussed in this paper have been explored and the results are summarized in the following tables.

Table 2.4 Simple energy storage units available in energy building simulation software

Building simulation software		PVSYST	EnergyPlus	SAM	PVSOL	TRNSYS	Developed Model
Simple storage unit (Energy bucket)	Availability	-	√	-	-	√	√
	Self discharge	-	×	-	-	×	√
	Capacity degradation	-	×	-	-	×	√

Table 2.5 Lead-acid battery models available in energy building simulation software

Building simulation software		PVSYST	EnergyPlus	SAM	PVSOL	TRNSYS	Developed Model
Voltage model	Type	Steady state ECM	Steady state ECM	Steady state ECM	Empirical model	Steady state ECM (Shepherd equation)	Steady state ECM (Copetti)
	Temperature incorporation	V_{OC}	×	×	×	×	R_{int}
Capacity	Charge/discharge rate	Peukert law	KiBaM	KiBaM	Experimental data	×	Peukert law
	Temperature incorporation	√	×	√	×	×	√
	degradation	×	×	√	×	×	√
	Self-discharge	√	×	×	×	×	√
State of Health (SOH)	Cycle aging	Rainflow	Rainflow	Rainflow	Customized model	×	Avg cycle counting
	Capacity degradation	×	×	√	×	×	√

Table 2.6 Lithium-ion battery models available in energy building simulation software

Building simulation software		**PVSYST**	**EnergyPlus**	**SAM**	**PVSOL**	**TRNSYS**	**Developed Model**
Voltage model	Type	Steady state ECM	Steady state ECM	Steady state ECM	-	-	1st and 2nd order ECM
	Temperature incorporation	V_{OC}, R_{int}	×	×	-	×	V_{OC}, R_{int}
Capacity	Charge/discharge rate	Peukert law	KiBaM	KiBaM	-	×	Peukert law
	Temperature incorporation	√	×	√	-	×	√
	degradation	×	×	√	-	×	√
	Self-discharge	√	×	×	-	-	√
State of Health (SOH)	Cycle aging	Rainflow	Rainflow	Rainflow	-	-	Avg cycle counting
	Capacity degradation	×	×	√	-	-	√
Supported Chemistry		NMC, NCA	NMC	NMC	-	-	LFP, NMC, NCA

2.3 Objectives of the battery model library

The main objective of this chapter is to develop a unified TRNSYS battery model library allowing users to model generic batteries and the most relevant specific battery types with a range of component models sharing the same formalism and general definitions. The library includes 3 component models:

- A technology-agnostic model for feasibility studies, predesign and system-level design. The model will perform an energy balance but will not model battery voltage.
- A lead-acid battery model representing all sub-classes of lead-acid technologies (Flooded, Gel, AGM).
- A Lithium-ion model representing all sub-classes of technologies (NCM, LFP, NCA, LTO/LMO).

The literature review has illustrated the strengths and weaknesses of different available models in TRNSYS and other energy simulation programs. Based on the review, we have selected the following requirements for the library.

While some software programs come with large databases of commercially available components, TRNSYS does not, so requiring detailed data would likely result in example values or data files being used in most cases. So the general philosophy of the library is to avoid relying on detailed manufacturer data:

Obj 1:	All models should be generally applicable to a class of technology (or battery chemistry).

In terms of implementation, the models should be flexible within the TRNSYS environment:

Obj 2:	All models should allow interaction with relatively simple components using power flows as inputs and outputs, and more detailed models should also allow interaction with more detailed components using voltage and current as inputs/outputs.

In terms of features, all models should allow to perform realistic energy balances, i.e. include battery losses:

Obj 3:	All models should consider the most significant impacts on battery efficiency: coulombic efficiency, polarization voltage, self-discharge (possibly through simple efficiency factors for the technology-agnostic model).

Models should allow to perform realistic economic analyses by modelling battery performance degradation.

Obj 4:	All models should represent battery performance degradation and report the battery state of health. They should also offer the option to use the degraded performance during the simulation.

TRNSYS offers the advantage that electrical systems can be simulated within the same environment as a building. The more detailed models should include temperature effects and be able to interact with building models.

Obj 5:	The more detailed models should allow taking into account the impact of battery temperature on performance and include a thermal model capable of interacting with building models.

Finally, while detailed model validation is outside the scope of this thesis, some quality assurance should be performed to ensure the validity and applicability of developed component models.

Obj 6:	The developed models should be assessed by comparing them to other established models and to experimental data when available.

2.4 Developed battery library

The next sections will first discuss to common features of the developed models: capacity, self-discharge, state of health, and the thermal model. Then, the simple generic model (energy balance) and the specific models for lead-acid and Lithium-ion batteries will be discussed.

2.4.1 Capacity

The battery capacity is the main battery design parameter in PV+Battery system analysis, so it is entered by the user as a rated capacity and the corresponding discharge time (e.g. the rated capacity

for a 10-h discharge, C_{10}). This value is internally converted to C_{10} using a Peukert coefficient approach:

$$\frac{C_n}{C_{n_{ref}}} = \left(\frac{n}{n_{ref}}\right)^{k-1} \tag{2.36}$$

The Peukert coefficient k is user-selectable with recommended values of 1.02 for Li-ion and 1.12 for lead-acid.

During the simulation, the capacity will be corrected at each time step depending on the charging/discharging current, and depending on the battery state oh health.

The capacity is also corrected for temperature. The user enters a capacity reduction factor at -20 °C (the reference being 25 °C), with a suggested value of 50 %, and the model linearly interpolates between those values. The capacity is kept constant above 25 °C.

The capacity correction for temperature and current are not applied in the simple (energy balance) model.

2.4.2 Self-discharge

The self-discharge current at reference temperature is entered by the user as a percentage of the rated capacity per month, with suggested values of 3 % for Li-ion and 5 % for lead-acid. This value is then converted to a self-discharge current in amperes. The self-discharge current is corrected at each time step for temperature effects using the equation adopted by PVSYST:

$$I_{sd}/I_{sd,ref} = 1 + \alpha_{sd} \cdot \left(T - T_{ref}\right)^2 \tag{2.37}$$

Where I_{sd} is the self-discharge current and α_{sd} is a user-selected parameter, with suggested values of 0.005 for lead-acid batteries and 0.01 for Li-ion batteries. This correction is not applied in the generic (energy balance) model.

2.4.3 State of health

All battery models in the library share the same approach for state of health (SOH) modelling. The selected indicator for battery health is the usable capacity C. The state of health SOH is equal to 1

when the battery is new, and the threshold for replacement is left to the user. A threshold of 80 % is often used in the literature, but lower thresholds can be applicable so some use cases.

The model selected to assess battery degradation combines static (or calendar life) degradation with dynamic (or cycle-dependent) degradation.

Static degradation is applied as in PVSYS. It is entered by the user as a lifetime (with a suggested value of 10 years). The static degradation at each time step is simply assumed to be the time step (expressed in years) divided by that value. The amount of degradation is then corrected for temperature using the rule that it doubles for every increase by 10 °C over 25 °C. This results in a static variation of SOH, ΔSOH_{static}.

Dynamic (cycle-dependent) degradation is parametrized by the number of full cycles that the battery can perform (with suggested values of 1200 for lead-acid and 2000 for Li-ion). The model calculates the equivalent number of full cycles using a simple cycle counting method (Gundogdu et al., 2018). In this approach, the number of charge and discharge micro-cycles are computed separately through independent counters. The counters, keep tracking the sum of input and output energy to estimate the battery charge and discharge SOC respectively. The number of either charge or discharge cycles are incremented when the corresponding SOC reaches to the predefined maximum thresholds (DOD). At each point, the equivalent cycle number is the average of previous charge and discharge cycles. The flowchart in Figure 2.2, shows how the cycle counter operates at each time step over the simulation period.

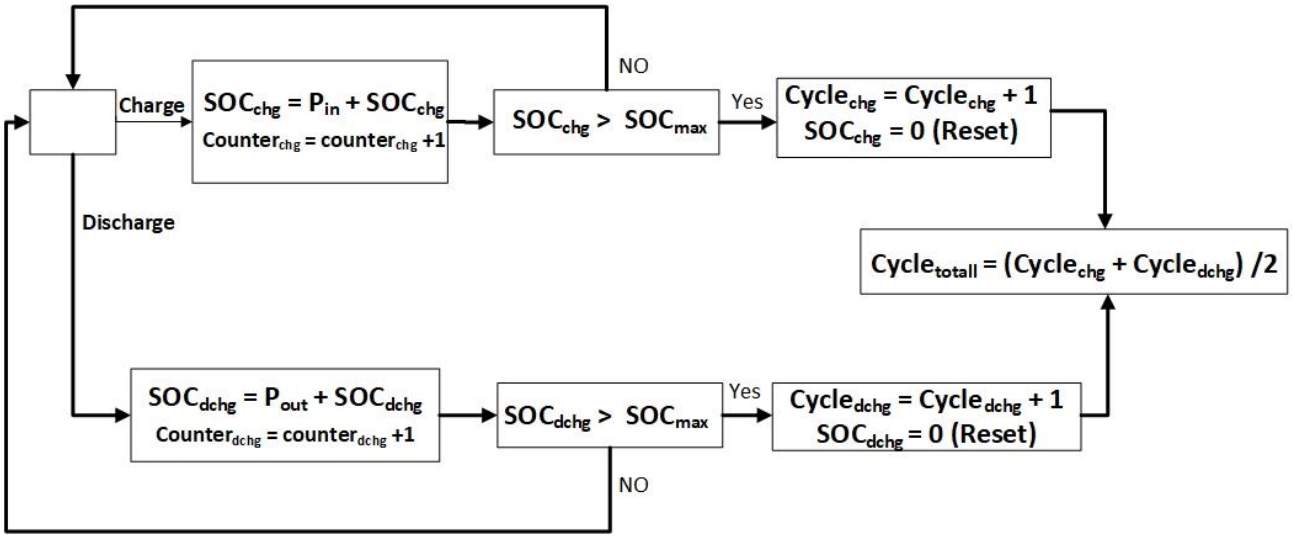

Figure 2.2 Flow chart of cycle counting method for estimating the equivalent cycles number

The number of completed equivalent full cycles is used to calculate a dynamic degradation, which is simply the ratio between the fractional full cycles completed during a time step and the lifetime number of cycles, which provides the dynamic variation of SOH, $\Delta SOH_{dynamic}$.

At each time step, the variation of SOH is calculated as the maximum of the static and dynamic variations:

$$SOH_{n+1} = SOH_n - \max\left(\Delta SOH_{static}, \Delta SOH_{dynamic}\right) \tag{2.38}$$

2.4.4 Thermal model

Temperature has a significant impact on different aspects of battery performance, and it cannot simply be assumed that the battery temperature is equal to the room temperature. The experimental results in Figure 2.3 (collected from experimental setup), show the difference between the ambient (room) temperature and the battery surface temperature.

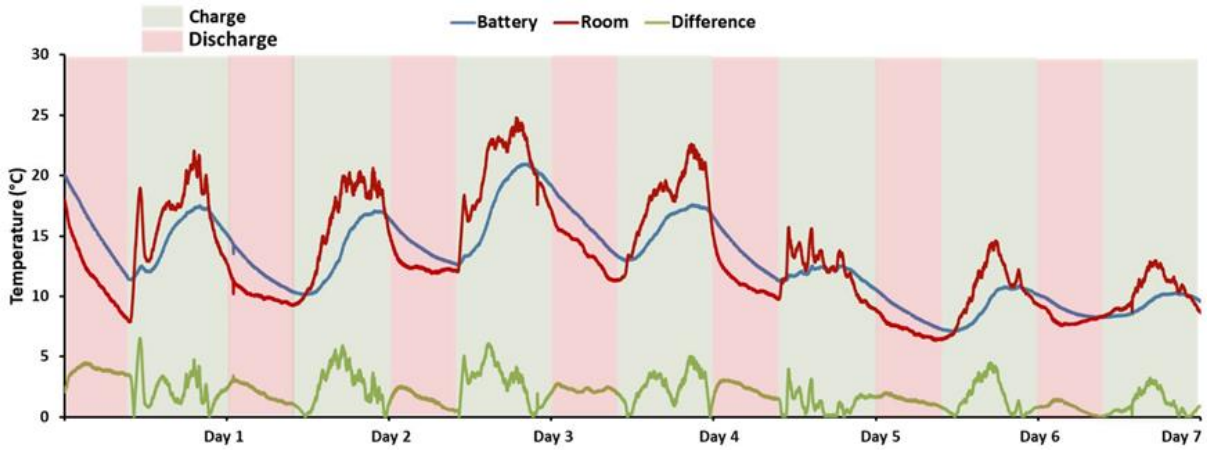

Figure 2.3 Battery surface and room temperature at dynamic loading operation mode (Barzegar Bafrouei, 2014)

The green line indicates the trend of temperature difference between battery and surrounding in charge and discharge mode of operation over sunny (e.g. day 3) and hazy days (e.g. day 5). The higher temperature difference at sunny days is related to higher input current during solar window (charge mode) which increase the internal heat generation (that is correlated to the current).

The summary of recorded data corresponding to battery surface temperature deviation from room temperature is shown in the following table for cycle, charge and discharge mode of operation.

Table 2.7 Difference between battery and room temperature

Operation mode	Average(°C)	Max(°C)	Standard deviation
Cycle	2.24	8.49	1.46
Charge	2.38	8.49	1.75
Discharge	2.05	4.67	1.19

The thermal model performs a heat balance on the battery assuming a lumped capacitance model and using a global heat transfer coefficient representing convection and longwave radiation (no shortwave radiation is assumed):

$$m\, c_p \frac{dT_{Bat}}{dt} = h\, A\, (T_{Bat} - T_{room}) + \dot{Q}_{loss,Bat} \tag{2.39}$$

Where T_{Bat} is the battery (lumped, or bulk average) temperature, T_{room} is the room temperature (provided as an input to the component model by other TRNSYS components), h is the global heat transfer coefficient, A is the surface area of the battery, m is its mass, and c_p the average specific heat of the battery. $\dot{Q}_{loss,Bat}$ includes all battery losses calculated by the other part of the model: ohmic dissipation, coulombic efficiency, gassing losses (for lead-acid), and self-discharge.

The value of C_p in lead-acid battery depends on the battery type, it varies between $0.7 - 0.9\ J/(g\ °C)$ for the valve regulated category (VRLA) and slightly more than $1\ J/(g\ °C)$ for the flooded batteries (Rand & Moseley, 2017). For the Li-ion batteries, as it expected similar to other LIB characteristics, the C_p also depends on the chemistry class of battery. For the LIB of interest (LFP) the C_p ranging from $1.005 - 1.103\ J/(g\ °C)$ (Kim et al., 2013). So a value of 1 kJ kg^{-1} K^{-1} seems appropriate and is hardcoded in the model (the user can correct the mass if required).

Given the availability of detailed building models in TRNSYS, it would have been possible to treat long-wave heat exchange in more detail, but this has not been implemented at this stage. The heat exchanged by the battery is provided as a single output and it is suggested to use it as a convective gain in building models. The global heat exchange is provided as an input (so that forced ventilation could for example be implemented), with a suggested constant value of 8 W m^{-2} K^{-1}. Battery mass and surface area are user-selected.

2.4.5 Simple electrical storage unit (Energy bucket)

This simple model performs an energy balance. Its capacity is entered by the user and only affected by SOH degradation. The thermal model is not implemented, and the model neglects all impact of battery temperature. A constant value is entered by users for charging and discharging efficiency values, which should account for coulombic efficiency and ohmic losses. Self-discharge is also implemented. Battery losses are calculated and outputted, so they could be used in a building model to account for heat gains, but there is no feedback loop to the battery.

This simple component is convenient for preliminary design of electrical storage in PV+Battery systems (or other energy systems using batteries), but it does not represent the battery voltage.

2.4.6 Lead-acid battery model

2.4.6.1 Model selection

Temperature has an impact on different aspects of battery performance: open-circuit voltage, internal resistance (or polarization voltage), capacity, and degradation. Among the reviewed models for lead-acid batteries, none of them models all these aspects. The PV*SOL and existing TRNSYS models do not consider temperature. The SAM and EnergyPlus models neglect any impact on degradation and voltage (either through the open-circuit voltage or through the internal resistance). Finally, the PVSYST model neglects the impact on internal resistance. This last model also relies on manufacturer data, which contradicts Objective 1 (generalization). So none of the reviewed model is suitable to address objectives 1 and 5.

The Copetti model (Copetti et al., 1993) was selected as a basis for the voltage and capacity assessment. The model implements a simple steady-state ECM where V_{CO} and R_{int} are taken into account through empirical relationships that are meant to represent all batteries based on a lead-acid chemistry. These relationships include the effects of SOC, current, and temperature on all parts of the model. The model also accounts for gassing current through an "overcharge" equation.

Interestingly, DiOrio (DiOrio et al., 2015) mentions that the Copetti model was not considered for SAM because it lacks generality (i.e. it is only applicable to lead-acid batteries, not to lithium-ion batteries). But the SAM model then evolved to become extremely specific to some technologies for other aspects than voltage (e.g. for capacity and degradation), so it is unclear why the requirement for the voltage part of the model was different. As indicated above, the selected voltage model in SAM is technology-independent but requires parameters identified from manufacturer data, and neglects any impact of temperature.

The original Copetti model does not discuss self-discharge or performance degradation, so these will be addressed separately. Also, the Copetti model uses the battery temperature as an input, but does not address calculating that temperature. A lumped capacitance thermal model will be added to that effect.

2.4.6.2 The Copetti model

In their study (Copetti et al., 1993), the model authors tested several lead-acid batteries under charge/discharge regimes over wide range of operating conditions in order to develop a generic model. Their model is based on a modified version of Shepherd equations (Shepherd, 1965). The model includes expression for charge and overcharge phases which are not considered by the previous models such as Shepherd and Facinelli (Facinelli & A., 1983).

The basis of the voltage model is the same as for all models representing a steady-state ECM (here expressed for one cell rather than the whole battery):

$$V = V_{OC} - R_{int}\, I \tag{2.40}$$

Where V_{OC} (open-circuit voltage) and R_{int} (internal resistance) are calculated by different expressions in discharge and charge modes.

The discharge open-circuit voltage ($V_{OC,d}$) for a single cell, in V, is:

$$V_{OC,d} = 2.085 - 0.12\ (1 - SOC) \tag{2.41}$$

While the charge open-circuit voltage ($V_{OC,c}$), in V, is:

$$V_{OC,c} = 2 + 0.16\ \ SOC \tag{2.42}$$

The expression for R_{int} represents 3 terms: a constant term, a term that depends on the cell current I, and a term that depends on the state of charge SOC. These terms are then multiplied by a correction factor depending on the battery temperature T, which is expressed as a difference with the reference temperature $T_{ref} = 25$ °C:

$$\Delta T = T - T_{ref} \tag{2.43}$$

The discharge equivalent resistance $R_{int,d}$ is:

$$R_{int,d} = \frac{1}{C_{10}} \left(0.02 + \frac{4}{1 + I^{1.3}} + \frac{0.27}{SOC^{1.5}}\right) (1 - 0.007\ \Delta T) \tag{2.44}$$

Where C_{10} is the battery capacity for a 10-h discharge.

The charge equivalent resistance $R_{int,c}$ is:

$$R_{int,c} = \frac{1}{C_{10}} \left(0.036 + \frac{6}{1 + I^{0.86}} + \frac{0.48}{(1 - SOC)^{1.2}}\right) (1 - 0.025\ \Delta T) \tag{2.45}$$

The full voltage equations are obtained by replacing V_{OC} and R_{int} by the appropriate values in equation (2.40).

The coulombic efficiency in charging mode, η_c, is calculated by an empirical equation:

$$\eta_c = 1 - e^{\left(\frac{20.73}{I/I_{10} + 0.55}(SOC - 1)\right)} \tag{2.46}$$

The equation for the charge voltage is only valid in the absence of gassing current. The threshold for gassing process can be expressed by the cell voltage, and the equations above for charging will only be valid when the cell voltage V is below the gassing voltage V_g ($V \leq V_g$) with:

$$V_g = \left(2.24 + 1.97 \ln\left(1 + \frac{I}{C_{10}}\right)\right)(1 - 0.002\Delta T) \tag{2.47}$$

Above the gassing voltage ($V > V_g$), the charge cell voltage follows a dynamic behavior before reaching its final value, V_{ec} (voltage at the end of charge):

$$V_{ec} = \left(2.45 + 2.011\ \times \ln\left(1 + \frac{I}{C_{10}}\right)\right)(1 - 0.002\Delta T) \tag{2.48}$$

Between V_g and V_{ec}, the voltage can be expressed as:

$$V_c = V_g + \left(V_{ec} - V_g\right)\left(1 - e^{\frac{\int_{t_g}^{t} I\, dt - SOC_g\, C}{I\, \tau}}\right) \tag{2.49}$$

Where t_g and SOC_g represent respectively the time and the state of charge at the onset of gassing (i.e. when the voltage became higher than V_g), and τ is a time constant expressed as:

$$\tau = \frac{17.3}{1 + 852\left(\frac{I}{C_{10}}\right)^{1.67}} \tag{2.50}$$

So in charging mode, the voltage is expressed differently depending on the charge level:

- Charge $V \leq V_g$: $V_{OC,c}$ from (2.42) and $R_{int,c}\, from$ (2.45) with the general expression (2.40)
- Overcharge $V > V_g$: Dynamic expression (2.49)

In charge mode, when the battery voltage reaches the certain point (transition from bulk to absorption stage), the charge controller reduces the current to keep charging the battery with constant voltage (to avoid overcharging). Therefore, without investigating the right transition point among charge stages, the model is unable to estimate the voltage accurately. Since the Copetti equation uses the voltage as an indicator parameter to switch among various stages of charge and voltage is a function of input current, the Copetti model fails to simulate the battery behaviour (in absorption stage) when it is coupled with charge controller. To solve this problem, the newly developed model employed the combination of battery SOC and terminal voltage to appropriately investigate the turning points among various charge stages and apply the corresponding equations.

The synoptic diagram of battery which is illustrated in Figure 2.4 demonstrates the inputs and outputs of battery model. The mathematical algorithms and detailed explanation associated with this component is provided in the following section.

2.4.6.3 Developed model

The developed lead-acid battery model uses the Copetti model for voltage and internal resistance. Its schematic is described in the figure below.

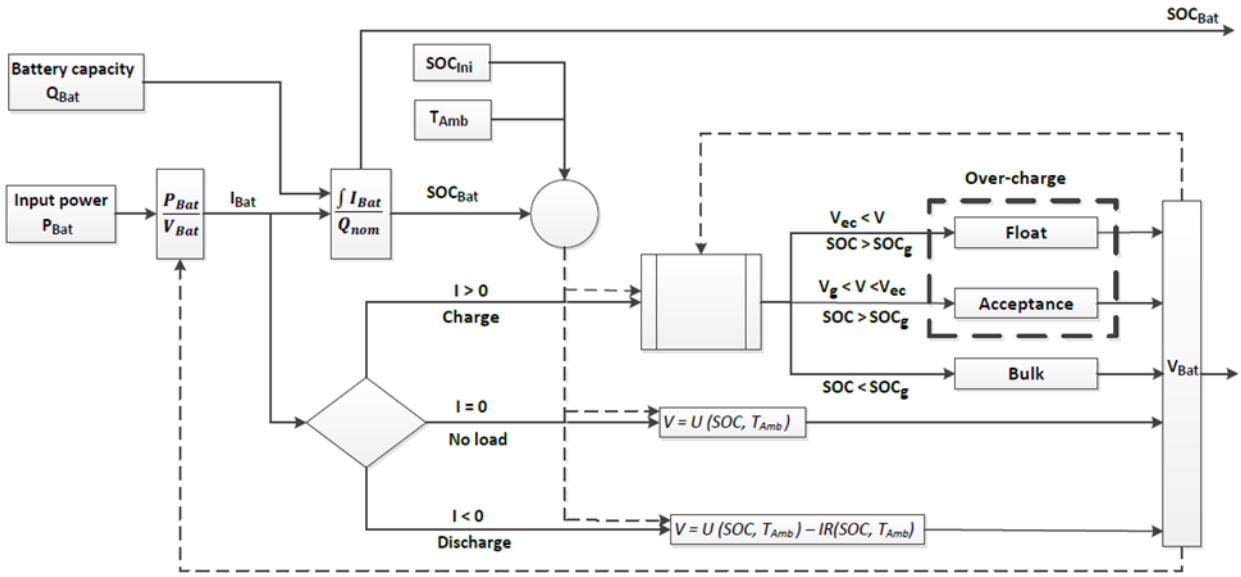

Figure 2.4 Schematic diagram of general lead-acid battery model

2.4.7 Lithium-ion battery (LIB) model

As mentioned previously, the LIB subcategories have different features corresponding to the battery chemistry class. This chemical variation needs to be taken into consideration in the LIB modelling procedure.

2.4.7.1 Modelling approach

Equivalent circuit model (ECM) was used as modelling strategy to replace the electrochemical reaction of LIB with network of electrical elements under dynamic loading condition. This modelling approach has been described previously in the subsection corresponding to battery modelling strategies. In trade of between accuracy and complexity level, commonly one or two RC blocks are employed to meet the required accuracy level while keeping the number of parameters under control. The general 2nd order ECM is presented in Figure 2.5.

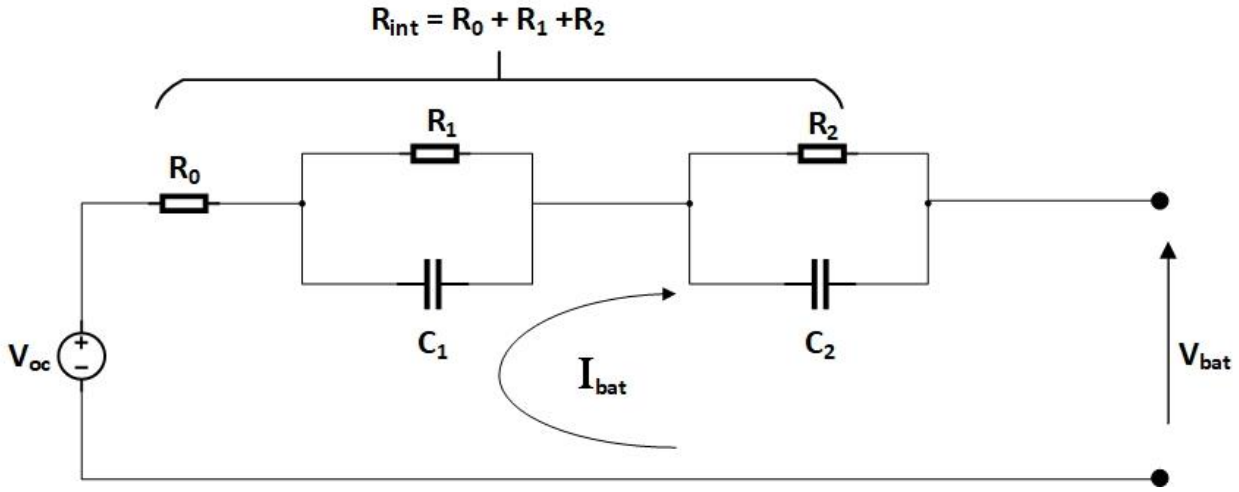

Figure 2.5 Schematic diagram of the 2nd order ECM

The internal voltage source (V_{oc}) models the open circuit voltage and the series resistor (R_0) is the minimal ohmic internal resistance of the battery. The parallel RC branches comprised of polarization resistance and capacitance (R_1, C_1) and (R_2, C_2) represent the impact of short and long dynamic transient response respectively. Based on Kirchhoff's law, the terminal battery voltage (V_{Bat}) consists of four parts (the open circuit, series resistance, the first (V_1) and second (V_2) RC block) can be written as:

$$V_{bat} = V_{oc} - V_1 - V_2 - R_0 I_{Bat} \tag{2.51}$$

The voltage-drop of RC branches over the time (dt) can be calculated through the following formula expressed like a derivative:

$$\frac{dV_1}{dt} = -\frac{1}{R_1.C_1} V_1 + \frac{1}{C_1}.I_{bat} \tag{2.52}$$

$$\frac{dV_2}{dt} = -\frac{1}{R_2.C_2} V_2 + \frac{1}{C_2}.I_{bat} \tag{2.53}$$

Or in the integrated form:

$$V_{bat} = k_0 - k_1.\exp(-a.t) - k_2.\exp(-b.t) \tag{2.54}$$

Where:

$$k_0 = V_{oc} - R_s . I_{bat}$$

$$k_1 = R_1 . I_{bat} \quad k_2 = \frac{R_2}{I_{bat}} \tag{2.55}$$

$$a = \frac{1}{R_1 . C_1} \quad b = \frac{1}{R_2 . C_2}$$

During charge and discharge mode of operation, the ECM elements vary differently as a function of SOC, temperature, and state of health (SOH). The challenge in this modelling approach is to formulate the ECM elements based on influential parameters.

The most cited test procedure to provide data for parameter identification is called a charge-discharge current impulse test. During the test, a current pulse for charging/discharging the battery will be applied to measure the corresponding terminal voltage. It is necessary to impose adequate rest time (e.g. 30-60 min) between charge and discharge current pulses to ensure the battery reaches the equilibrium to be stable at certain open-circuit voltage. Parameters are identified based on the test data as illustrated in Figure 2.6, and then expressed as polynomial functions or lookup tables. These functions or table encapsulate the variation of all parameters as functions of temperature and state-of-charge:

$$ECM\ parameter_i = f_i(SOC, Temperature\ ) \quad i = 1, 2, \dots, N \tag{2.56}$$

N illustrates the number of ECM parameters which can varies based on model structure (for a 2nd order ECM, these would be $V_{OC}, R_0, R_1, R_2, C_1, C_2$, i.e. $N = 6$). The dependency on state-of-health requires longer tests and is generally addressed separately.

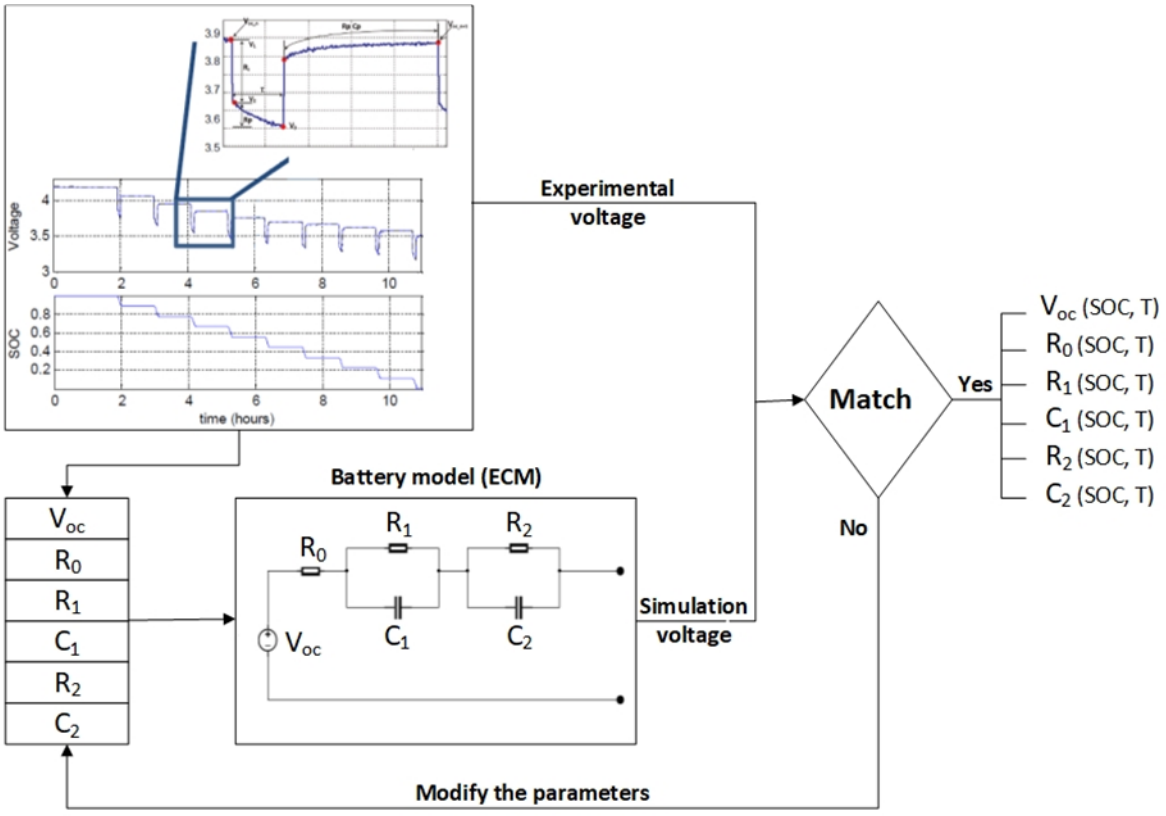

Figure 2.6 Schematic diagram for parameters identification of 2nd order ECM

Detailed testing of a wide range of batteries is outside the scope of this thesis, so the parameters described below are extracted from the literature, with an objective of selecting parameters applicable to a broad range of batteries using a given technology.

The developed LIB component model is applicable to 3 chemistries which are the most frequently employed for on-site storage-based hybrid systems (Hesse et al., 2017): NMC, LFP, and LTO.

2.4.7.2 Lithium Iron Phosphate ($LiFePO_4$) – LFP

The developed LFP battery model (Lam et al., 2011) has capability to work in two modes of operation to simulate battery performance with and without incorporating the temperature effect respectively. Both modes of operation use the second order ECM to estimate the battery terminal voltage. Regardless of the operation mode, the open-circuit voltage is calculated through the following equation, which is temperature independent:

$$V_{oc} = a_1 e^{-a_2 SOC} + a_3 + a_4 SOC + a_5 e^{-\frac{a_6}{1-SOC}} \quad (2.57)$$

The temperature is not considered in the above equation since the open-circuit voltage variation remains below $2\,mV$ in a temperature range from -20℃ to 40℃ (Lam et al., 2011).

In the first mode the values corresponding to ECM elements are based on battery SOC:

$$f_i(SOC) = b_1\, SOC^6 + b_2\, SOC^5 + b_3\, SOC^4 + b_4\, SOC^3 + b_5\, SOC^2 + b_6\, SOC + b_7$$

$$f_j(SOC) = c_1\, e^{c_2\, SOC} + c_3\, SOC + c_4 \quad (2.58)$$

$$R_0, C_1, C_2 = f_i(SOC)$$

$$R_1, R_2 = f_j(SOC)$$

Where a_1- a_6, b_1-b_7 and C_1- C_4 are the constant parameters which are identified separately for charge and discharge operation in (Lam et al., 2011).

The second mode of operation taking into consideration the effect of temperature on battery performance. Two series of equation has been defined for the temperature range above and below the 20℃ to improve the model accuracy for predicting the battery terminal voltage:

In the following sets of equation, the c and d subscripts refer to charge and discharge mode of operation respectively. T is the battery temperature in kelvin and ΔT indicate the temperature deviation from reference (20℃). The ECM terms with "*" superscripts represent the corresponding parameters in equation (2.58) which is dedicated to temperature independent model.

High temperature (> 20℃)

$$R_{0C} = R^*_{0C}(SOC).\, 0.7192\, \exp\frac{33.91}{T - 199.9}$$

$$R_{0d} = R^*_{0d}\,(SOC).\, 0.7613\, \exp\frac{10.14}{T - 260.8} \quad (2.59)$$

$$R_{1C} = 9.86E8\ \exp(-0.1479T - (-01178T + 13.99).SOC) - 18970T + 705.4$$
$$R_{1d} = R^*_{1d}(SOC) - (0.00036.97\,\Delta T) + 0.0002225\ \Delta T\,.SOC \quad (2.60)$$

$$C_{1C} = C^*_{1C}(SOC) + 8.814\,\Delta T$$
$$C_{1d} = C^*_{1d}(SOC) - 6.58\,\Delta T\,.SOC + 12.11\,\Delta T \quad (2.61)$$

$$R_{2C} = R^*_{2C}(SOC)\,.(-134.4\,T + 5.011)$$
$$R_{2d} = R^*_{2d}(SOC) + (0.006718\,\Delta T)\exp(-20SOC) - 0.0005967\ \Delta T \quad (2.62)$$

$$C_{2C} = C^*_{2C}(SOC).0.00002611\exp(0.03541\ T)$$
$$C_{2d} = C^*_{2d}(SOC).3128\ \exp(-\frac{2398}{T}) \quad (2.63)$$

Low temperature ($<$ 20℃)

$$R_{0C} = (0.2192\ SOC^4 - 0.3968\ SOC^3)(-0.08297\ T + 24.82) + (0.0002136\ T^2 - 0.1422\ T + 2348)\ SOC^2 + (-0.0001795\ T^2 - 01077\ T - 16.2)SOC + 0.04968\ \exp\frac{28.78}{T - 237.6} \quad (2.64)$$

$$R_{0d} = (-0.00000593\,T^3 + 0.005011 2d\,T^2 - 1.411\,T + 132.5)SOC^4 - 0.2819\,SOC^3 + 0.2448\,SOC^2 - 0.0963\,SOC + 0.06297\exp\left(\frac{24.37}{T - 236.3}\right)$$

$$R_{1C} = 7.008\text{E}29\exp(-0.03051\ \text{T} + (0.2782\ \text{T} - 63.04)SOC) + 0.00000284\,T^2 - 0.001733\,T + 0.2786$$

$$R_{1d} = (19230\,T^2 - 0.1166\,T + 17.66)\,.\exp -(0.01098\,T^2 - 5.644\,T + 729.9)SOC + 0.01827 - 0.006462\,SOC \quad (2.65)$$

$$C_{1C} = (-11.23\,T^2 + 5941\,T - 784800)SOC^4 + (16.18\,T^2 - 8523\,T + 1.12E6)SOC^3 - 368.8\exp(426.1\,T)\,SOC^2 + (-1.199\,T^2 + 710.3\,T - 102700)SOC + 8.493\,T - 1902$$

$$C_{1d} = -1173\,\left(SOC + (142.8\,T - 4.068)\right)^3 + 827.8\left(SOC + (0.01428\,T - 4.068)\right)^2 + 100.5 + (-0.06807\,T^2 + 400.2\,T - 57690\,)\left(SOC + (0.01428\,T - 4.068)\right) \quad (2.66)$$

$$R_{2c} = 3.726E8\exp(-495.1\,T + 32.23\,SOC) + 592100\,T^2 - 350.7\,T + 5.225 + 157.1\,SOC \quad (2.67)$$

$$R_{2d} = 0.008238 \exp\left(\frac{180.5}{T - 232.1} - 20\,SOC\right) + 15.89E\text{-}8 \exp\left(\frac{3779}{T}\right) - 2.208E\text{-}8 \exp\left(\frac{4202}{T}\right) SOC$$

$$C_{2c} = ((6.343E\text{-}6)\,SOC^5 - 1.817E\text{-}5\,SOC^4 + 188700\,SOC^3).\exp(855.1\,T) - (1.414E\text{-}5)\exp(838.1\,T)\,.\,SOC + 696.2 \quad (2.68)$$

$$C_{2d} = (2.4E\text{-}4SO\,C^4 + 21.54E\text{-}6\,SOC^3 + 2.8)\exp(759\,T) + 157300\,SOC^2 \exp(435.3\,T) + 378.3\,SOC \exp(\frac{4980}{T - 243})$$

2.4.7.3 Lithium Nickel Manganese Cobalt Oxide ($LiNiMnCoO_2$) — NMC

The selected parameters for the NMC model implement a first-order ECM (i.e. $R_2 = 0$, $C_2 = \infty$), as proposed by (Ceraolo et al., 2019). For this chemistry, temperature effects are mainly affecting capacity and degradation, but their impact on ECM parameters can be neglected. The ECM elements are described through a series of polynomial equations where the corresponding parameters are defined as a function of SOC:

$$ECM\ element_i = a_1\,SOC^3 + a_2\,SOC^2 + a_3\,SOC + a_4 \quad (2.69)$$
$$ECM\ element = V_{oc}, R_0, R_1, C_1$$

Where a_1 to a_4 are are tabulated below.

Table 2.8 Li-ion NMC model parameters

ECM elements	a_1	a_2	a_3	a_4
V_{oc}	-0.1558	0.625	0.0776	3.643
R_0	0.0082	-0.0113	0.003	0.0114
R_1	0.036	0.0551	-0.0251	0.0103
C_1	82419	-119776	50522	7415.9

2.4.7.4 Lithium Titanate (LTO)

The model for LTO estimate the battery terminal voltage through the second order ECM based on the proposed model in (Li et al., 2018). Again, for this chemistry, temperature effects are mainly affecting capacity and degradation, but their impact on ECM parameters can be neglected. The extracted parameters values are expressed through the following equations where the ECM components are quantified as a single-variable function of battery SOC:

$$V_{OC} = a_1 e^{a_2 SOC} + a_3 SOC^3 + a_4 SOC^2 + a_5 SOC + a_6 \tag{2.70}$$

Where a_1 to a_6 are the constant parameters that are presented in the table below.

Table 2.9 Constant parameters for V_{oc}

a_1	a_2	a_3	a_4	a_5	a_6
-0.018	-83	0.642	-0.642	0.5673	2.0633

The other components of ECM including the series resistor as well as RC block's parameters (resistor and capacitor) are quantified by the following equations:

$$ECM\ element_i = b_1 e^{b_2 SOC} + b_3$$
$$ECM\ element = R_0, R_1, C_1, R_2, C_2 \tag{2.71}$$

The b_1, b_2 and b_3 are the constants corresponding to ECM parameters equation which are identified in the table below.

Table 2.10 Constant parameters of ECM components

ECM elements	b_1	b_2	b_3
R_0	15.62	-24.37	7.75
R_1	18.08	-25.14	4.67
C_1	-596	-11.01	703.6
R_2	31.1	-155.2	4.98
C_2	-3956	-27.12	4475

2.5 Battery library model evaluation

The battery library including the generic lead-acid and several Li-ion battery chemistries models is implemented in the TRNSYS environment in order to determine the terminal voltage of battery as a function of input current/power, load and ambient temperature at various modes of operation. The battery was cycled under operating conditions and the parameters of interest were recorded over the test period (e.g. battery current, voltage and temperature).

The TRNSYS project as it is shown in Figure 2.7 has been defined to evaluate and compare the accuracy level of developed and currently existing battery model (Type 47) through comparison among simulated and experimental battery voltage.

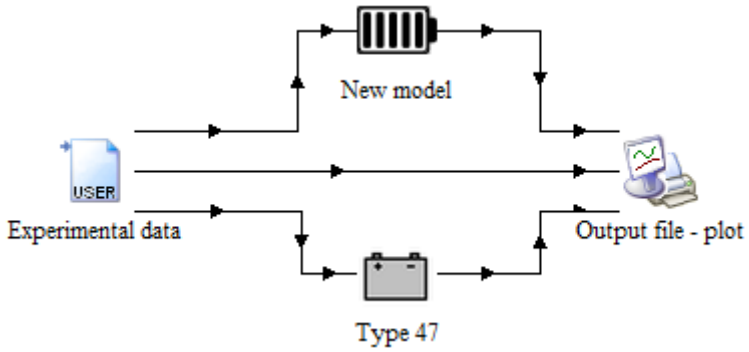

Figure 2.7 TRNSYS project for model evaluation

The recorded experimental data include the current and voltage at the charge controller output, as well as ambient temperature. The battery model receives the measured current and calculates the voltage.

2.5.1 Experimental setup and tests

The experimental setup (Solar street light), was installed at Sexton Campus of Dalhousie University in Halifax, Canada to collect the data corresponding to battery operation under dynamic supply and demand condition. The installation data is provided in Table 2.11.

Table 2.11 Installation site specification

Latitude	Longitude	Elevation	PV tilt angle	PV direction
46.67˚N	63.61˚E	145 m	45˚	South

The data logger recorded the parameters corresponding to battery behaviour over the two months period from 14/05/2014 to 14/6/2014. The stored data including battery input/output current and voltage as well as ambient and surface temperature.

2.5.2 Lead-acid battery model evaluation

The tested battery is a sealed advanced glass mat (AGM) battery, type Hoppecke solar bloc 6 V 250 Ah. Each module consists of three internal cells; the weight is $41.4\ kg$ and the dimension are (L, W, H) $308, 107, 275\ mm$. The battery bank comprised of two lead-acid modules ($6\ V, 250\ Ah$) connected in series. In order to carry out the steady phase of the test, a power-cycler (Arbin BT2000) is employed to put the battery under deep charge and discharge cycles. For the second stage (dynamic loading), the utilised experimental setup operates as an off-grid solar streetlight. The setup is comprised of two 135 W PV panels which are connected in parallel to supply the required electricity for 55 W LED lamp unit (SAT-48S model). The setup has light controlling functionality to turn on/off the LED based on surrounding radiation level.

2.5.2.1 Deep charge-discharge cycle

In the first phase of test, in order to characterize the battery performance, the discharge cycles were carried out based on the provided set point limits by manufacturer in battery specifications sheet. The discharge and charge schedules are described briefly in the following.

The discharge cycle with constant current equal to $22.9\ A$ takes approximately 9 h until the voltage drops to $5.4\ V$ per module. The charge cycles consist of two stages including constant current (CC) and constant voltage (CV) which take 8 h and 3 h respectively. During the first step the power cycler charges the battery with constant current ($22.9\ A$) until the battery voltage reaches $7.05\ V$. This step is followed immediately by a CV phase of charging where the terminal voltage remains

constant and current decreases until the cutoff point (minimum current of 3.43 A). The simplified description and set point values corresponding to deep discharge cycles are presented in Table 2.12.

Table 2.12 Deep discharge-charge schedule description

step	Phase	Description and values
1	Discharge	Current at -22.9 A to a minimum voltage limit of 5.4 V
2	Charge	Two step CC/CV: current +22.9 A to a maximum voltage limit of 7.05 V and a minimum cut-off current of +3.43 A

The characteristic voltage and current profiles corresponding to experiment and simulation data are given in Figure 2.8.

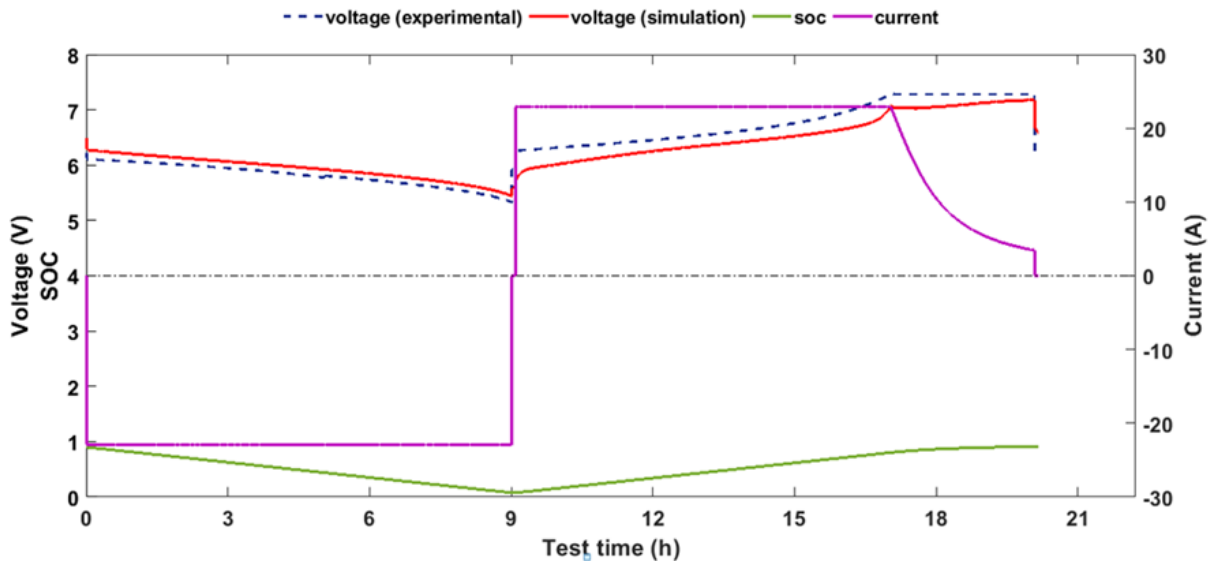

Figure 2.8 The battery voltage (experimental and simulation results) versus current and SOC profile

As it is anticipated the voltage experienced steady decline over constant discharge phase which is typical of lead acid battery. Charging the battery (CC) increases the voltage gradually until the end of bulking stage where the transition to rapid rise occurred and voltage reaches the maximum value. Throughout the floating charge stage (CV) the voltage remains constant while current drops steadily.

2.5.2.2 Dynamic loading

During the second phase of the test, the system operates continuously for a whole month and the required load value as well as supplied electricity level varies daily due to the change on working hours of LED lamp and input solar radiation intensity. Consequently, during one-month time span of monitoring the experimental setup, the battery experienced various charge and discharge regimes over the different SOCs and DODs. These various realistic working conditions provide opportunity to examine the model at three states of charging (bulk, absorption and float) as well as autonomous operation mode which is crucial for evaluation procedure. Moreover, the repeated discharge cycles with different initiation SOCs (ranging from 90% to 30%) and working operation events enable the possibility to assess the battery performance in wide range of DODs.

Any type of inaccuracy during either mode of operation (charge/discharge) will be accumulated and has impact on the (starting point of) following cycles. Therefore, precise measurement of charge-discharge efficiency as well as initial SOC at the start of the test are key parameters to minimize the model evaluation error. A fully charged battery at the start of the test facilitates the SOC tracking through coulomb counting method over the whole period. Since the model utilizes current integration method, determining the cycle efficiency necessitate measuring the columbic capacity corresponding to charge and discharge cycles. The cycle efficiency would be estimated through dividing the columbic capacity (Ah) value for discharge, by the charge. The measured values of columbic efficiency throughout the deep discharge cycling test ranged from 95% to 98% for the corresponding battery module.

Figure 2.9 presents the comparison among predicted and experimental battery voltage by developed and currently existing TRNSYS model (Type 47 with Shepherd-Hyman model) during six arbitrary selected consecutive days. The solid red line indicates the measured battery voltage and the blue and green dash line represent the simulated data by developed model and Type 47 respectively.

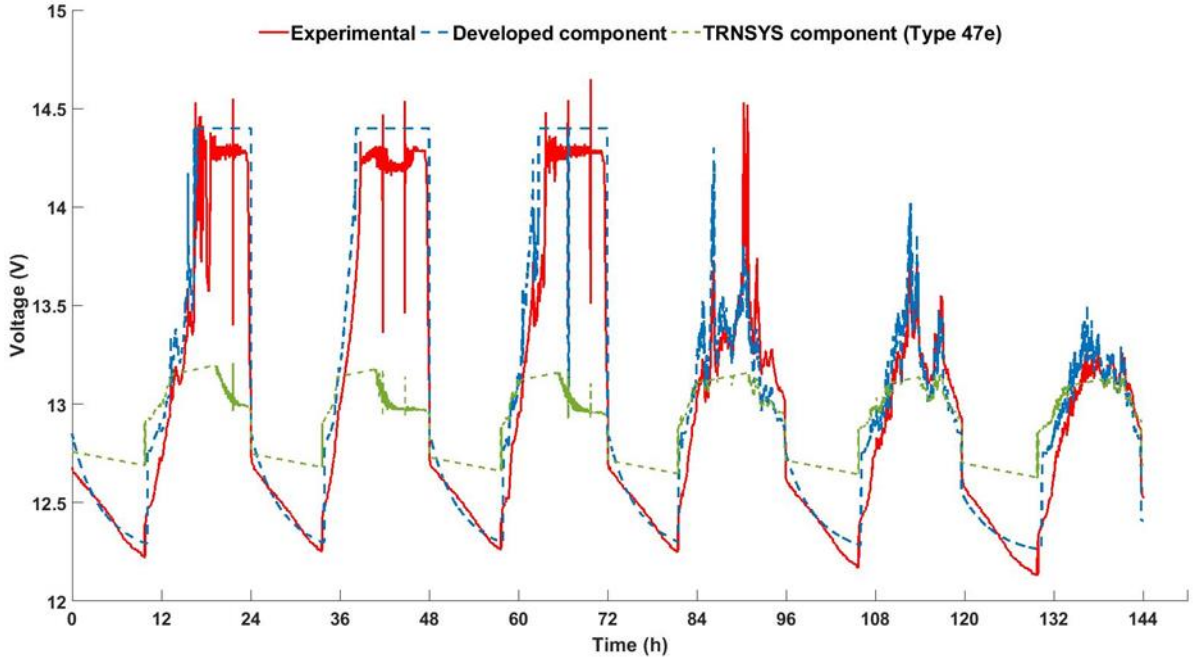

Figure 2.9 Comparison among measured and simulated battery terminal voltage

The good level of agreement between experimental and predicted data which are presented in Figure 2.9 during whole test timespan (after several dynamic loading cycles ~ 30) demonstrates the model capability to predict the battery electrical behaviour over long-term periods. Two days were selected as representative of sunny and cloudy days when the battery experience full and partial charge respectively. The corresponding days were selected according to the amount of daily generated solar electricity parameters (columbic capacity in Ah) and the related information is presented in Table 2.13

Table 2.13 Selected days for model assessment

Climatic condition	Day No	Electricity production (Ah)
Sunny	3	66.3
Cloudy	26	29.7
Average	1-30	46.6

Figure 2.10 and Figure 2.11 contain three graphs to present the model input and output parameters as well as experimental data over a sunny and cloudy day respectively. The top graph displays the (measured and simulated) terminal voltage and the middle chart shows how battery SOC changes

over the battery operation. Finally, the recorded parameters which are used as model input data including the ambient temperature and battery current are provided in the bottom graph.

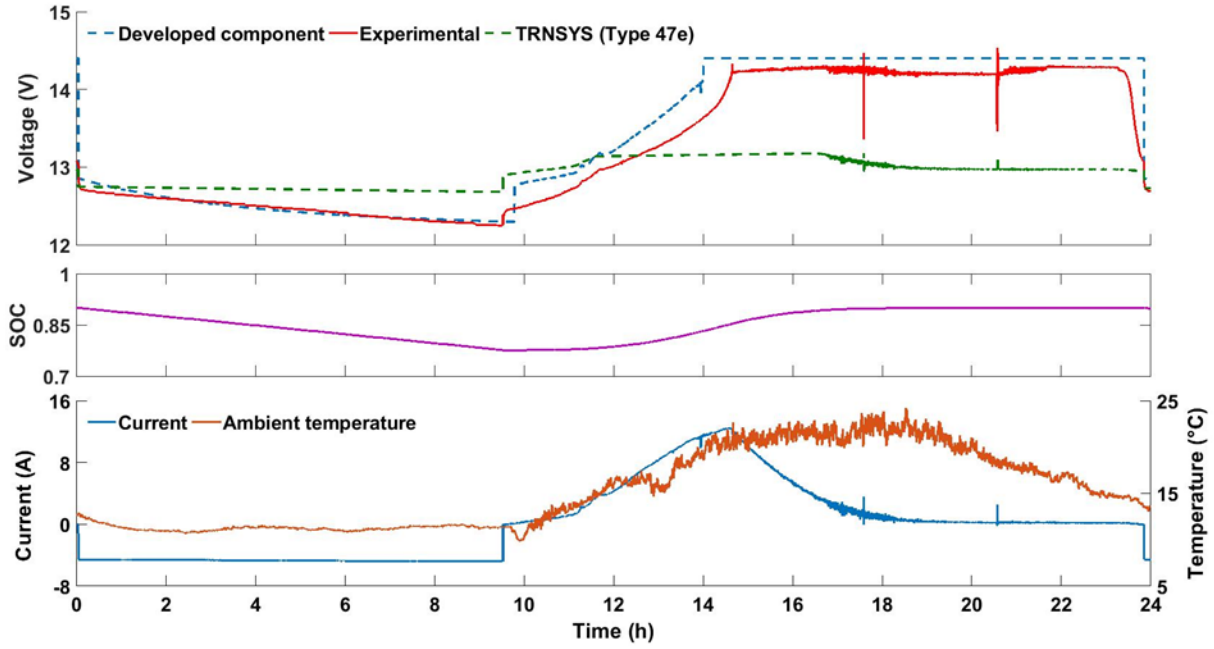

Figure 2.10 Battery model inputs and outputs for sunny day (Top: measured and experimental battery voltage. middle: the battery SOC bottom: measured input current and ambient temperature)

As can be seen in top graph in Figure 2.10, during the discharge mode (between 0-8th hour), the TRNSYS component (type47e) fails to estimate the battery voltage accurately while, acceptable match exists between measured and developed model's simulated results. The root mean square error (RMSE) of Type 47 and the developed model corresponding to the discharge phase during the sunny day is 50 mV and 7 mV respectively. During the transition stage from discharge to charge when the current value is approximately zero the battery voltage represents the open circuit voltage at corresponding SOC.

For model assessment during the charge mode, several aspects need to be considered including the investigation of charge stage (e.g. bulk, absorption) and reaction to charge controller device (which works in conjunction with battery). During the first stage of charge (bulk) – between 10th to 14th hour – the predicted voltage by the developed model closely follows the experimental results and the offset between two data series remains below 70 mV. As can be seen, Type 47 is unable to investigate the final point of bulk charging (transition to the absorption stage) which results in a

considerable gap between predicted and experimental data over the rest of the cycle. During the charge stage, the RMSE is 40 mV for the developed model compared to 130 mV for Type 47.

Figure 2.11 presents the same series of data (simulated and experimental battery input/output parameters) for to the cloudy day. The developed model predicts the measured voltage with a reasonable accuracy, while Type 47 is unable to follow the trend of the recorded battery voltage in discharge and during the majority of the charge phase. Apart from a short period (between 8th - 10th hour) at the start of the charge mode, the voltage predicted by the developed model precisely follows the acquired data from the experimental setup, and the root mean square error (RMSE) is 19 mV.

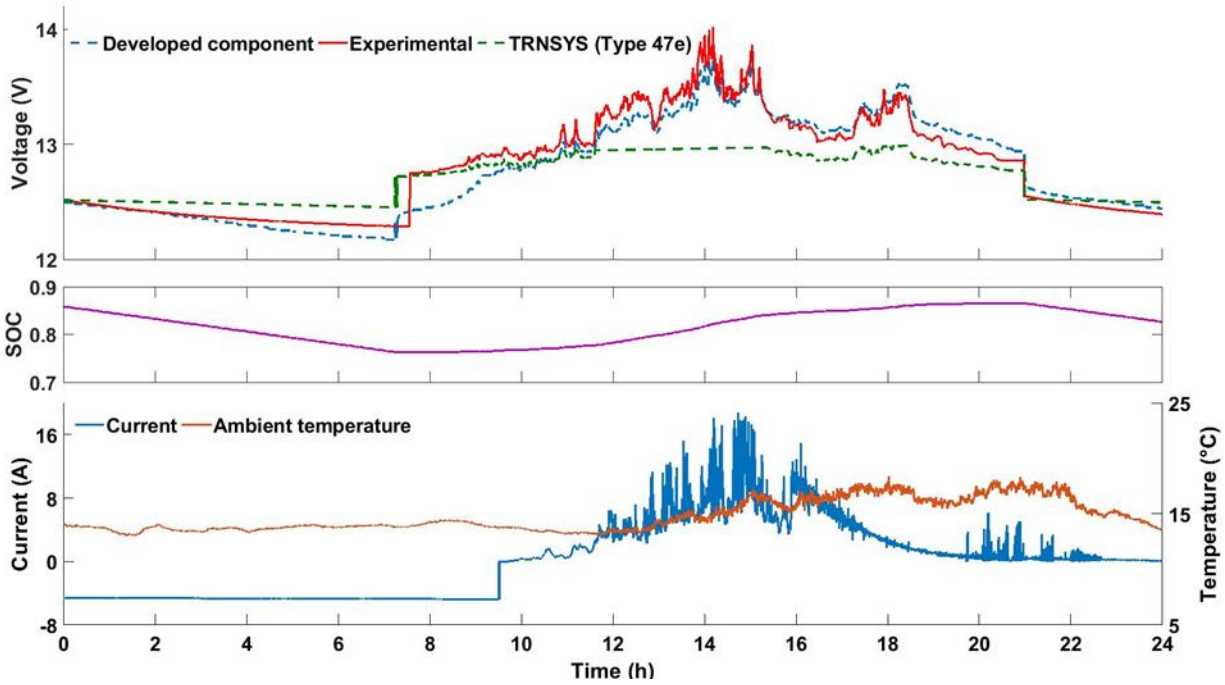

Figure 2.11 Battery model input and outputs for cloudy day (Top: measured and experimental battery voltage. middle: the battery SOC bottom: measured input current and ambient temperature)

The table below presents an overview of RMSE values for the different tests.

Table 2.14 RMSE values [in V] for simulated battery terminal voltage

Day No (climatic condition)	Operation mode	TRNSYS type	Developed model
3rd (Sunny)	Charge	0.13	0.04
	Discharge	0.05	0.007
	Cycle	0.12	0.03
25th (Cloudy)	Charge	0.06	0.018
	Discharge	0.03	0.023
	Cycle	0.04	0.0196
1st – 30th (Random)	Charge	0.12	0.052
	Discharge	0.092	0.015
	Cycle	0.096	0.05

2.5.3 Lithium-ion battery models evaluation

The measured voltages which are used in this evaluation are provided by Calce Battery research group (Zheng et al., 2016) who applied the dynamic stress test current profile, on batteries with LFP and NMC chemistries.

2.5.3.1 Lithium Iron Phosphate (LFP)

The battery specifications corresponding to the LFP which is used for model evaluation by experimental data (Zheng et al., 2016) is presented in Table 2.15.

Table 2.15 LiFePO4 Battery specifications

Cell chemistry	Capacity rating (Ah)	Weight (gr)	Dimension (mm)	Length(mm)
$LiFePo_4$	2.23	67	25.4	65

Three plots including the measured and estimated voltage (top graph), the battery soc (middle graph) and the current profile are presented in Figure 2.12. According to the provided current profile in the bottom graph, the test comprised of two stages:

- Static charge including two steps (constant current/constant voltage)
- Dynamic charge/discharge

As can be seen in the top graph, acceptable agreement exists between experimental and estimated voltage over two parts of the test. In the first part (static charging) the model error remains below 0.05 V and over the dynamic charge/discharge the offset between two data series never exceeds 0.15 V.

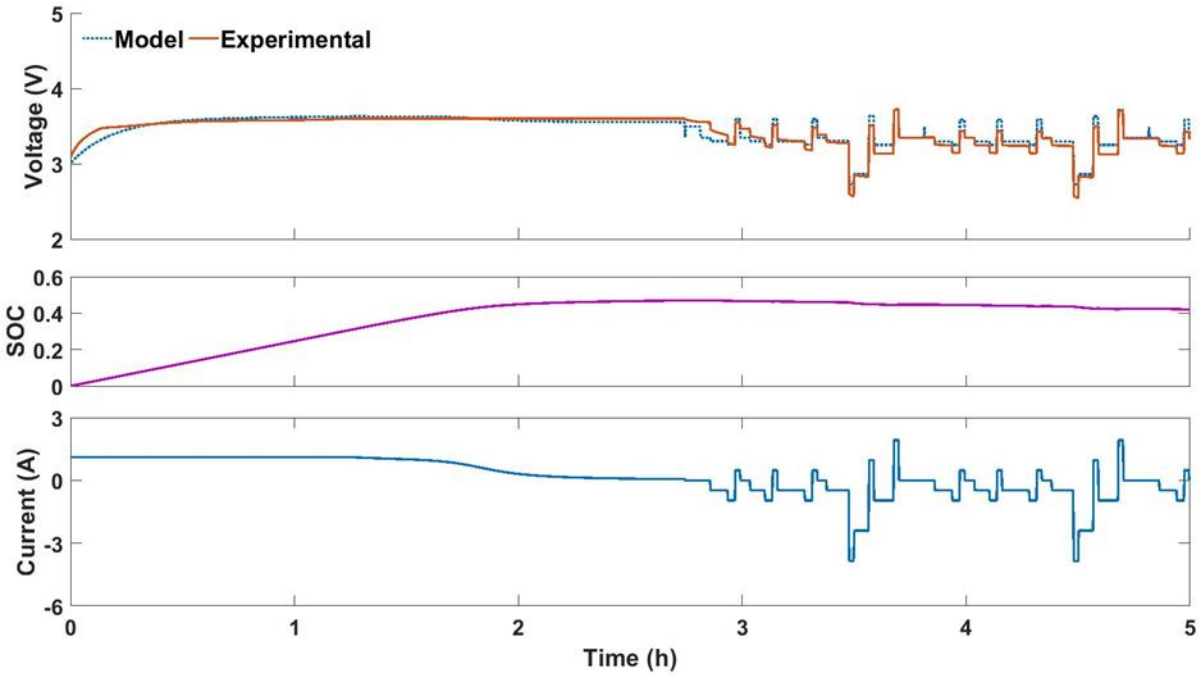

Figure 2.12 The estimated and measured voltage (top), the battery SOC (middle) and battery input current profile (bottom)

The acquired results from this evaluation indicated the developed battery model has the capability to estimate the battery voltage over both static and dynamic loading mode of operation with reasonable error for considered application.

2.5.3.2 Lithium Nickle Manganese Cobalt Oxide (NMC)

The properties of utilised battery for implementing the experimental test (Zheng et al., 2016) are shown below

Table 2.16 NMC battery specifications

Cell chemistry	Capacity (Ah)	Weight (gr)	Diameter (mm)	Length (mm)
NMC/Graphite	2	45	18.33	64.85

The model input and output data as well as measured battery voltage are presented in Figure 2.13 through three plots. The top plot shows the model estimated and measured voltage, the middle plot indicates the battery SOC variation and finally the bottom graph is allocated to the input current profile.

The operating conditions include different phases:

- Constant current (CC)-constant voltage (CV) charge steps
- Constant current discharge phase
- Rest-time (where the terminal voltage is equal to battery OCV)
- Dynamic charge-discharge mode

The first stage of the test (static loading) is comprised of two steps (CC and CV) in charge mode which is followed by single step (CC) in discharge phase. In order to attain the equilibrium, the current remains zero for approximately two hours before starting the second stage of the test. Over the rest time period the battery terminal voltage represents the battery OCV at the corresponding SOC. The second stage is a dynamic stress test to put the battery under fast changing charge and discharge phases.

Table 2.17 Battery test schedule explanation

Stage	Phase	Description and values
1st	Charge	Two step CC/CV: current 1 A to a maximum voltage limit of 4.2 V and a minimum cut-off current of 0 A
1st	Discharge	Current at -1 A to a minimum voltage limit of 3.5 V
-	Rest	zero charge or drawn current for 2 hrs
2nd	Charge/discharge	The dynamic stress current profile for rest of the test

The comparison between estimated and measured voltage at top graph indicate the model has capability to appropriately predict the battery voltage even at low currents.

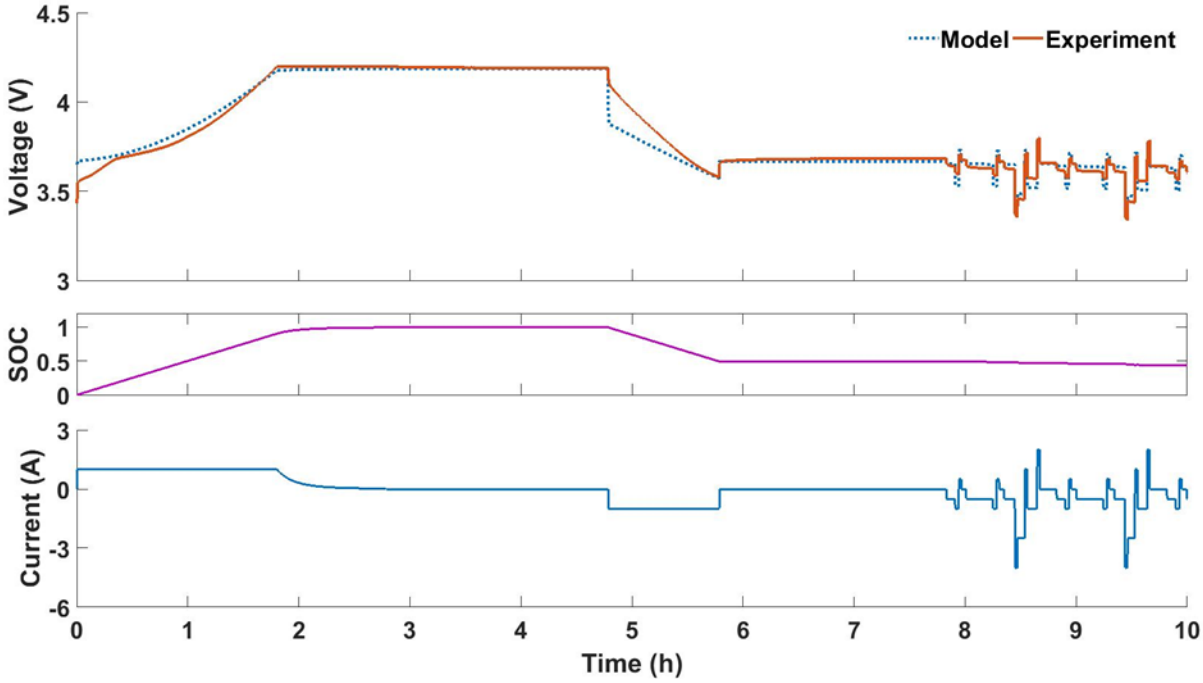

Figure 2.13 The estimated and measured voltage (top), the battery SOC (middle) and battery input current profile (bottom)

During the charge mode the error at first and second step remains below 50 mV and 20 mV respectively. The model capability to accurately estimate the battery SOC and OCV can be evaluated through comparing the data sets over the rest time period. A good agreement is also shown among simulated and experimental voltage at rest (hours 6 to 8) where the offset never exceeds 16 mV. The model error is higher during short transients in discharge mode (around hour 5), reaching 0.2 V, which is still acceptable in the context of yearly or multi-year PV+Battery analyses.

2.6 Chapter summary

This chapter presented the most relevant battery technologies for PV+Battery systems, and reviewed the models implemented in building performance and energy systems simulation tools. The literature review identified the main desirable characteristics for component models, and highlighted the fact that none of the implemented models combines all those characteristics. In particular, the component models available in TRNSYS lack several key features such as health

degradation and the ability to represent Li-ion batteries. Temperature effects are generally poorly represented in building performance tools such as EnergyPlus and TRNSYS.

The proposed TRNSYS battery library responds to the identified need by proposing 3 distinct component models addressing the modelling of generic batteries, lead-acid batteries, and lithim-ion batteries. They have been compared to experimental data to confirm their validity.

CHAPTER 3 RESIDENTIAL ARCHETYPE

This chapter describes the residential archetype used in this study. The archetype consists of a typical building (house), its heating, ventilation and air-conditioning (HVAC) system, and the PV+Battery system.

3.1 Building

The selected residential building for modelling purpose in this thesis is a two-storey single-family detached house (210 m^2 of floor area) with a basement and an attached garage constructed in Canadian Center of Housing Technology (CCHT)(Swinton et al., 2001). It represents a typical North-American wood-frame structure compliant with Canadian R-2000 building standard which is set on a poured concrete basement. In order to implement the house model, the detailed information regarding the insulation materials, windows specifications and airtightness assumptions are extracted from building specification provided by Swinton et al.(Swinton et al., 2001).

3.1.1 HVAC system (baseboard and conventional AC)

The heating, ventilation and air conditioning (HVAC) system is comprised of all-electric baseboard heating unit and conventional air conditioner. The considered electric resistance heating system is commonly used for space heating application in Canadian buildings. The HVAC load is calculated through modelling the corresponding HVAC system in TRNBuild using the idealized heating and set-point control strategy.

3.2 Occupant-driven load profiles

The accurate estimation of electricity consumption plays a crucial role in achieving more accurate and reliable results in implementing and modelling the load management strategies. The pie chart in Figure 3.1 indicates the share of major end-use in total consumed energy in residential sector.

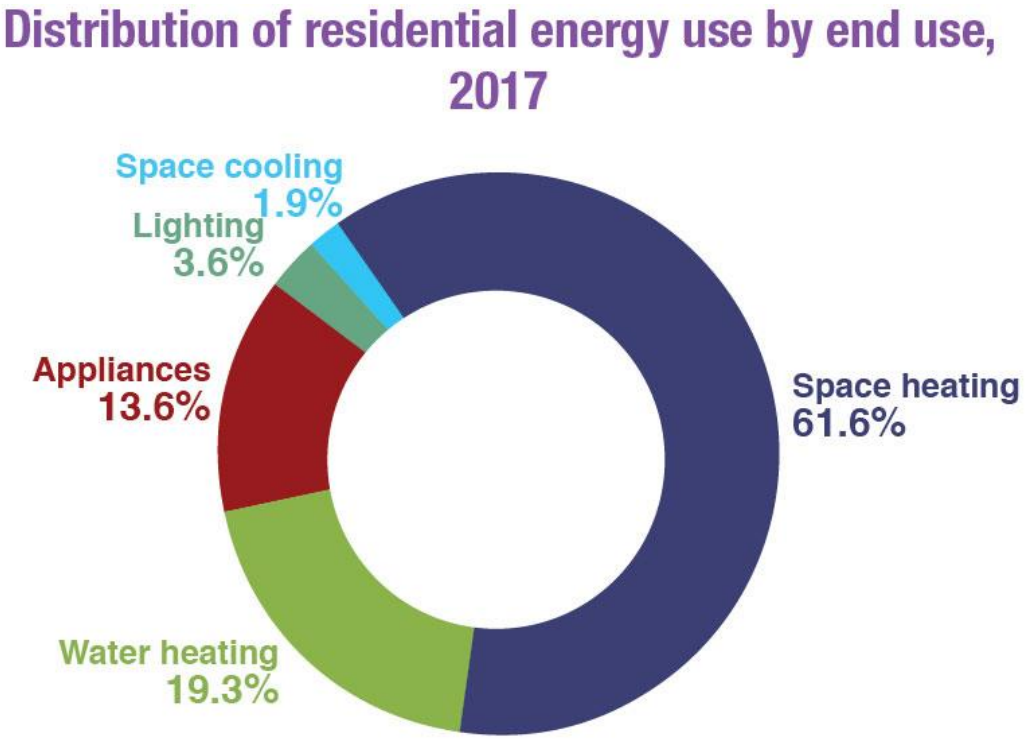

Figure 3.1 Total residential energy consumption by major end-use (NRCan, 2021)

As it is illustrated in Figure 3.1, approximately 64 % of the whole consumption is associated with HVAC loads (heating and air-conditioning), and even 83 % when domestic hot water is added. Lighting and other electrical appliances account for the remaining 17 %. In all-electric homes, the electricity consumed by HVAC systems also has a notable impact on the electricity grid peak demand. In Québec for example, residential space heating contributes 30% of the winter peak demand (Kummert et al., 2011). The electricity demand profile used in this study is comprised of three load components:

- HVAC system (space heating and cooling)
- Hot water system
- Electrical appliances (e.g. washer, dryer, dishwasher, freezer, refrigerator, light and small appliances)

3.2.1 HVAC load (space heating)

The detailed model of considered residential archetype as well as corresponding HVAC system

(electric resistance) is implemented in a validated building model in TRNSYS to estimate the HVAC load regarding the commonly assumed occupant comfort conditions (K. Zhang, 2018). The impact of internal heat gains which is generated by operation of electrical appliances are considered in the simulation model.

A typical meteorological weather data file for Montreal, Canada (CWEC) (Environment Canada, 2010) is utilised in this study to provide the associated climatic conditions (e.g. temperature, radiation level and etc.) for system components over the simulation periods.

3.2.2 Appliances, lighting, and plug loads

The employed non-HVAC load profile (e.g. appliances, lighting and etc.) in this study is based on measured data for non-HVAC electricity load from 22 Canadian houses ranging from 6 to 30 kWh usage per day (Johnson & Beausoleil-Morrison, 2017). The non-HVAC load profiles are categorized into three classes (low, average and high) based on daily electricity consumption. The 8 households with lower than 10.8 kWh daily electricity consumption are labelled as low demanded profile, while high load profile category consist of 6 households with daily electricity usage more than 17.8 kWh. The remaining load profiles including 8 households have daily electricity consumption between 10.8 and 17.8 kWh which are tagged as average. For more clarification the information related to the classified load profiles are presented in the Table 3.1.

Table 3.1 Load profiles classifications according to daily electricity consumption

Daily electricity consumption	**< 10.8 kWh**	**10.8 kWh < < 17.8 kWh**	**17.8 kWh <**
Number of households	8	8	6

In this study, one load profile in each category was selected following a methodology that imitates the selection of typical months for a Typical Meteorological Year: the cumulative distribution frequency (CDF) of all load profiles within one category were plotted, and the CDF that was the closest to the “average” of that class was selected. This allowed us to keep only 3 non-HVAC profiles, corresponding to high, average, and low usage categories. The selected electricity demands are added to the electrical load of the house but they are also used in the detailed

simulation, as most of these usages are converted to internal gains.

3.2.3 Domestic hot water

The domestic hot water (DHW) load is derived from eight series of measured data containing DHW draw profiles (Edwards et al., 2015). The water draw profiles were categorized in three groups based on daily usage (low, average and high). The daily usage thresholds as well as quantity corresponding to the profile's classification is shown in Table 3.2.

Table 3.2 DHW profiles classifications

Daily hot water consumption	$< \mathbf{130}\ (\frac{L}{D})$	$\mathbf{130}\ (\frac{L}{D}) << \mathbf{170}\ (\frac{L}{D})$	$\mathbf{170}\ (\frac{L}{D}) <$
Number of water draw profiles	3	3	2

The same method based on CDF comparison is used to select one profile in each category. The electricity usage associated with domestic hot water is obtained by running a separate 5-min simulation using a typical 270 L, 2-element water heater (Allard et al., 2011) and the 15-min integrated electrical load is then used in the main simulation.

3.2.4 Electric vehicle (EV)

According to the published vehicle survey by NRCan (*Canadian Vehicle Survey: Annual*, 2009), the average yearly mileage for the typical Canadian vehicle is around 15200 km. Depending the model and driving habits, the electric vehicle can travel between 4.8 and 6.4 *km* by using 1 *kwh* of electrical energy (Buchmann, 2011). The technical specifications corresponding to the various EV model's battery are provided in Table 3.3 (*Electric Vehicle (EV) – Battery University*).

Table 3.3 Electric vehicle battery capacity, range and energy consumption

EV make/Model	**Battery capacity** (kWh)	**Range** (km)	**Electricity/distance** (kWh/km)
BMW i3 (2019)	42	345	8.2
GM Spark	21	120	5.7
Fiat 500e	24	135	5.6
Honda Fit	20	112	5.6

Nissan Leaf	30	160	5.3
Mitsubishi MiEV	16	85	5.3
Ford Focus	23	110	4.8
Smart ED	16.5	90	5.5
Mercedes B	28	136	4.9
Tesla S 60	60	275	4.6
Tesla S 85	90	360	4.0
Tesla 3	75	496	6.6

The efficiency of EV supply equipment, varies between 74.2 and 90.6 % depending the charger level (e.g. level 1 and level 2) and ambient temperature (Sears et al., 2014). According to the provided data, the typical EV electricity consumption as well as considered assumptions are presented in Table 3.4.

Table 3.4 Electricity load corresponding to the typical EV

Electricity/distance	5.6 km/kWh
Charger efficiency	85 %
Yearly mileage	15200 km
Yearly Electricity consumption	3193 kWh

Therefore, the demanded electricity for charging one EV according to Canadian driving habits is estimated to be 8.75 kWh per day.

3.3 Electricity demand profile

The average daily electricity demand (non-HVAC, HVAC and DHW) for various end-user categories (low, average and high) ranges from 70 to 90 kWh/day. The non-HVAC load stands for the electricity used by appliances (frig, stove, TV and etc.), lighting and plug loads which is extracted from measured data (22 Canadian households). The HVAC load represent the consumed electricity for space heating and air conditioning which is estimated from the calibrated TRNSYS model of employed archetype. The DHW load is the amount of electricity utilised by the electric water heater to supply the measured water draw profile corresponding to the real consumption patterns (8 Canadian households). The detailed information related to the employed load profiles (low, average and high) including the yearly electricity used in each sector are shown in Table 3.5.

As expected, the HVAC consumption (mainly heating) increases for cases with a lower energy demand for appliances, as those appliances contribute to internal heat gains (the buildings and HVAC setpoint profiles are identical in all cases, so the contribution of internal gains is the only changing parameter in calculating the HVAC loads.

Table 3.5 Yearly load profile for various consumption patterns

Consumption pattern category	HVAC (kWh/year)	Non-HVAC (kWh/year)	DHW (kWh/year)	Total (kWh/year)
Low	19734	2642	3573	25948
Average	18281	4525	4808	27614
High	17041	6510	4948	28498

The average daily electricity demand corresponding to the three major part of load profile is demonstrated graphically in Figure 3.2.

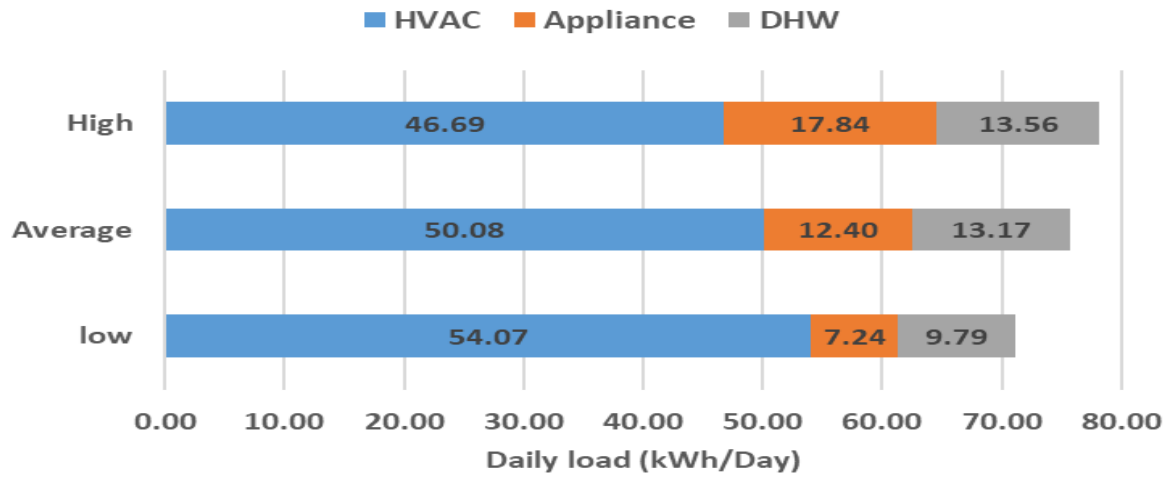

Figure 3.2 Average daily load profile for various consumption patterns

In order to investigate the variation of electricity demand corresponding to each end-use over the year, the average daily load profile associated with the moderate consumption pattern (average) for non-HVAC and HVAC +DHW load are presented separately within 15 minutes interval time in

Figure 3.3 and Figure 3.4 respectively. The corresponding profiles represent the average consumption class (with 27616 kWh/year).

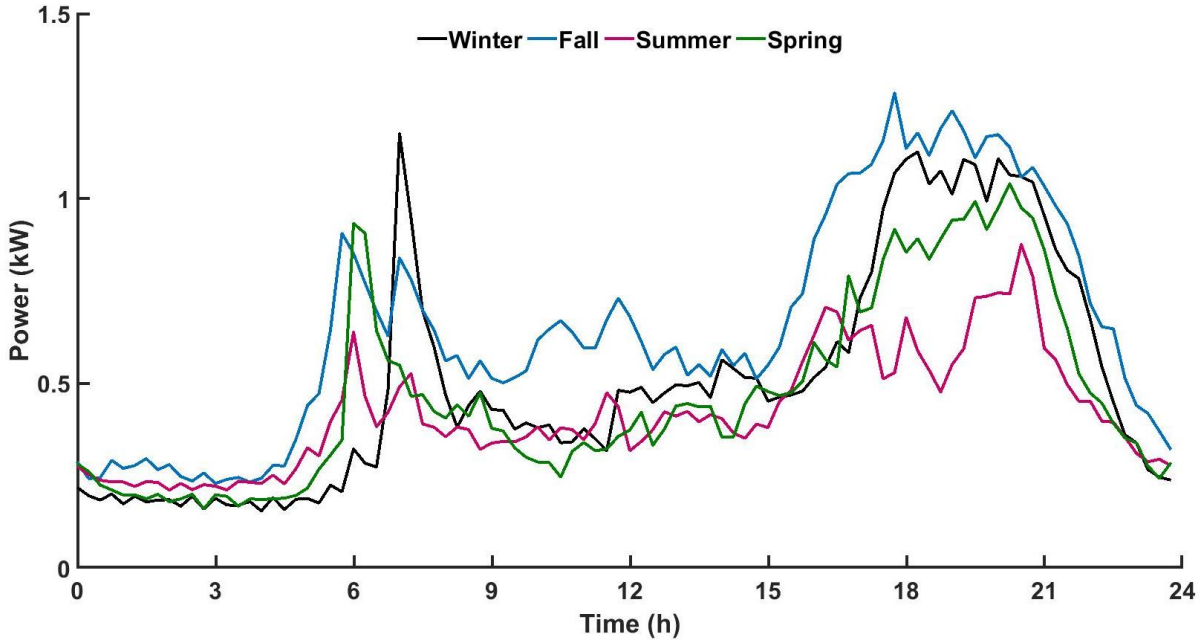

Figure 3.3 Daily average load profile for non-HVAC load (average electricity use)

The presented graph in Figure 3.3 shows the daily load average of electrical appliance (e.g. lighting, fridge and etc.) for average consumption pattern (12.4 kWh/day). As it is illustrated the trend of non-HVAC load profile approximately stays constant over the year since apart from lighting, the usage patterns for the other appliances-which depend on occupants' behaviour- remain unchanged. The presented graph in Figure 3.4 is related to the sum of daily average consumed energy by HVAC (50.08 kWh/day) and hot water system (13.7kWh/day) over the whole year.

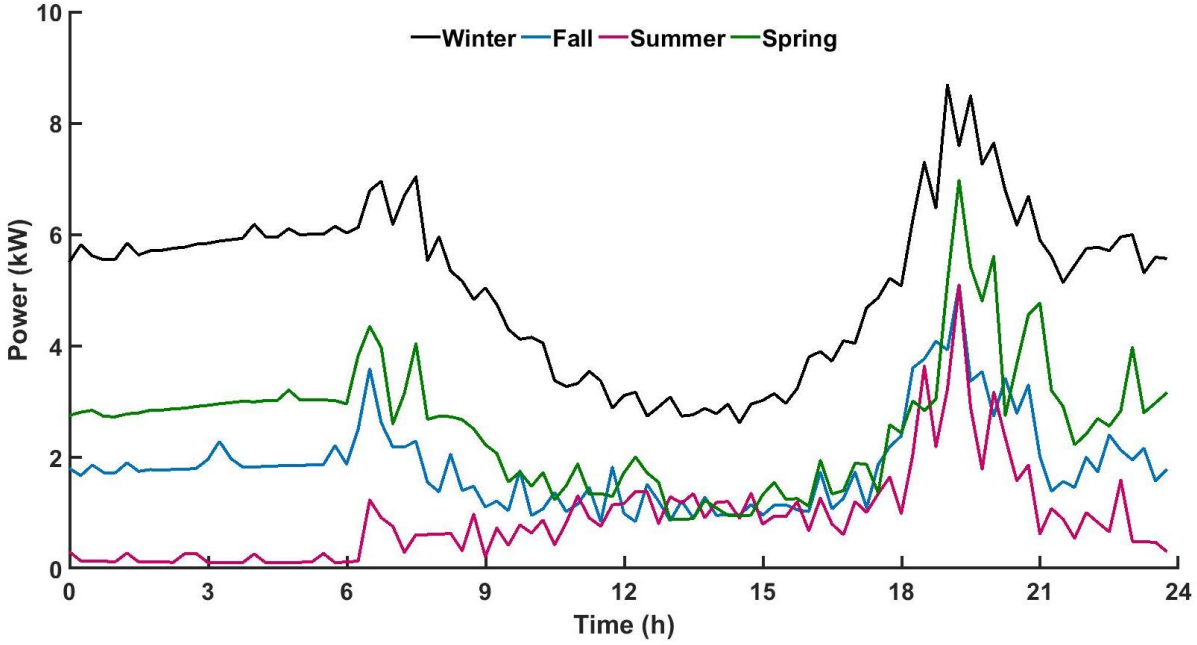

Figure 3.4 Daily average load profile for HVAC load (Including hot water)

As it is anticipated the HVAC load and hot water usage varies significantly over the year based on climatic conditions. The notable drop in ambient temperature over heating seasons results in higher electricity consumption by HVAC system.

The total electric demand is shown in Figure 3.5. The presented load profile is the average of total electricity demand within 15 minutes interval over the whole year.

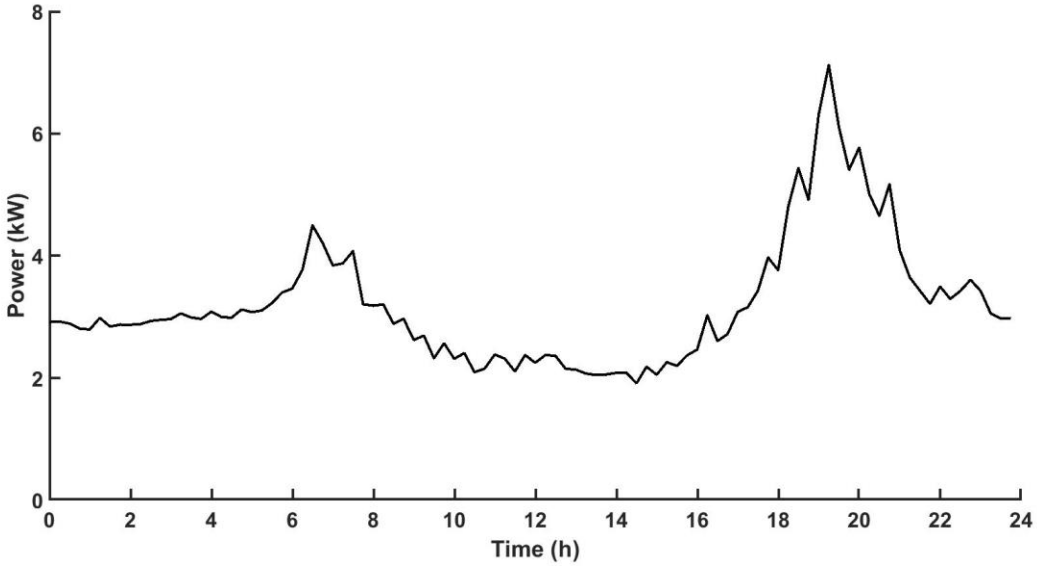

Figure 3.5 The average daily load electricity profile

The 15-min electrical demand is presented for selected winter and summer days (January 15th and July 15th) in Figure 3.6 and Figure 3.7. The top, middle and bottom plots show the low, average and high consumptions pattern categories respectively. These days were selected randomly, and are presented to illustrate the dynamic profile of the simulated demand. They are not necessarily "typical", hence they do not necessarily match the average shapes shown in the average profiles above.

The same zoning and comfort conditions are considered for all three archetypes regardless of electricity consumption patterns, therefore the HVAC loads associated with three classes (low, average and high) are similar in all cases (except for the influence of internal gains, as discussed before).

The presented load profiles in Figure 3.6 indicates the electricity consumption in January 15th when the HVAC load accounts for significant percentage of total demanded energy.

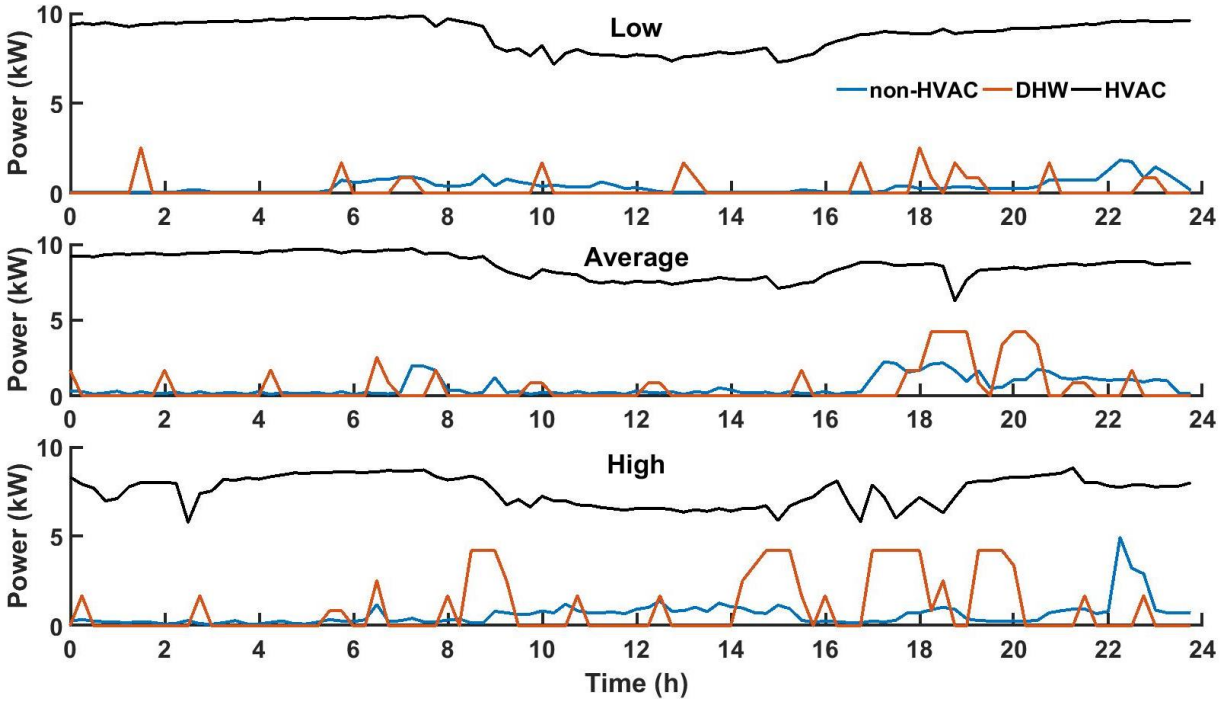

Figure 3.6 Load profiles - January 15th

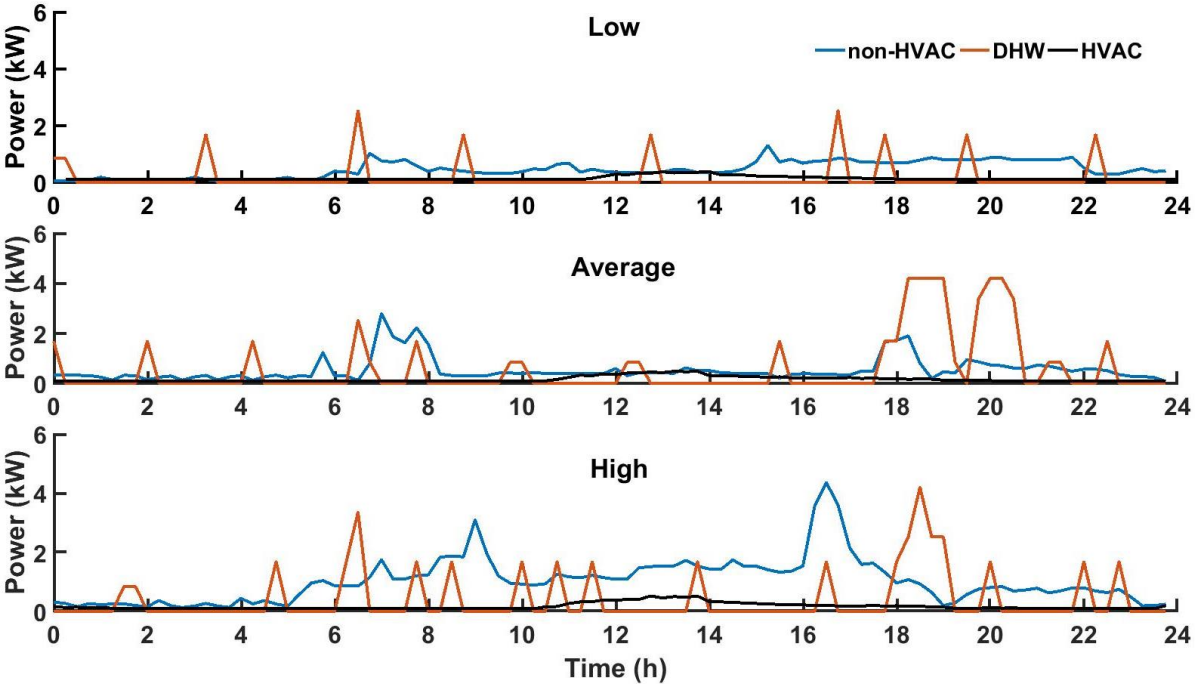

Figure 3.7 Load profiles - July 15th

Regardless of consumption pattern the electricity demand (for electrical appliances) in residential building usually remains negligible during 12-6 AM while the load profile experience significant rise over the morning and evening peak hours. The morning and evening peak periods usually occur between 6-9 AM and 16-20 PM respectively. The load over the remaining hours entirely depends on occupancy present/absence status and reflect the electricity consumption profile.

The nature of occupancy-driven electricity demand corresponding to hot water, appliances and plug loads, as well as ambient temperature fluctuations that affect the energy used by the HVAC system, the load profile pattern varies significantly from day to day. The plots in Figure 3.8 show the load profile from three electricity usage classes over a whole week (April 10th to 17th). As can be seen the load pattern changes over the consecutive days regarding the occupants' energy consumption schedules and habits.

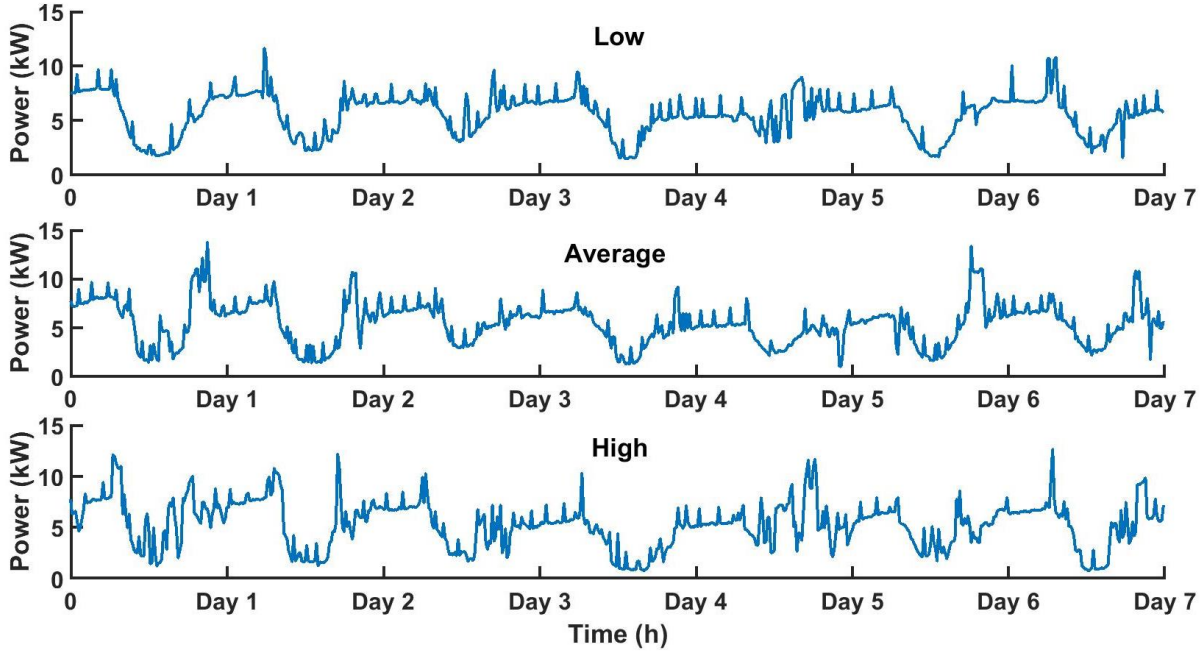

Figure 3.8 The load profiles corresponding to the typical week

3.4 PV+Battery system

A typical grid-connected solar system with battery backup is presented in Figure 3.9. It is comprised of PV panels, a bi-directional inverter, a charge controller, and battery bank components.

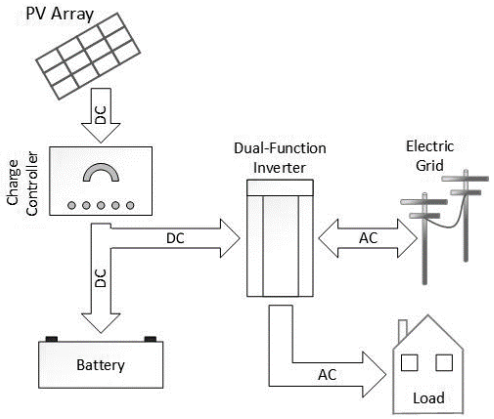

Figure 3.9 One-line diagram of grid-tied PV+Battery system

Appropriate sizing of the system components plays a major role in improving the system efficiency and performance while optimizing the system economically. The main parameters for sizing are the assumed/target daily critical load (i.e. the load that must be satisfied in case of power outage), battery depth of discharge, number of autonomy days for battery capacity, and the constrain of available roof area for panels installation. These parameters are discussed in the continuation of this subchapter.

3.4.1 Autonomy day

The number of autonomous days refers to the system potential to supply the demanded electricity in absence of grid or solar electricity.

3.4.2 Critical load

Batteries are an expensive part of the system, so they are typically not sized to meet the average or peak demand in case of power outage, but rather according to a "critical" load. For an average house, the essential items which are needed to be powered during the critical events include the refrigerator, some lights, microwave oven, cellphone battery charger, radio and security systems.

The critical load can also include minimum heating in selected rooms in winter. This requires meeting peak power demands from 3 to 5 kW (running) and up to 7 kW (starting) – the autonomy is not proportional to these peak demands, as the average critical load is supposed to be much lower, in the order of 400 W to 600 W (or approximately 10 to 15 kWh/day). This is confirmed by multiple commercially available solutions like E-Gear (*E-Gear™ BESS*,) and Tesla (*Powerwall | Tesla Canada*,) that provide 10 to 12 kWh storage for residential backup/stand-by battery banks. These banks are intended to provide one day of autonomy, which can be extended to 2 to several days in a PV+Battery system, depending on available solar energy.

3.4.3 Battery Depth of Discharge (DOD)

The battery DOD is the percentage of battery capacity that can be used during charge or discharge cycles. The predefined cycle depth is one of the primary parameters that affect the battery degradation rate and lifetime. A higher DOD range increases the autonomy, but reduces battery life. Results obtained by testing a battery in grid-connected applications indicated that increasing the DOD by 15% (from 0.6 to 0.75) reduce the battery effective life by more than 30 % (from 10 to 7 years) (Smith et al., 2017).

A economical trade-off must be reached between purchasing a larger battery and using it with a reduced DOD, versus purchasing a smaller battery and using it with its maximum DOD. According to the conducted research by NREL(Smith et al., 2017) on lithium ion battery life-cycle in grid-connected application, for prolonging the battery life up to 10 years ,the battery DOD should be set to 60 % of its nominal capacity. This decreases the storage cost over the energy system lifetime and minimize the battery operation and maintaining expenditures. In this study, the battery SOC thresholds are set between 0.3 and 0.9 over the whole simulation to maintain the cycle depth at 60 %.

3.4.4 PV panels and battery bank sizing

In order to investigate the impact of PV nominal power and battery storage capacity on potential energy flexibility of the hybrid solar system, nine system size configurations are defined through combining the three PV and battery size variants. The information regarding the employed sizes of PV and battery are shown in Table 3.6.

Table 3.6 PV nominal power and battery capacity

PV size (kW)	Battery capacity(kWh)
16.2	30.1
12.2	61.2
8.1	122.4

In the case of a PV system which cannot export to the grid, the amount of curtailed PV energy is a simple and practical indicator of the performance of a PV+Battery system. This indicator represents the amount of energy that would have been available at the output of the PV panels but was curtailed (by disconnecting the PV panels or rejecting part of their power output) because the battery was full and the load was insufficient.

The results obtained with the average occupant-driven load profiles are shown in Table 3.7.

Table 3.7 Curtailed solar electricity data

PV power (kW) / Battery capacity (kWh)	8.1 kW	12.2 kW	16.2 kW
0 kWh	5208 kWh	9010 kWh	13837 kWh
30 kWh	225 kWh	1868 kWh	5141 kWh
60 kWh	36 kWh	1503 kWh	4506 kWh

Due to the mismatch between the generated solar electricity and load profile, installing the PV panels without battery storage, results in considerable amount of dumped energy. The simulation results indicate 48 % of generated solar electricity is curtailed for on-site solar system with 8.1 kW PV panels where this ratio is 58 % and 64 % for 12.2 kW and 16.2 kW PV panels respectively

Adding the battery bank with 30 kWh of storage capacity to the PV systems enables storage of excess generated solar electricity to accommodate the demanded load, out of solar window period to reduce the curtailed energy.

As the data shows, contrary to the notable drop on curtailed energy when the storage capacity rises to 30 kWh, doubling the size of battery bank to 60 kWh shows diminishing returns for all PV sizes.

This can be explained by the fact that apart from storage capacity, the daily load also affects the amount of curtailed energy. In cold climates, this daily energy load (dominated by heating) decreases during the sunniest months (May-August), which results in energy curtailment during these months.

For better interpretation, the monthly grid-imported electricity as well as curtailed energy, corresponding to the solar power system of 16.2 kW PV (the largest PV size) with 30 kWh and 60 kWh battery is shown in Table 3.9 and Table 3.9 respectively.

Table 3.8 Monthly grid usage and curtailed energy for PV (16.2 kW) + Battery (30 kWh)

Month	**Jan**	**Feb**	**Mar**	**Apr**	**May**	**Jun**	**July**	**Aug**	**Sep**	**Oct**	**Nov**	**Dec**
Curtailed (kWh)	0	0	81	443	999	1168	1376	626	401	46	0	0
From Grid (kWh)	4126	3314	2348	1323	44	16	2	71	115	999	2554	3883

As the results indicate, 80 % of curtailed energy is related to the period between May to August where the total grid imported electricity corresponding to this period is 133 kWh. Since the estimated values, show the reasonable saturation level for the battery size to accommodate the demanded load, increasing storage capacity (from 30 kWh) will not lead to a notable rise on harvesting the dumped energy.

Based on the presented data in Table 3.9, doubling the battery capacity to 60 kWh results in just 11 % reduction on the total curtailed energy.

Table 3.9 Monthly grid usage and curtailed energy for PV (16.2 kW) + Battery (60 kWh)

Month	Jan	Feb	Mar	Apr	May	Jun	July	Aug	Sep	Oct	Nov	Dec
Curtailed (kWh)	0	0	0	45	982	1185	1412	572	309	0	0	0
From Grid (kWh)	4093	3301	2264	1033	0	0	0	0	0	942	2550	3880

3.5 Chapter summary

This chapter describes the employed residential archetype in our simulation studies. A typical North-American wood-structure single-family house is simulated using a validated model. A simple HVAC system is modelled (electric baseboard heating, typical central air-conditioning, electrical hot water tank). Occupant-driven load profiles for domestic hot water and non-HVAC loads (lighting, appliances, plug loads) are taken from Canadian empirical studies in the literature. A preliminary PV+Battery sizing study shows that increasing the battery size beyond 30 kWh for the simulated buildings shows diminishing returns, for all PV peak power sizes.

CHAPTER 4 ENERGY FLEXIBILITY

This chapter analyses the benefits of PV+Battery systems in the residential sector in terms of energy flexibility. The employed key performance indices (KPIs) in the flexibility assessments are defined and quantified for the developed archetype (introduced in chapter 3) representative of Canadian residential building and electricity consumption pattern. The flexibility analyses accommodate both utilities and end-users' sides through grid interactive and yearly KPIs (e.g. self-generation and self-consumption) respectively.

This study investigates the impact of two key design parameters of a PV+Battery system – PV peak power and battery storage capacity – on yearly KPIs, using a simple control strategy commonly implemented by commercially available inverters ("grid support", detailed below).

In the second part, dynamic flexibility KPIs are assessed for one PV system configuration and two basic control strategies ("grid support" and "UPS", explained below). In this study, the desired load is assumed to remain constant, i.e. the occupants' comfort is not affected by flexibility events (whether the thermal comfort, the hot water temperature, or the ability to use any appliance at a given time).

4.1 PV+Battery integration to the electricity grid – the role of flexibility

4.1.1 The challenges and opportunities (utility perspective)

Financial incentives, a notable drop in market prices of photovoltaic (PV) panels and global concern for environmental issues over the last decade encouraged the electricity consumers to install and operate rooftop solar power systems. Due to generous subsidies and substantial decrease of solar power cost, PV panels are close to reach grid parity over the world (i.e. the cost of solar electricity becomes close to utility rates) (Branker et al., 2011). However, increasing the share of solar energy in producing electricity without appropriate load management has major drawbacks for power utilities: over-generation during sunny days, and a high power ramp rate before evening peak hours, which increases the risk of failure in power plant facilities (Denholm et al., 2013). Adding well sized and well managed batteries to PV systems could allow to reduce these negative

impacts, and even to improve the overall grid performance, in addition to providing distributed backup power to end-users.

Demand side management (DSM) in smart grid includes balancing the supplied electricity and load, which is more effective through appropriate interaction of the grid and buildings. Croce et al., (2017) discussed centralized management as a solution for smart grid which is equipped with local storage devices.

O'Connell & Riverso, (2016) evaluate energy flexibility provided by the integration of solar power system with batteries over different conditions (e.g. heating season, on/off peak hours and etc.) and energy control approaches. They confirm that PV+Battery systems have the capability to improve grid stability through responding grid signals for increasing/decreasing the load.

4.1.2 Energy flexibility associated with PV+Battery

According to the proposed definition by the International Energy Agency's (IEA) Energy in Buildings and Communities (EBC) Annex 67, energy flexibility is reshaping the load profile through distributed generation, storage and demand-side responses in reaction to the grid request while providing secure and reliable supply with least impact on occupants (Jensen, Marszal-Pomianowska, et al., 2017).

The energy flexibility concept can be used to assess the performance of different systems and control strategies to implement demand-side management for the smart grid. Integrating batteries within solar photovoltaic (PV) systems enables to control the power flow dispatch (based on supplied electricity and required load). In addition to modifying the electrical load profile (e.g. peak shaving, load shifting), battery storage units add resiliency to system in the case of power failures.

Due to a lack of a uniform methodology for assessing the energy flexibility, performance is often assessed on a case-by-case basis (O'Connell & Riverso, 2016). The energy flexibility KPIs should be selected with reference to the objective and proposed sources of flexibility. Clauß et al., (2017) conducted comprehensive review on previous research in the area of flexibility and provided complete list of existing KPIs in a broad range of applications (e.g. on-site generation and storage).

For instance self-generation and self-consumption appropriately identify the range of flexibility in the contexts of supplying the electricity demand through the renewable energy power system (Clauß et al., 2017). The aforementioned KPIs also play crucial role in the economic assessment of adding roof-top solar systems for the site owners through quantifying the reduction in the grid usage.

Apart from commonly used KPIs such as self-generation and self-consumption as the label of installed PV system characteristics, it is also necessary to investigate dynamic performance indicators for complementing the flexibility assessment. These flexibility indicators quantify the building's dynamic interaction with the electricity grid. As an example the forced flexibility could be defined as photovoltaic (PV) system capability to increase (positive or upward flexibility) or decrease (negative or downward flexibility) the amount of imported electricity from the grid over the predefined events (Clauß et al., 2017).

4.2 Methodology

4.2.1 Energy flexibility scenarios

The study considers two opposite flexibility events: upward (or positive) and downward (or negative). During **upward flexibility**, the controller reduces on-site generation (by dumping PV power) and forces the battery to store energy through grid charging. It generally takes place over the solar window when the produced solar electricity is beyond the demand.

During **downward flexibility,** the system uses the stored energy to reduce the amount of energy imported from the grid. This solution is usually applied to avoid high ramp rate over the peak hours. Currently the time of use scheme encourages the end-users to reduce their consumption on high demand hours. The example of flexible energy demand for downward flexibility event is demonstrated in Figure 4.1.

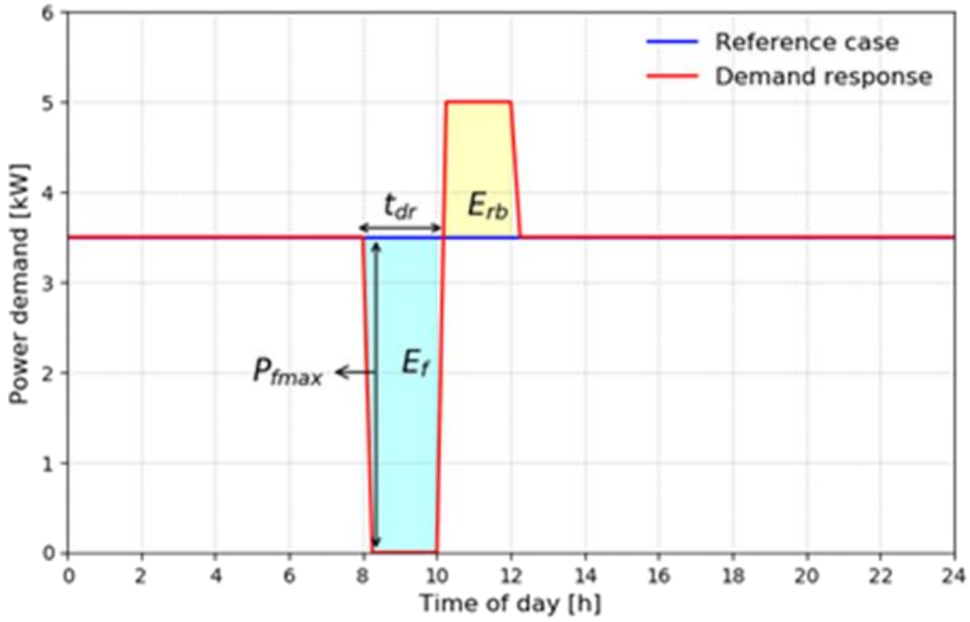

Figure 4.1: Flexible energy demand of building (downward flexibility)

4.2.1 Control strategies

The employed load management approach has a notable impact on the provided energy flexibility offered by hybrid solar power system. The implemented rule-based control methods in this study represent two extreme operation modes typically available in commercial grid-tied inverters.

- Grid support (PV priority)

In the grid-support mode, the system supplies the required load by prioritizing the electricity generation sources as the following order: 1st. PV panels, 2nd. Battery and 3rd Grid. This reduces the dependency on the grid, but it will not necessarily minimize the electricity bill since discharging the battery during off or mid peak hours is not always economically beneficial.

- Uninterrupted power system (UPS)

In UPS mode the primary task is to keep the battery fully charged in order to back up the grid for supplying the load over interruption or instability. Utilizing this mode of operation let the households have access the electricity over blackout as well as supporting the sensitive AC loads.

In this mode, since the battery bank is always fully charged, the surplus electricity is either dumped or exported to the grid. Therefore, the system is unable to store the extra-generated electricity during the day to meet the load in absence of solar energy. It is interesting to note that, since the battery is not used under normal operation, this references scenario is very close to what a PV system without battery would provide.

4.3 Key Performance Indices (KPIs)

The considered KPIs for evaluating the provided energy flexibility by the PV+Battery are briefly explained in this section.

4.3.1 Yearly KPIs (Salom et al., 2014)

- The **self-generation** (or load cover factor) estimates the share of demand met by on-site generation through various generator types (e.g. PV panels).

$$\boldsymbol{Self-generation} = \frac{\int_0^T \min[g(t) - S(t) - \zeta(t), l(t)]\, dt}{\int_0^T l(t)\, dt} \qquad (4.1)$$

Whereby the g(t) is the solar panels power at time t and s(t) represent the battery power balance. $\zeta(t)$ is corresponding to the losses and l(t) indicates the load power.

- The **self-consumption** (or supply cover factor) displays the proportion of on-site generation which is utilised by the end-user. In fact, this indicator quantifies the system potential to store and use the surplus generation.

$$\boldsymbol{Self-consumption} = \frac{\int_0^T \min[g(t) - S(t) - \zeta(t), l(t)]\, dt}{\int_0^T g(t) dt} \qquad (4.2)$$

4.3.2 Grid interaction (Dynamic) KPIs (Jensen, Marszal-Pomianowska, et al., 2017)

The system capacity to modify the electricity demand upon receiving the grid signal needs to be evaluated for both upward and downward flexibility scenarios. Figure 4.1 provides a graphical

explanation of grid interactive KPIs for downward energy flexibility corresponding the two hours event (occurs at 8:00 AM).

- The **flexible energy** ($\boldsymbol{E_f}$) reflects the amount of load that can be shifted (shed or added) through on-site generation and (de)store energy. This indicator measures the system flexibility in interaction with grid.

$$\boldsymbol{E_f} = \int_0^{t_{dr}} (Q_{dr} - Q_{ref})dt \qquad (4.3)$$

Here Q_{dr} and Q_{ref} show the corresponding power consumptions at reference and demand response scenario respectively. This KPI evaluates the system interaction with the grid during a particular event; however, it does not assess the impacts after the event, which is the focus of the next KPI.

- The **rebound energy** ($\boldsymbol{E_{rb}}$) characterizes the change in the energy demand after the event. The battery state of charge will be affected by the system behaviour during the flexibility event, and this will have an impact on the system behaviour down the line, sometimes several hours after the event has taken place. In this study t_∞ is approximated by the end of a yearly simulation.

$$\boldsymbol{E_{rb}} = \int_{t_{dr}}^{t_\infty} (Q_{dr} - Q_{ref})dt \qquad (4.4)$$

4.4 Case study

The specifications corresponding the residential archetype which is selected for implanting the flexibility analyse is presented in Chapter 3.

In order to study the impact of PV size and storage capacity on yearly energy flexibility KPIs, nine sizing variants were defined by combining 3 PV sizes and 3 battery sizes, as illustrated in Table 4.1.

Table 4.1 PV nominal powers and battery capacities

PV size (kW)	Battery capacity(kWh)
16.2	30
12.2	60
8.1	120

For the grid-interactive KPIs, one PV and battery size are selected to investigate the impact of load-management scenarios. The selected PV array nominal power is 8.1 kW (three 270 W panels are wired in series at each string) and the storage capacity of the battery bank is $30\,kWh$ ($48\,V - 600\,Ah$). Eight Lithium-ion ($LiFePO_4$) battery (model-CLI300-12LT), 12V 300Ah, are connected in two paralleled groups of 4 modules in series mode.

4.5 Simulation setup

The simulation uses a detailed TRNSYS model of the house, the grid-tied solar system (composed of PV panels, charge controller, inverter and battery bank), as well as an all-electric HVAC system (Baseboard heating and conventional Air conditioner).

4.5.1 Controller

The control strategy which is employed in the TRNSYS model consists of two control layers: supervisory and real time. The supervisory layer implements the considered mode of operation by sending control commands to the inverter. Additionally, during the event it applies the associated rule-based scenario to govern energy dispatch to/from system components.

The real-time layer utilizes the equations and equalities to address the system operation constraints such as battery SOC set-points, voltage thresholds and the limits for the main components power rate.

- $P_{Loads}(t) = P_{grid}(t) + P_{battery}(t) + P_{PV}(t)$
- $SOC_{min} < SOC(t) < SOC_{max}$

- $P_{battery}^{min} < P_{battery}(t) < P_{battery}^{max}$
- $P_{grid}(t) < P_{grid}^{max}$

The battery SOC remains constant at 0.9 when the system operates in UPS mode while the minimum and maximum SOCs for grid support mode are 0.3 and 0.9 respectively.

4.5.2 Implementation of flexibility event

As mentioned above, when the inverter operates in grid-support mode the amount of electricity usage from the grid is minimized, so there is no potential for downward flexibility. During an upward flexibility event, the controller applies the following rules to minimize generation and maximize the delivered energy from the grid. The inverter shuts down the PV system and forces the battery to stop discharging in order to employ the grid for supplying the required load and charge the battery with maximum allowed current.

When the inverter works in UPS mode, the system has the capability to shift energy during upward and downward flexibility events. For the upward flexibility, the controller shuts down the PV and meets the load with the grid. Downward flexibility is obtained by readjusting the pre-set low set point of battery SOC to meet the load by discharging the battery. To put it simply, the controller switches to the grid-support mode and use the battery potential to offset the load that is not met by the solar panels.

4.5.3 Running the simulation setup

For the assessment of yearly KPIs with different system sizing configurations, results are simply obtained by running 27 independent simulations (9 system designs combined with 3 usage classes).

For the assessment of dynamic KPIs, only one load profile is kept, and an independent simulation is run for each one-hour flexibility event. So for example the first simulation will have an upward flexibility event from 0 AM to 1 AM on January 1st, the second simulation will have an event from 1 AM to 2 AM, etc. This results in 8760 simulations for upward flexibility events and 8760 simulations for downward flexibility. Note that the calculation time is limited for this study, so no attempt was made to reduce it. Under tighter constraints, it would be possible to fix a given limit

to assess the rebound effect (t_∞ above) and simulate several flexibility events in the same simulation. For example, if a 1-week period is assumed to be long enough for the impact of the flexibility event to be "forgotten", each simulation could include one event per week and the total number of simulations to run would be reduced to 168. MATLAB scripts were used to generate the input files, run TRNSYS simulations in batch mode, read and analyse the results.

4.6 Results

4.6.1 Yearly KPIs

Figure 4.2 shows the self-generation for a whole year for three different load profiles associated with low, average, and high electricity consumption patterns. The results are related to the "grid-support" mode of operation where the battery stores the surplus generation to supply the load over peak hours.

Points with a zero value on the x-axis represent conventional grid-tied photovoltaic systems without batteries. As mentioned above, the performance obtained is the same as a PV+Battery running in UPS mode, as in that case the battery is maintained fully charged under normal operation and not used to compensate for the solar generation variations.

Adding a battery to a PV system allows to almost double the self-generation and more than double the self-consumption, and there appears to be a saturation of the battery benefits above a value of 4 kWh/kW_p for the selected load profiles.

Figure 2 shows that the installed PV capacity has a large impact on self-generation, which was expected. A more surprising result is that self-generation is also strongly affected by the total electrical load, with higher loads corresponding to higher self-generation. For the same PV+BATTERY configuration, the solar fraction (the potential share of on-site generation to cover the load) will decrease if the building load increases, but in all cases (with the selected assumptions and configurations) the self-generation will increase. This KPI does not "credit" the system for any exported energy, and increasing the building load will shift some of that exported energy towards directly used energy, therefore improving the self-generation.

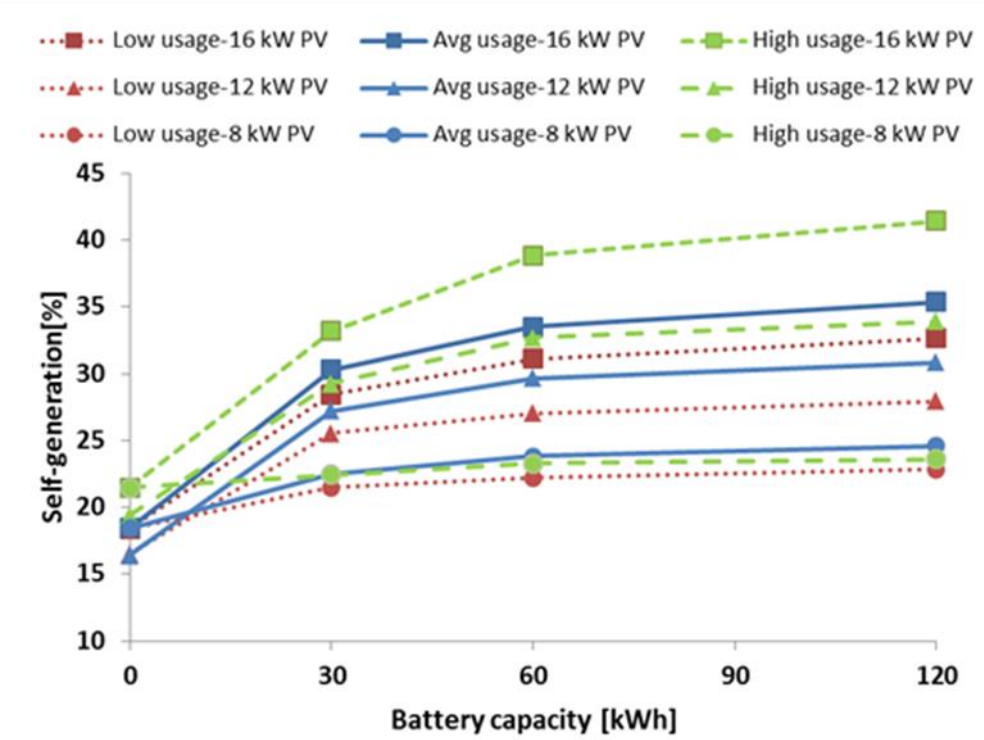

Figure 4.2 Self-generation versus battery capacity

Figure 4.3 shows the results obtained for self-consumption. There is a direct relationship between the amount of exported (or dumped) energy and self-consumption, so adding a battery has a large impact on that KPI. The saturation effect observed for self-generation is even more present, showing that the sizing of PV+Battery systems will have a large impact on their energy flexibility, without necessarily requiring much larger investment costs than conventional (battery-less) PV systems.

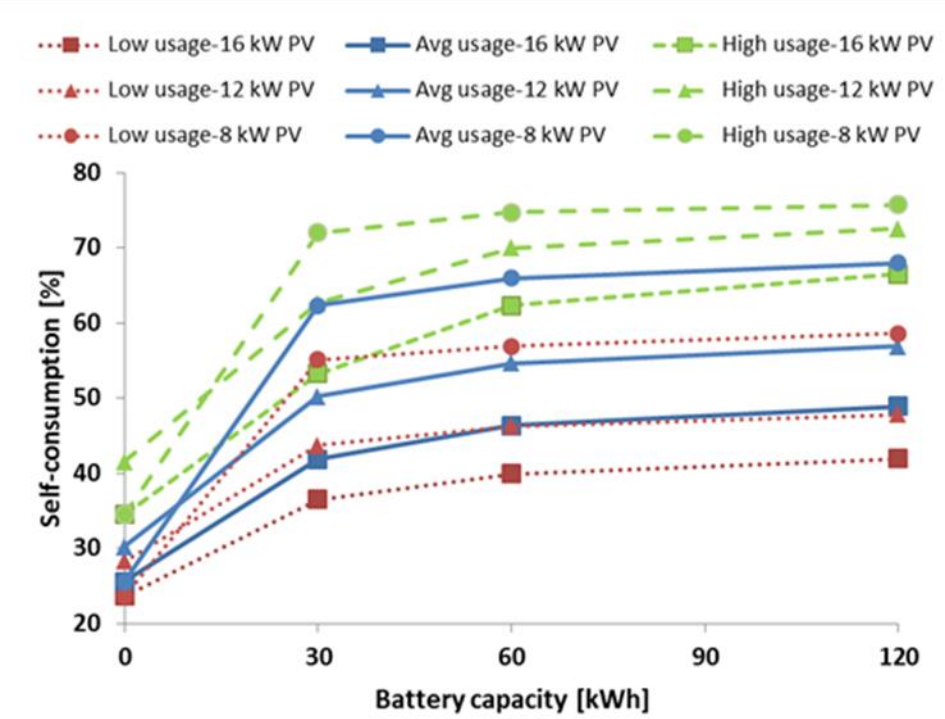

Figure 4.3 Self-consumption versus battery capacity

A possible explanation for the relatively quick saturation of the two KPIs with increasing battery sizes is that the system performance is largely influenced by two extreme periods. In winter, an all-electric building load will be very high due to space heating, and solar generation will be low. So, the need for storage is relatively small, only representing a few extremely sunny days. In summer, on the other hand, the building load will typically be much lower, and the solar generation will be much higher. Adding a relatively small battery capacity allows dealing with the winter period, but not with the summer period. And the results seem to show that the investigated battery sizes (up to 15 kWh/kWp) do not result in significant improvements over much lower battery sizes – improving the self-consumption significantly would require a longer-term energy storage (closer to seasonal storage than to the type of short-term storage investigated in this study).

4.6.2 Dynamic KPIs

The KPIs presented above show a picture of the yearly system performance and are very relevant to end-users. This section will address dynamic KPIs which may be better suited to the priorities of utilities that need to balance demand and supply at a shorter time scale, typically a few hours.

All the results in this section were obtained for the system configuration with a 12 kW PV array and 120 kWh of battery capacity, using the "average" non-HVAC load profiles.

Figure 4 and 5 show how the system reacts to an upward flexibility event (i.e. an event when the grid requests that the building use more energy) in grid-support mode. The event occurs at 12:00 PM and lasts for one hour. Figure 5 shows that the inverter starts to charge the battery by using the grid, so that the battery SOC rises up to 0.35.

The system also shuts down the PV panels, so that the grid is used to supply the entire building load. The left graph (Figure 4) shows the large impact on grid import during the flexibility event.

After the event at 1:00 PM the inverter reverts to normal operation, using the battery to cover the load. A rebound effect can be observed between 1:00 PM and 4:45 PM, when the energy stored in the battery is used. The rebound effect ends when the battery SOC reaches the same value as for the reference scenario. The situation in Figure 4.4 and Figure 4.5 show a favourable case, since the battery SOC at the start of the flexibility event is low.

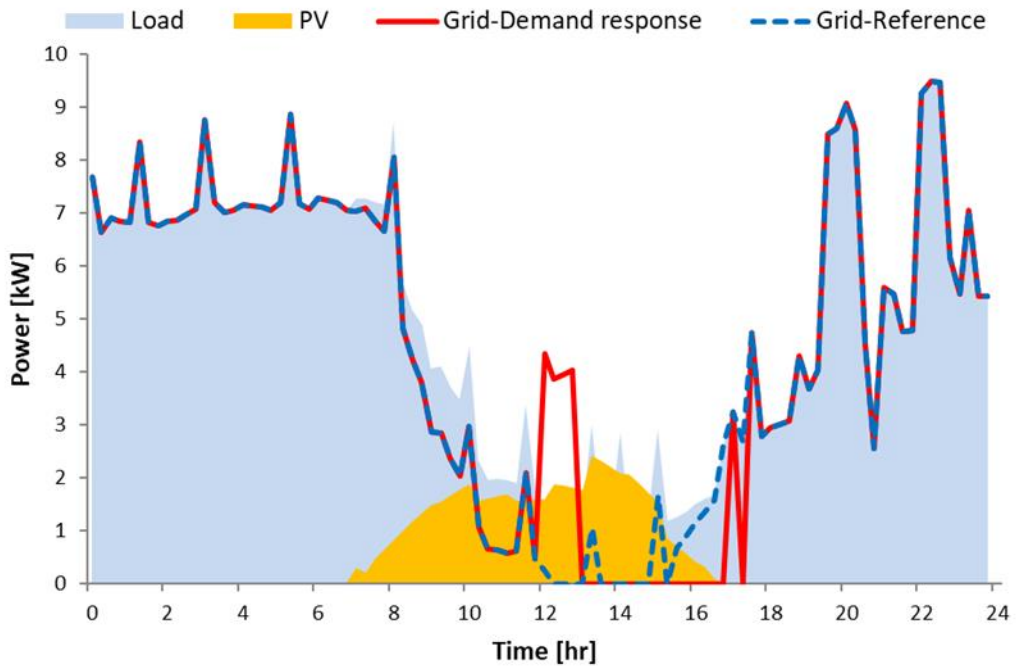

Figure 4.4 One-hour flexibility event for upward energy flexibility scenario (grid support mode)

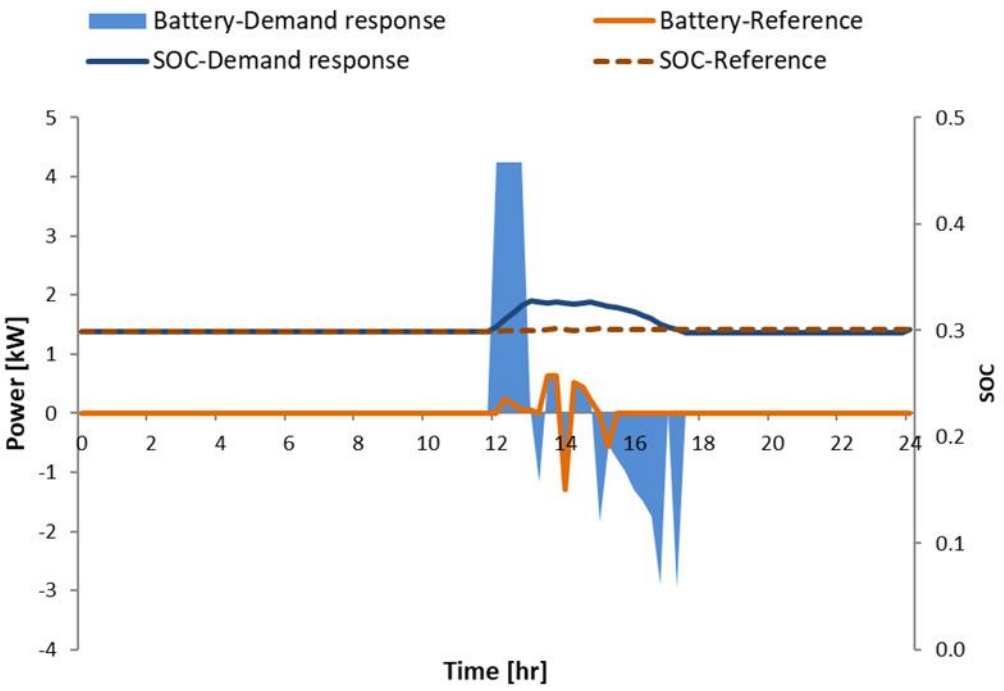

Figure 4.5 One-hour flexibility event for upward energy flexibility scenario (grid support mode)

Figure 4.6 shows a downward flexibility event when the UPS mode of operation is selected. The event occurs at 9:00 AM and the controller acts to discharge the battery for supplying the load.

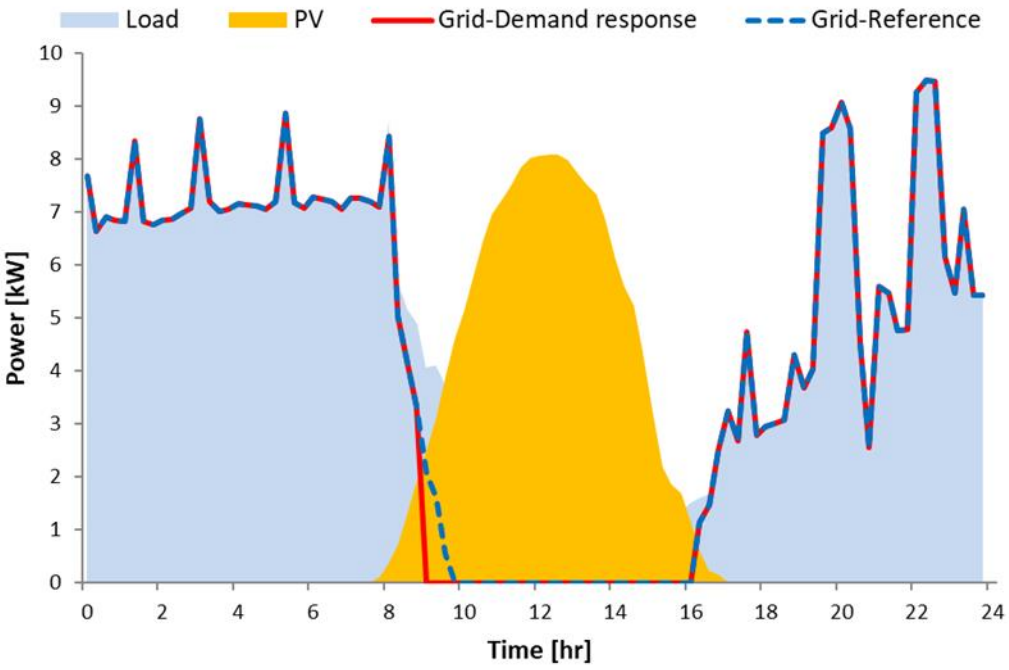

Figure 4.6 One-hour flexibility event for downward energy flexibility scenario (UPS mode)

Figure 4.7 indicates that while the discharging phase lasts for the whole period of the event, the discharge rate has been reduced gradually. This reduction is caused by solar electricity generation over the second half of the event. At the end of the event he battery charge level (SOC) has dropped to 0.87.

After the flexibility event (at 10 AM), the battery will be recharged to its setpoint in UPS mode (0.9 here), in this case using PV generation. There is no rebound effect since the amount exported to or imported from the grid is not affected. The controller could be set to allow battery charging from the grid in UPS mode, in which case a rebound effect would be possible (although not on the day represented here). In UPS mode, the maximum downward energy flexibility will be achievable at times when the whole load is supplied through the grid.

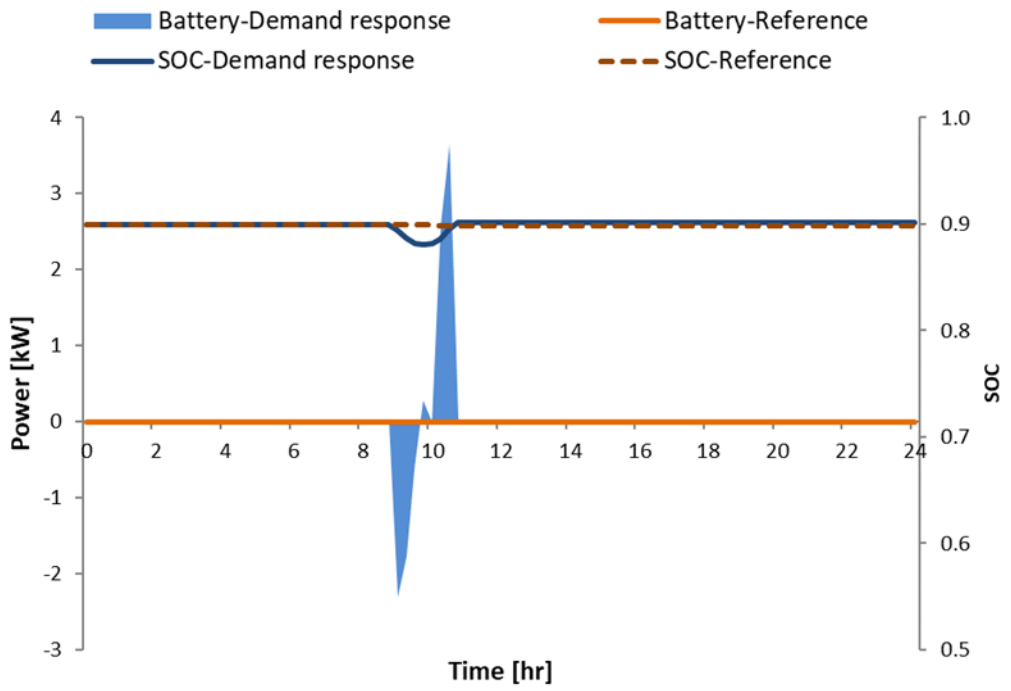

Figure 4.7 One-hour flexibility event for downward energy flexibility scenario (UPS mode)

The energy flexibility varies daily and hourly throughout the year. This KPI depends on various parameters including: on-site generation, demand, battery SOC and energy control approach. Figure 4.6 displays how this KPI varies depending on the start time of the event for the PV grid support mode. The PV power, load and battery SOC (at the start of the event) are presented in the same graph. On that graph, the blue line represents the flexibility KPI E_f defined above for a 1-h event that would occur at the given time. Since the event duration is 1 hour, E_f expressed in kWh has the same numerical value as the average power in kW.

Figure 4.8 shows hourly results for a typical day during the heating season. In the absence of PV power (in the period between 12:00 AM and 10:00 PM) the available upward flexibility is equal to the maximum battery charging power. It should be noted that over the mentioned period the whole demand is supplied through the grid for both reference and demand response scenario. Later in the day, when PV panels contribute to the load during the solar window, the upward flexibility increases as it represents the sum of the load that was covered by PV and the maximum battery charging power.

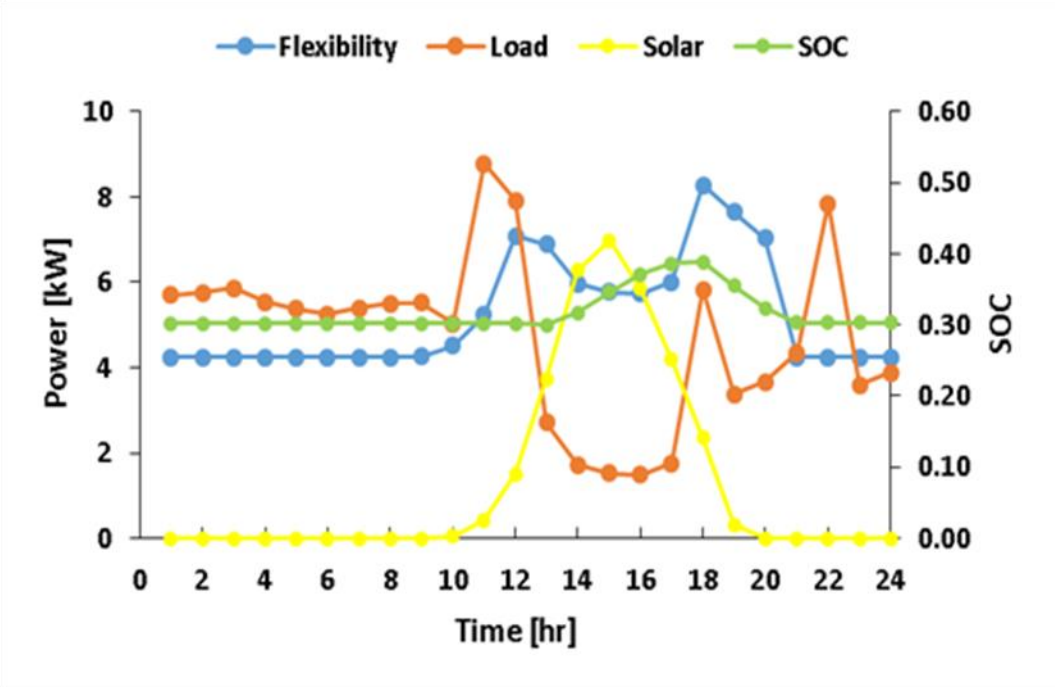

Figure 4.8 Hourly flexibility power (upward flexibility-grid support mode-heating season)

The maximum battery charging power (about 4 kW here) represents the minimum achievable flexibility during the day, as long as the maximum battery SOC is not reached.

Figure 4.9 presents the same results for a very sunny mid-season day. The low demand and high on-site generation keep the charge level of battery around the high limit over the major part of the day. Between 3:00 PM and 9:00 PM, the battery is full and the KPI is equal to the amount of the load that was covered by solar electricity. Consequently, the energy flexibility is equal to the portion of the demand, which is supplied by the battery and PV.

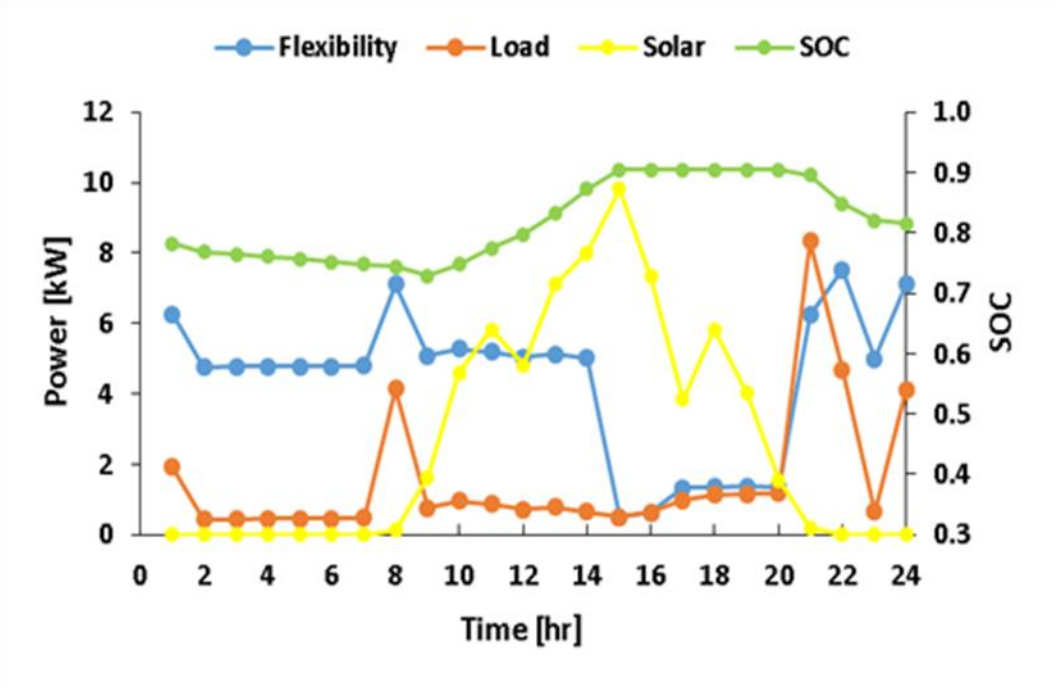

Figure 4.9 Hourly flexible power (upward flexibility-grid support mode-sunny day)

For the UPS mode of operation, the upward energy flexibility is the same as for the grid-support operation when the battery is full: it is equal to the part of the load that is covered by PV, and it is always zero at night.

Downward flexibility is mainly affected by the maximum battery discharge power. Figure 10 displays how downward energy flexibility fluctuates hourly over a typical heating season day.

Hereby the SOC indicates the battery charge level at the end of the event. As it is illustrated in Figure 4.10, when the PV power is negligible the downward energy flexibility is equal to the load as long as it is smaller than the maximum discharge rate.

For instance, at 10:00 PM the discharged energy is not adequate to cover the whole load which results in a lower KPI compared to the demand. When part of the load is covered by the PV and/or the battery, the available downward flexibility is equal to the share of the load which is still covered by the grid. Since we do not consider potential exports as "flexibility", it is 0 the whole load is already met by the sun and or the battery.

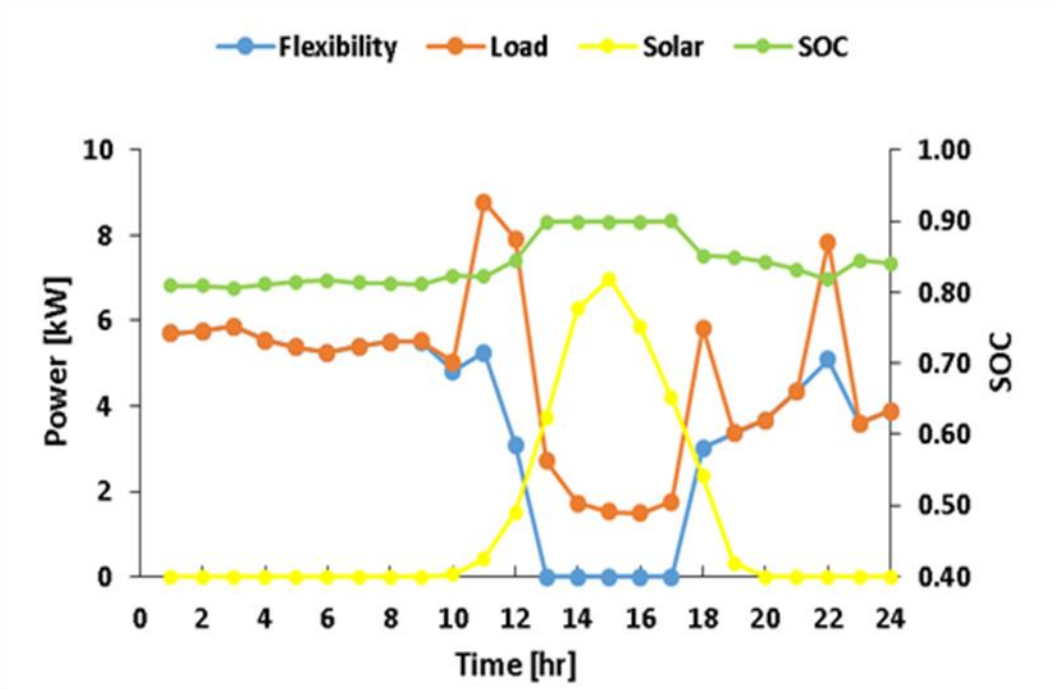

Figure 4.10 Hourly flexible power (downward flexibility-UPS mode)

Figure 4.11, Figure 4.12, and Figure 4.13 represent the same results as the figures above but combining all the days and event times for the entire year. Each data point in these figures depicts the value of E_f as a result of one simulation with one flexibility event taking place at the given time on one particular day. The colour of each point denotes the month in which that day is falling. The blue line represents the median value of the KPI, while the boxes represent the 25th and 75th percentiles.

Figure 4.11 shows that the available energy flexibility E_f ranges from 0 to slightly over 12 kWh, the lower values taking place during the day. The minimum flexibility at night is at 4 kWh except when the battery is full, as discussed above. The median value is relatively constant during the day, with higher values immediately after the solar day, when the battery is more likely to be charged and the load increases with late PM / early evening activities.

During the night time the higher E_f occurred over the months with higher solar radiation (e.g. June and July), when the surplus of generation during the day can be used at night to meet the load.

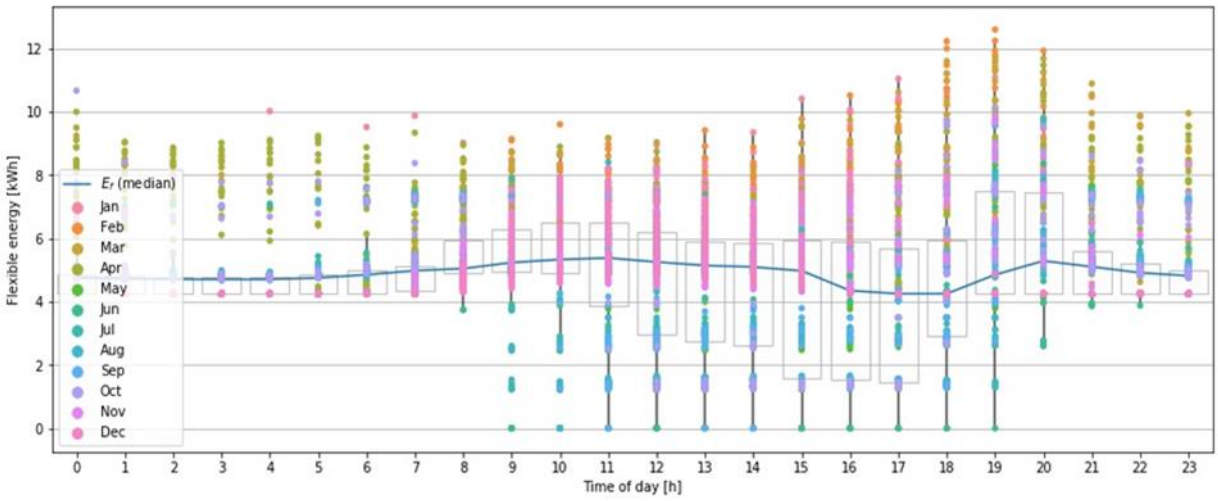

Figure 4.11 Upward flexible energy-grid support mode

Over the day time, usually on-site generation supplies the load and the system operates in semi-standalone mode. In these conditions, upward flexibility is gained by shutting down the PV panels and supplying the load with the grid, so that the shape of the flexibility matches the shape of the building load, and is higher during the winter months (e.g. December and January).

Figure 4.12 and Figure 4.13 display the upward and downward energy flexibility for UPS mode respectively in a same format as shown in Figure 4.11.

As it is expected and explained previously in both upward and downward energy flexibility, the correspondent KPI depends on the share of on-site generation in supplying the load. The upward flexibility is a direct representation of PV generation that can be shut down, and the downward flexibility represents the share of the load that is not covered by PV, up to the maximum battery discharge current (about 8 kW here).

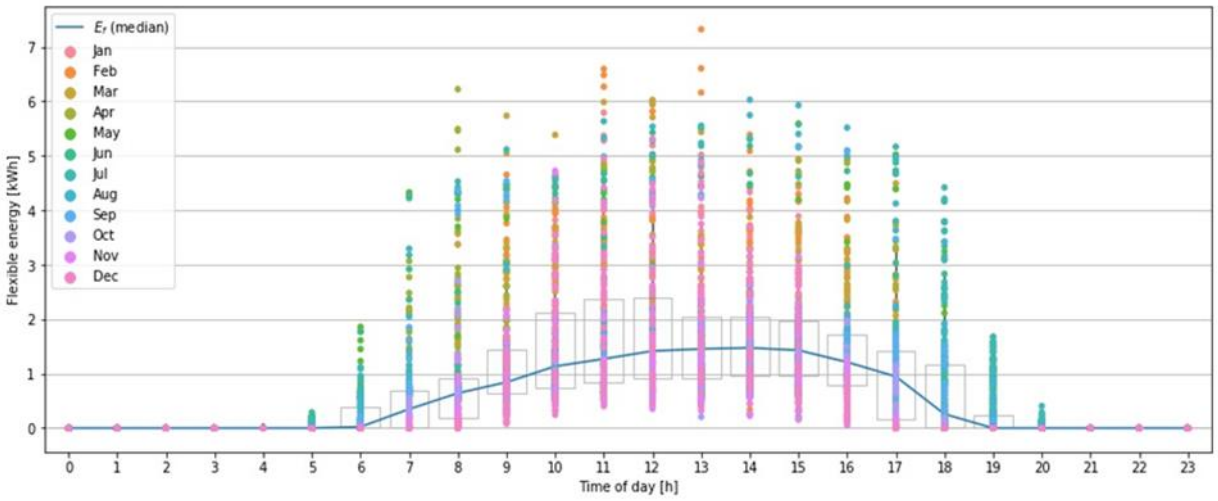

Figure 4.12 Upward Flexible energy-UPS mode

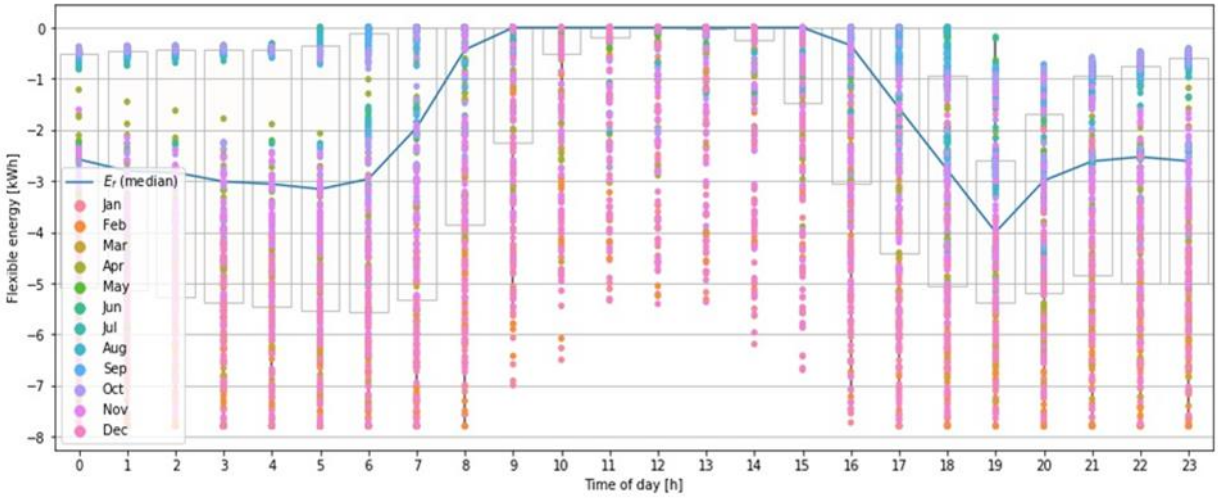

Figure 4.13 Downward flexible energy-UPS mode

4.7 Chapter summary

This chapter assesses the energy flexibility provided by a PV+Battery system. Yearly and dynamic flexibility Key Performance Indicators (KPIs) are assessed for different system configurations (sizing) and non-HVAC load profiles through system simulation in TRNSYS. The simulated house is a typical Canadian single-family home and high-resolution load profiles are used for non-HVAC loads and domestic hot water.

Default control strategies in commercially available inverters are used: Grid support (or PV priority) and UPS-mode. No attempt is made to optimize these strategies in this study.

Yearly KPIs such as self-generation and self-consumption show that adding batteries to a conventional grid-tied PV system can improve dramatically the available flexibility, with a saturation of the effects for battery capacity higher than 4 kWh/kWp under the selected assumptions.

Dynamic KPIs calculated for 1-h upward and downward flexibility events show that there is a large variability in available flexibility, depending on the day and time of the year and on the inverter control strategy. The UPS mode, which results in the lowest yearly self-generation and self-consumption, presents a significant downward flexibility potential, limited by the maximum battery discharge current, which resulted in a potential of up to 8 kWh per 1-h event, with a median value between 0 and 4 kWh depending on the time of the day (the downward flexibility is limited by the load itself, the PV+Battery system cannot do better than removing the entire load). Its upward flexibility results from the ability to shut down PV generation and is entirely dependent on solar radiation. On the other hand, the grid-support (or PV priority) operation mode, which already minimizes grid imports, offers no potential for downward flexibility under the current assumptions. Its upward flexibility is variable between 0 and 12 kWh in this study, with a relatively constant median value around 5 kWh.

CHAPTER 5 ECONOMIC ASSESSMENT

This chapter investigates the economic performance of PV+Battery systems in the Canadian residential context. The conducted analysis considered two parameters of capital cost and potential cost savings on electricity bill. The conventional grid-support mode of operation is compared with a proposed "battery pre-charging" strategy and they are assessed for the two most frequent billing policies: predefined (e.g. Time of Use) and dynamic (e.g. price signal) flexible rates. The case study residential property, which has been described earlier in Chapter 3, is used for modelling purpose (e.g. load profiles, hybrid system sizes and etc.) to conduct the economic analysis.

The Net Present Value (NPV) and the payback period corresponding to the defined PV and battery capacity configurations are estimated to analyze overall cost of offered power flexibility during peak hours. The net levelized cost of provided flexibility to electricity grid through residential PV+Battery system is estimated for comparison purpose with other electricity generation technologies (e.g. hydropower, natural gas, coal, wind and etc.).

5.1 Methodology

Figure 5.1 shows the workflow of our economic analysis.

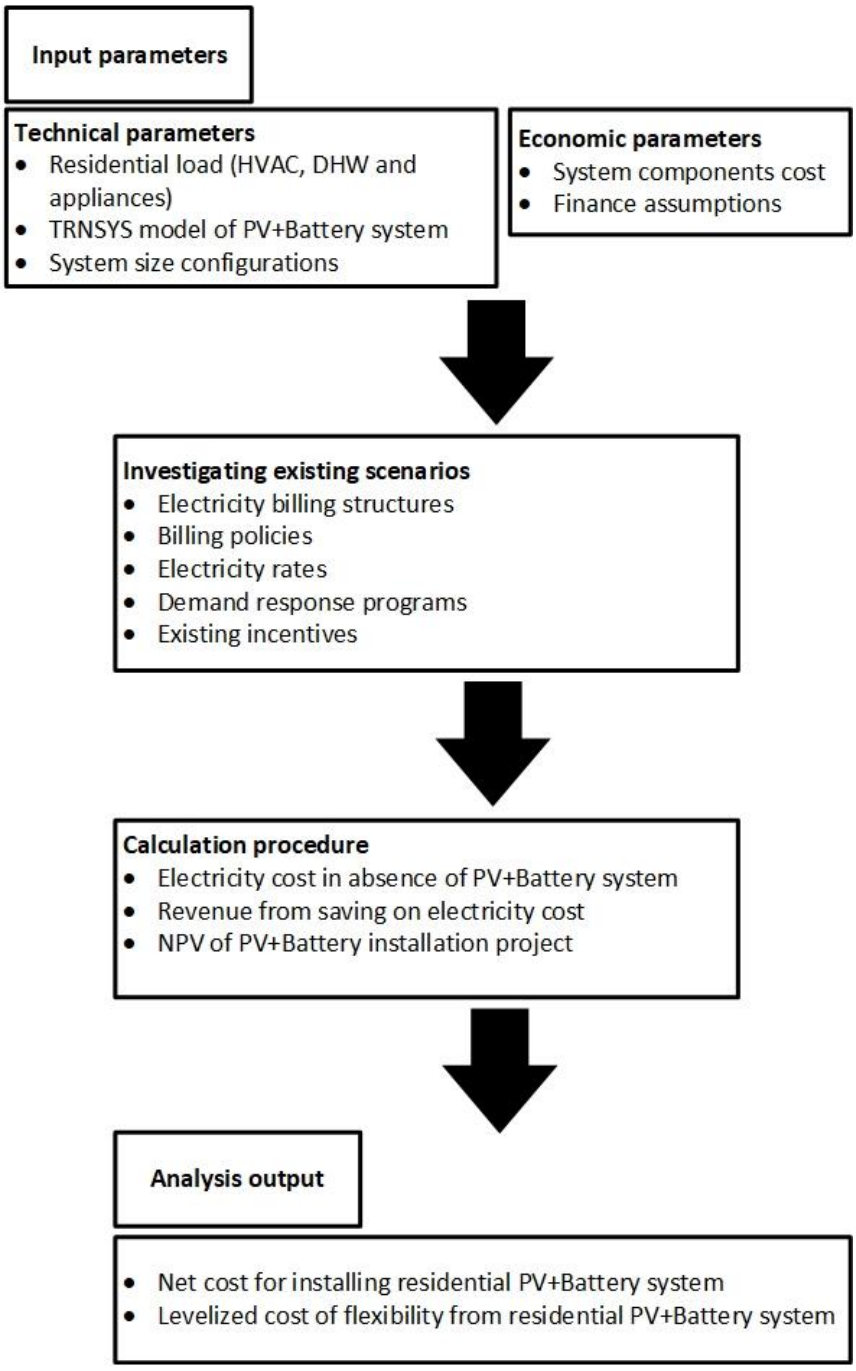

Figure 5.1 Economic analysis workflow

The TRNSYS model of residential archetype presented in chapter 3, including PV+Battery system and load profile (HVAC, DHW, appliances and EV) corresponding to average consumption pattern, was used for performing all simulations in this chapter.

Table 5.1 presents monthly produced solar electricity for the corresponding PV size variants which were discussed in chapter 3.

Table 5.1 Monthly produced solar electricity (kWh)

PV (kW)	Jan	Feb	Mar	Apr	May	Jun	Jul	Aug	Sep	Oct	Nov	Dec	Year	Day Avg
8.1	474	633	957	1090	1314	1394	1499	1143	977	640	307	304	10737	29
12.2	690	921	1392	1586	1911	2027	2180	1663	1421	932	447	443	15618	43
16.2	949	1267	1914	2181	2628	2788	2998	2286	1954	1281	615	609	21475	59

Since billing policies usually vary over a certain time interval (e.g. a few months) according to demanded energy by end-users, the implemented load management scenario must be modified accordingly. Table 5.2 shows the total monthly electricity load (HVAC, DHW and appliances) for the three consumption patterns which are described in chapter 3.

Table 5.2 The monthly electricity usage (in kWh) for three consumption patterns

Load kWh	Jan	Feb	Mar	Apr	May	Jun	Jul	Aug	Sep	Oct	Nov	Dec	Year	Day Avg
Low	4599	4008	3470	2245	612	650	785	731	606	1453	2698	4091	25948	71
Avg	4631	4035	3429	2301	900	892	898	1030	973	1635	2780	4110	27614	76
High	4297	4013	3444	2087	1107	1272	1448	1388	1027	1585	2714	4117	28498	78

EV charging (which is assumed to occur over the off-peak nigh hours) increases the residential daily electricity consumption by 8.75 kWh.

The Table 5.3 (Feldman et al., 2021; Masson & Kaziuka, 2020) summarizes the cost breakdown for installing a PV+Battery system in Canadian residential properties. Although system components (PV, battery and inverter) are sold in discrete size values, the following table provides an approximative estimation through modelling total cost for installing an 8 kW PV with 30 kWh back up battery and a 48V-8KW dual function grid-tied inverter.

Table 5.3 Cost breakdown for installing PV + Battery system in a Canadian residential property

PV panel	
	Cost (CAD/W)
Module	0.63
Structure and electrical	0.75
Installation	1.55
Total expenditure	2.93

Battery bank	
	Cost (CAD/kWh)
Module (li-ion)	550
Structure and electrical (including the inverter, switch and back up circuits)	220
installation	30
Total expenditure	800

The employed parameters in economic assessment, including project timespan and components lifetime, as well as financial assumptions are shown in Table 5.4 (Macklem et al., 2021).

Table 5.4 Financial parameters for economic assessment of installing residential PV+Battery

Parameter	**Value**
Project lifespan	20 years
PV panels lifetime	25 years
Battery lifetime	10 years (operating at 60% DOD)
Inflation rate	2 %
Discount rate	3 %

With the selected assumptions (e.g. SOC thresholds, chemistry, and DOD), the lifetime of the employed battery is 10 years, which necessitates one replacement during project lifetime (20 years). For the economic assessment analysis, the cost corresponding to the battery unit replacement in the 11th year is limited to module price (excluding structural and electrical expenses).

Table 5.5 shows capital cost corresponding to different system sizes.

Table 5.5 capital cost for various PV + Battery system size variants

PV power (kW)	**0 kW**	**8 kW**	**12 kW**	**16 kW**
Battery capacity (kWh)				
0 kWh	0 $	23733 $	35746 $	47466 $
30 kWh	24480 $	48213 $	60226 $	71946 $
60 kWh	48960 $	72693 $	84706 $	96426 $

The considered load management strategies are implemented through scheduling the inverter to control power dispatch between the electricity grid and system components (e.g. battery bank and PV panels).

The economic viability of employing a residential PV+Battery system in various billing structures is assessed through computing the net present value (NPV) over the project lifetime (Duffie & Beckman, 2013).

5.2 Electricity rate structures

Utilities have various policies for implementing their load management scenarios to strike a balance between production capacity and the required electricity load. Time of use pricing scheme and price/curtail signal are the more frequently used strategies by utilities; they are briefly explained in the following.

5.2.1 Time of Use (TOU) pricing scheme

Time of use (TOU) is a typical pricing policy which is employed by the vast majority of utilities to encourage electricity consumers avoiding unnecessary usage over peak hours. In this strategy the day is divided into few periods, namely off peak, mid peak, and peak hours. Electricity rates vary over these periods and TOU prices are usually updated monthly or seasonally.

5.2.1.1 Case study for TOU

The TOU data corresponding to Grimsby power Inc., which provides electricity service to residential/commercial customers in Ontario, is provided in Figure 5.2

Figure 5.2 Detailed TOU pricing schedule of Grimsby power Inc

The data corresponding to real TOU price is shown in Table 5.6 which indicates the electricity

rates during peak, off-peak and mid-peak hours.

Table 5.6 Grimsby power time of use electricity rate

Grid mode	Rate (¢/kWh)
Off-peak	10.5
Mid-peak	15
On-peak	21.7

The data corresponding to PV arrays output power as well as load profile are presented in Figure 5.3 where the TOU periods are specified according to data provided by Grimsby power.

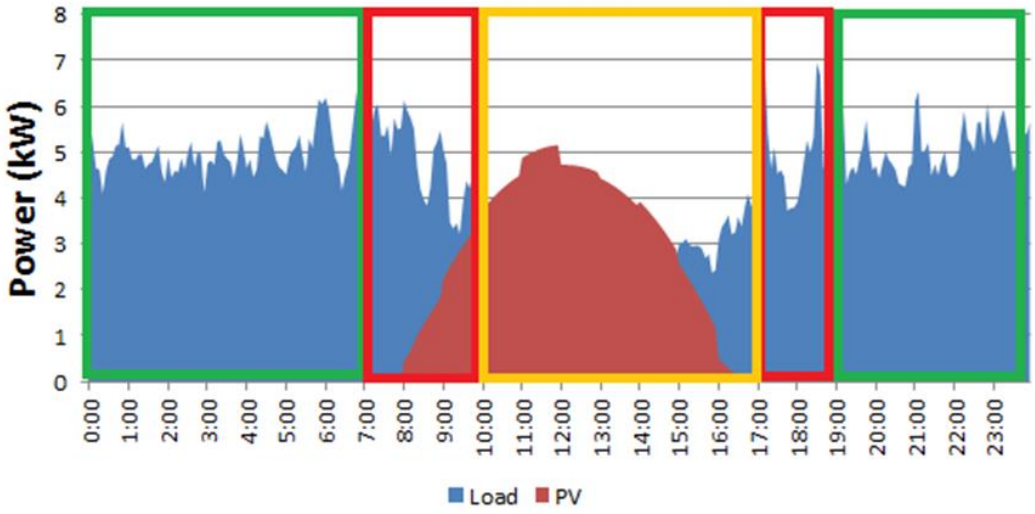

Figure 5.3 Daily average load and load profile over TOU periods

In Figure 5.3, the green frame is associated with off peak hours when electricity price has the lowest rate. The orange and red frames indicate mid and peak hours respectively when the electricity rate increases significantly.

5.2.2 Price signal (peak power event)

A price signal rate structure modulates the electricity rate to incentivize consumers/prosumers to support the grid operation through matching their electricity consumption/supply with the grid generators capacity: a price increase will encourage demand reduction and more exports from prosumers, while a price decrease will encourage more demand and discourage exports. Day-ahead real price or curtail signal are the common approaches for implementing the demand response

program. This dynamic pricing provides opportunity for electricity consumers to adopt their consumption/grid-usage based on network supply potential to minimize the overall electricity cost.

5.2.2.1 Case study for price signal

Hydro-Québec, government-owned public utility in province of Québec in Canada, charges a flat rate for electricity in the residential sector. Recently, the utility has offered two optional demand response (DR) programs for winter season (when the utility peak occurs). These optional tariffs apply dynamic electricity rates for customer, with the objective of reducing demand during winter peak periods (downward flexibility). The DR events are defined during the morning and evening peak hours over 6:00 to 9:00 and 16:00 to 20:00 respectively. The participants receive a notification signal one day prior to the events which can occur during both morning and evening peak hours. The total number of events hours will remain below 100 hours during whole program period (December 1st - March 31st). The specifications corresponding to the power peak events are shown in Table 5.7.

Table 5.7 Peak events specifications data

Specification	hours
Maximum number of events per day	2
Minimum interval between 2 events	7
Event duration	3-4
Maximum total event duration per winter period	100

With the first optional tariff, customers receive credits equal to 50 ¢ for each kWh that they "save" during DR events, where "savings" are assessed by comparing their energy use over the DR period to their typical electricity consumption load profile for similar days. The reference energy use is estimated by the utility, based on historical energy use for each consumer, combining the day, time of day, and a linear regression versus ambient temperature. In this credit-option program, the electricity rate remains constant (6.08 ¢/kWh). There is no risk to consumers as the credit cannot be negative. In order to receive the credit, amount of curtailed energy must be above 2 kWh during a peak event. The second program is defined as "Flex D" rate, which offers a lower electricity rate compared to the flat rate outside of the peak event periods, at 4.28 ¢/kWh (a 30 % discount). The electricity cost is significantly higher during DR events, at 50 ¢/kWh (more than 800 % increase

over the standard flat rate and a 1200 % increase over the Flex D "non event" rate). The electricity rates corresponding to Hydro-Québec billing policies for the base and demand response programmes (winter credit option and rate flex D) as of 2021 are summarized in Table 5.8 .

Table 5.8 Electricity rates of various billing policies (Hydro-Québec rates as of 2021)

	1st tier (< 40kwh/day)	2nd tier (> 40kwh/day)	Peak event
Billing policy	Rate (¢/kWh)	Rate (¢/kWh)	Rate (¢/kWh)
Base rate	6.08	9.38	Unchanged
Rate flex D	4.28	7.36	50
Winter credit	6.08	9.38	50 (credit for difference with reference)

5.2.2.2 Peak events determination

The exact mechanism to determine peak events is not published by Hydro-Québec, but the "dual energy" rate (which switches between electricity and another energy source) uses ambient temperature to define the peak periods, with a threshold of -12 °C or -15 °C depending on climate zones within Québec. Peak demand events used in the winter credit option were logged over the 2020-2021 winter and compared to the temperature forecasts for Montréal and for the city of Québec. In most cases, the forecasted temperature was around or below -12 °C for one of the two cities or both (peak events are the same throughout the province). We assumed that using a threshold of -12 °C to cause DR events was a reasonable approximation. That limit was applied to the typical weather file used in this study (CWEC). The morning and evening peak events are assumed to occur when the average temperature drops below -12 °C over the period between 6-9 AM and 16-20 PM respectively. The results are shown in Table 5.9. According to the Hydro-Québec regulations, the maximum number of peak events and the total duration must be below 33 and 100 hours respectively.

Table 5.9 Peak power events analysis

Temperature threshold	-12 °C
Morning event	22 days
Evening event	7 days
Morning and evening events	6 days
Total number of events	29
Total events duration	97 hours

Figure 5.4 shows a histogram of simulated electricity demand for the modelled house over the peak demand events. Based on the estimated data, a battery bank with 30 kWh storage capacity and 60 % DOD, would be able to supply the required energy over 11 events (35 % of total peak events) without importing electricity from grid (operating in off-grid mode).

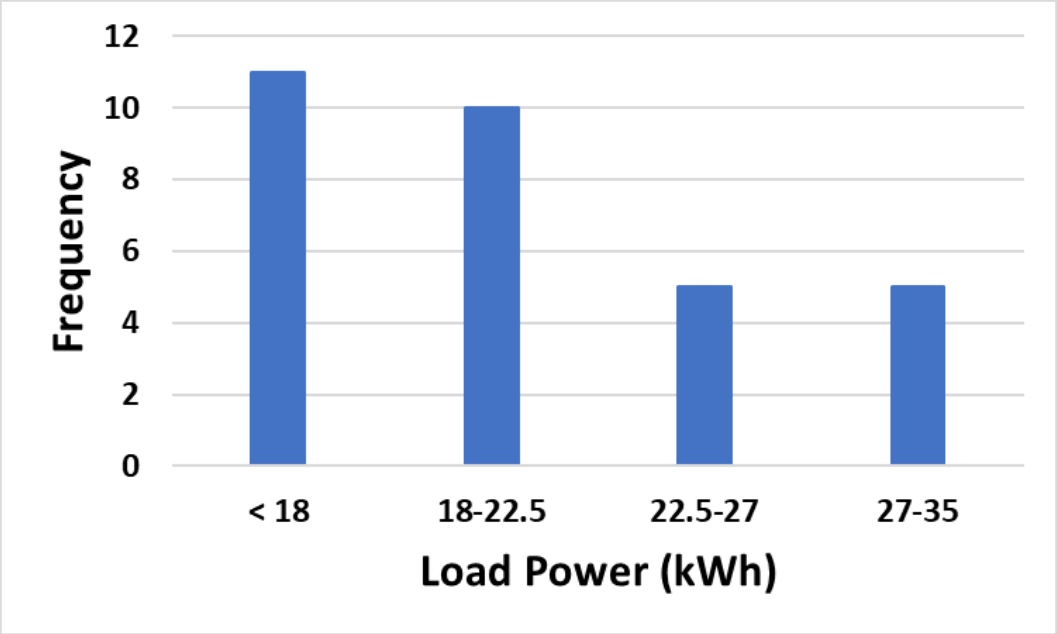

Figure 5.4 The distribution of the demanded load over peak power events period

Additionally, such a system could provide 85 % of the total energy demand over all peak events. Since all the load values during the peak events remain below 35 kWh, using a battery bank with a 60 kWh capacity (operating with 60% cycle depth), has potential to shift all the grid-imported electricity load during the peak events periods.

The same analysis is conducted to quantify the total produced solar electricity during the power peak events, with three PV nominal power values (8.1, 12,1 and 16.2 kW). The simulation results are shown in Table 5.10.

Table 5.10 Generated solar electricity during the power peak events

PV size (kW)	8.1	12.2	16.2
Solar electricity (kWh)	17	25	34

As it is anticipated, since the solar irradiance level is extremely low over the defined power events (6-9 AM or 16-20 PM from Dec 1st to Mar 31st), PV panels play a negligible role in reducing imported electricity from grid in winter credit or flex rate programs.

5.3 Control strategies

As shown above, PV panels will have little impact during peak events. Managing battery storage is a key control element to maximize a PV+Battery system economic performance. There are two main strategies to reduce the grid dependency over the peak hours:

- Force the system to charge battery over off-peak hours and simultaneously stop battery from discharging in this period. (constant rule-based controller)
- Scheduling charging/discharging period through forecasted deliverable solar electricity and load profile. (dynamic controller)

Commercially available grid inverters can be scheduled for grid charging over predefined periods. The inverter could be programmed with reference to the monthly average of PV output and electricity load as well as the TOU schedule. It would then manage dispatching the power flow from/to the grid on the basis of a pre-set schedule. This method would be simple to implement, the operator would have to modify inverter settings (e.g. monthly or seasonally) to minimize electricity bill.

This method does not account for daily variations in load and PV output. In the second strategy, day-ahead data (weather and load forecasts) are used in the controller to optimally schedule the inverter to minimize electricity cost. The controller charges the battery during off-peak periods (for a certain number of hours according to the forecasts) so that the amount of stored energy plus

generated solar energy over the daylit hours is sufficient to cover the load over peak times. As a result, the consumer does not have to buy electricity from the grid at high rates. The control strategies for each billing policy will be discussed under the corresponding subchapters.

5.3.1 Control strategy and cost-saving potential assessment for TOU

Time-of-use rates (TOU) provide an opportunity to reduce electricity bills by shifting demand from on-peak ("expensive") periods to off-peak ("cheap") periods. In PV+Battery systems, this can be achieved by storing and de-storing energy from battery. A quick, simplified energy analysis is useful in assessing the impact of energy losses on that strategy.

Using detailed simulations with the models described in chapters 2 and 3, the following estimates for efficiencies can be derived:

- AC to DC (inverter efficiency ~ 93%)
- Charging the battery (efficiency ~ 95%)
- Discharging the battery (efficiency ~ 95%)
- DC to AC (inverter efficiency ~ 93%)

The round-trip efficiency (also called AC/AC efficiency) is simply calculated by multiplying these values.

$$Round\ trip\ efficiency = 0.93 \times 0.95 \times 0.95 \times 0.93 = 0.781 \quad (1)$$

Consequently, for providing 1 kWh deliverable electricity energy in AC mode the required amount of energy from grid is equal to 1.28 kWh (1 kWh/0.78).

Using the Grimsby Power rates presented above, the cost associated to providing 1.28 kWh during off peak hours is:

$$1.28\ kWh \times 10.5\ ¢/kWh = 13.44\ ¢ \quad (2)$$

Given the electricity rates in mid-peak (15 ¢/kWh) and peak (21.7 ¢/kWh) periods, implementing

battery off-peak grid-charging results in potential savings up to 11 % and 38 % respectively. To maximize the economic efficiency of the corresponding strategy, the control layer is defined through the following rules:

- Priority for grid-charging period is off-peak and mid-peak hours, sequentially (no battery grid-charging is allowed during peak hours)
- Priority for drawing the stored energy to supply the load is peak hours and mid-peak hours, sequentially (no battery discharge is allowed over off-peak hours)
- Grid-charging will be scheduled based on estimated day-ahead PV output and load profile to avoid solar electricity curtailment

The implemented grid battery charging strategy is demonstrated graphically in Figure 5.5, showing the system interaction with grid over arbitrary selected winter day (February 9th).

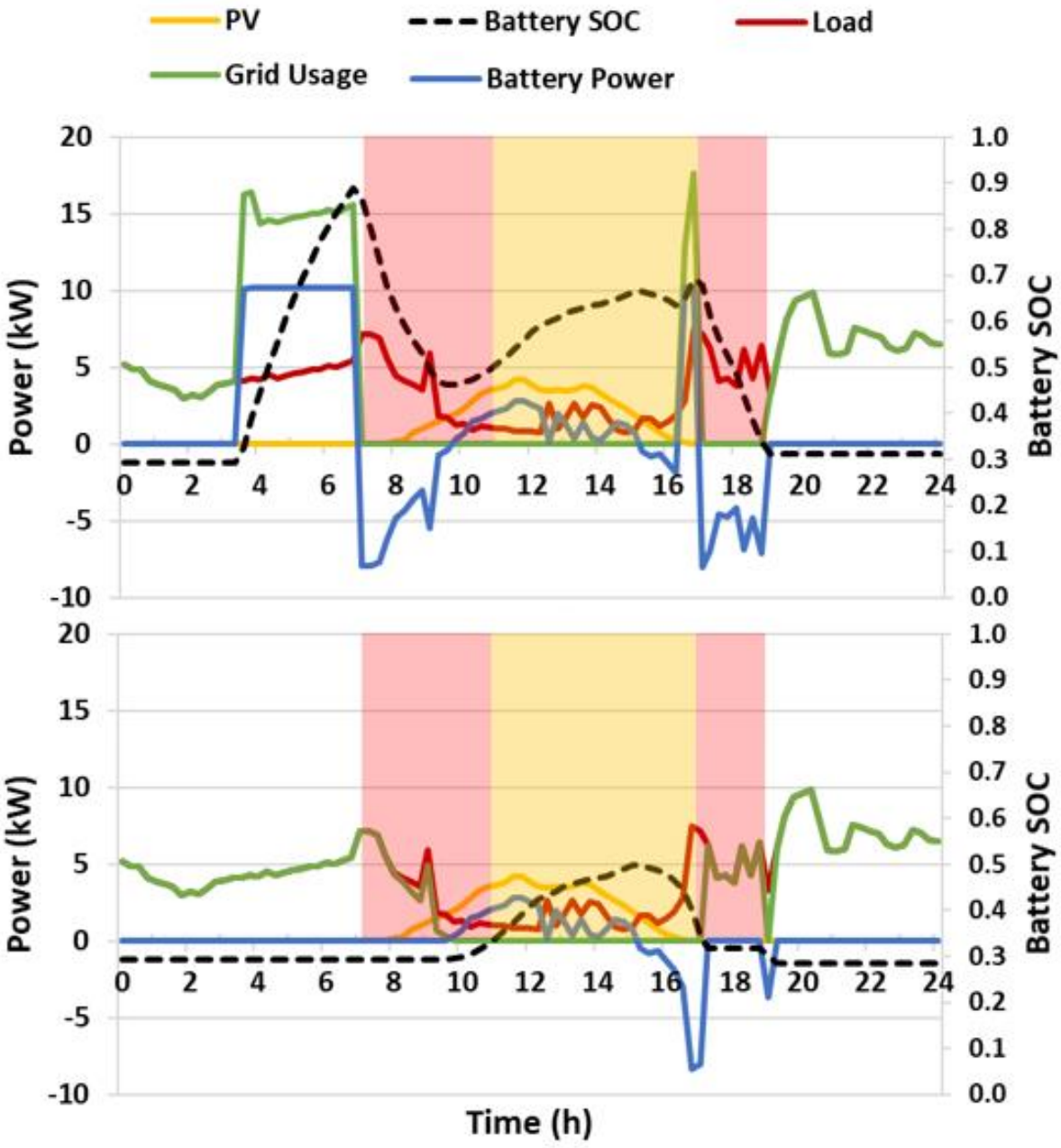

Figure 5.5 battery grid charging (top) versus grid-support load management strategy (bottom)

The imported electricity from the grid, in/output battery power as well as battery SOC level are compared between pre-charging (upper graph) and grid-support (lower graph) scenarios over peak, mid-peak and off-peak hours. The mid-peak and peak hours are marked in the corresponding graph by yellow and red background areas respectively.

In the pre-charging scenario (upper graph), the controller charges the battery at 3:30 AM until the start of the peak hours (7:00 AM). The battery supplies demanded load over peak hours (7:00 – 11:00 AM) without using the electricity grid. At the end of the mid-peak hours, the battery is charged for half an hour prior to the second peak-hours period (5:00 – 7:00 PM). Due to relatively high electricity rate (higher than off-peak hours) over the mid-peak hours, the battery grid-charging needs to be scheduled effectively to supply the load for the second peak-hours period (battery SOC needs to be close to 0.3 at the end of peak-hours).

As shown in the graph, the implemented strategy shifts the demand from peak hours to off-peak hours without energy curtailment or unnecessary battery grid-charging over mid-peak hours (the battery SOC reaches 0.3 at the end of second peak period at 7:00 PM).

In the grid-support scenario, the system supplies the required load over the entire mid-peak period without importing electricity from the grid, but it fails to accommodate the energy demand over the peak hours. Apart from a short period of time (one and half our) at the end of first peak hours, the controller had to supply the load using the electricity grid. This load management strategy effectively conducted load shifting over the mid-peak hours, where the stored excess solar electricity (mainly between 10:00-12:00 AM), compensated the lack of solar irradiance at the end of solar window period (3:00 – 5:00 PM).

As expected, the pre-charging scenario delivers significantly higher savings, but it also applies more cycles to battery. It should be noted that load and weather forecasts are assumed to be perfect.

5.3.2 Control strategy and cost-saving potential for price signal

The rate for the first tier of imported electricity from the grid (< 40 kWh/day) is 6.08 ₵/kWh while the remaining consumption will be billed at a higher rate of 9.38 ₵/kWh. Meeting a portion of the total load through the PV panels helps keeping the daily electricity grid consumption below the 40-kWh threshold and avoiding a 54 % raise.

Over the winter period (Dec-Mar), according to a signal received prior to the peak event, the inverter will be scheduled to charge the battery through the grid. Implementing this load management strategy (battery grid charging) minimizes the imported electricity from the grid during the corresponding peak periods to gain credit for reducing the consumption. With the winter

credit option, shifting 1 kWh of electricity demand from event period to off-peak time leads to a 50 ¢ credit, which is equivalent to 8 kWh of electricity consumption.

With the Flex D rate, the cost of electricity is reduced by 42 % and 22 % for the 1st and 2nd tiers respectively. But electricity used during peak events will be highly penalized, at 50 ¢/kWh – a "peak event" kWh is worth 12 "non peak event" kWh.

Figure 5.6 shows the implemented load management strategies. It compares power dispatch between electricity grid and system components in pre-charging (upper graph) and grid-support (lower graph) mode of operation during the day (January 11th) with morning and evening peak events.

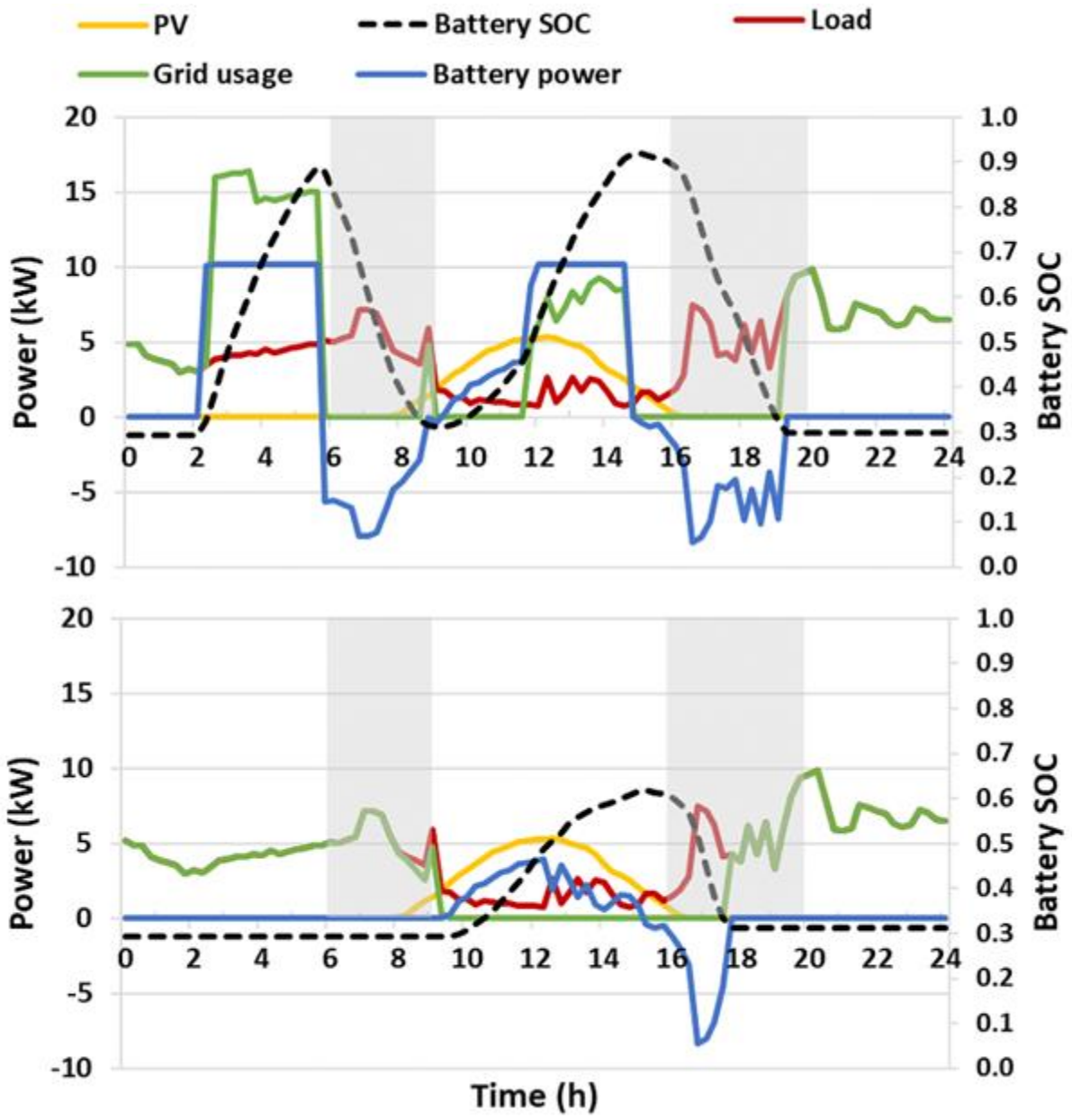

Figure 5.6 Battery grid charging (top) versus grid-support mode (bottom) in morning and evening peak

The solid lines show the input/output power related to system components and the battery SOC trend is presented with the black dash lines. The power peak events periods over the day are marked through two grey bands.

In grid support mode (bottom graph), the lack of solar input during the morning peak prevents any charging from battery (which was discharged overnight) so the morning peak load is entirely met

by the grid. Over the solar window time frame for the corresponding day (8 AM to 4 PM), the PV output power (yellow line) covers the load (red line) and the imported electricity from the grid stays close to zero for approximately the entire period. The excess produced solar electricity is stored in the battery bank to support the grid for supplying load during the evening peak hours. As presented on the lower graph, the stored energy meets the load roughly about half of the evening peak event duration (from 4 PM to 6 PM).

In pre-charging mode (upper graph), the inverter charges the battery (starting at 2 AM) according to the day-ahead estimated load and solar electricity during the upcoming peak event (from 6 AM to 9 AM). Apart from a short surge in the load profile at the end of the peak event period, the battery supplies the entire load, without using electricity from the grid (off-grid mode). The PV system then meets the load and contributes to charging the battery after the morning peak event. Battery grid charging starts at 11:45 AM and continues until 4 PM, leading to operation in off-grid mode for most of the evening peak event (until 7:30 PM).

With the pre-charging strategy, battery charging start time is the key parameter and it needs to be investigated appropriately. Efficient timing extracts the maximum potential of the system downward flexibility through using the entire storage capacity without dumping generated solar electricity. The battery SOC trend (black dash line) confirms the effectivity of the implemented scenario when it reaches the upper threshold (0.9) prior to the start of the peak events (6 AM and 4 PM).

5.4 Results

This subchapter presents the results of energy simulations and economic analyses for both electricity rate structures, TOU and price signal.

5.4.1 Economic analysis with TOU rates

The yearly electricity cost estimation, for the case study household with an average energy consumption pattern (for appliances and domestic hot water) using the private EV charger unit is 4193 $ based on the TOU rates. The results corresponding to load profile analysis are presented in Figure 5.7, which demonstrates electricity consumption dispersion over the off-peak, mid-peak and peak hours.

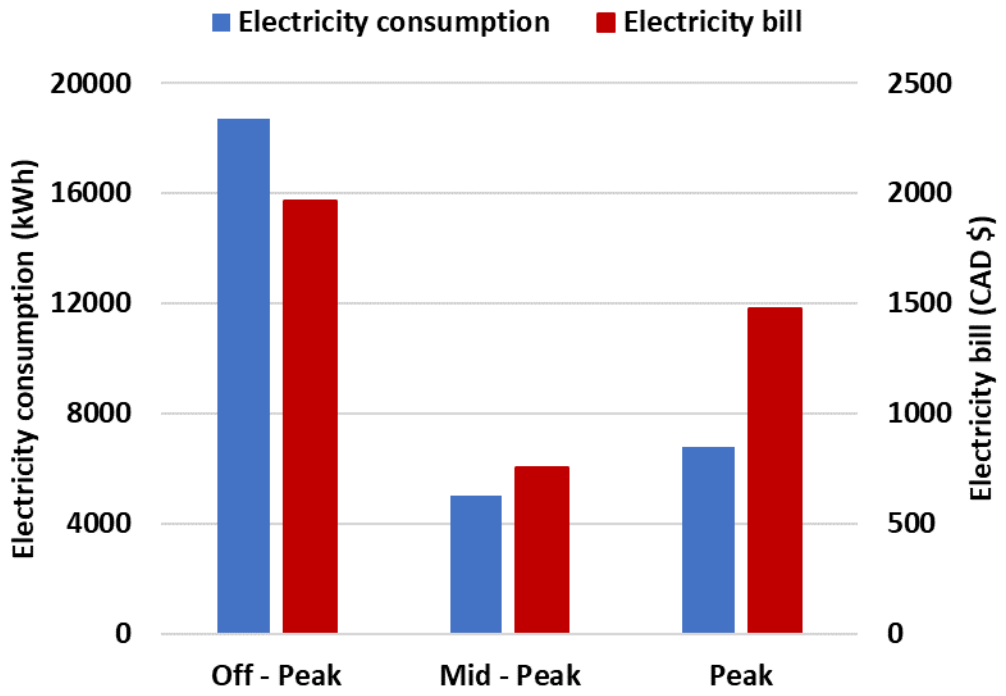

Figure 5.7 Electricity consumption and cost break down over off, mid and on-peak periods

5.4.1.1 Cost savings without grid export

With current policies, grid export is often not credited to PV+Battery systems (or battery-only systems). Excess PV production will be curtailed as dumped energy. The cost savings on annual electricity bills result from displacing part of grid imports from peak to mid-peak and from mid-peak to off-peak hours. Results are shown in Table 5.11 for the grid-support mode of operation.

The results indicate that by adding 30 kWh of battery capacity, the average increase on the electricity bill saving is approximately 55%. Doubling the battery size to 60 kWh leads to a further reduction, but with diminishing returns (14 % increase).

Table 5.11 Reduction on overall yearly electricity cost – grid support strategy, no grid exports

PV power (kW)	8 kW	12 kW	16 kW
Battery capacity (kWh)			
0 kWh	762 $	883 $	986 $
30 kWh	1154 $	1367 $	1539 $
60 kWh	1232 $	1530 $	1760 $

The pre-charging control strategy delivers extra savings, as shown in Table 5.12. Depending on the system size, implementing the grid battery charging increases savings by 22 % to 38 %.

Table 5.12 Extra savings from pre-charging control strategy – no grid exports

PV power (kW)	0 kW	8 kW	12 kW	16 kW
Battery capacity (kWh)				
30 kWh	462 $	391 $	362 $	334 $
60 kWh	577 $	470 $	428 $	385 $

The total savings on annual electricity bill are shown in Table 5.13

Table 5.13 Total cost savings on the annual electricity bill – pre-charging, no grid exports

PV power (kW)	0 kW	8 kW	12 kW	16 kW
Battery capacity (kWh)				
0 kWh	0 $	762 $	883 $	986 $
30 kWh	462 $	1545 $	1729 $	1873 $
60 kWh	577 $	1702 $	1958 $	2145 $

5.4.1.2 Cost savings with grid exports (net metering)

Even if this scenario is not currently possible in Canada, we have assessed the savings that could be achieved if grid exports were allowed and valued at the same rate as grid imports at the time. The results corresponding to the system size variants are shown in Table 5.14, as additional savings compared to Table 5.11.

Table 5.14 Extra savings gained from valuing grid exports (net metering) – pre-charging strategy

PV power (kW)	8 kW	12 kW	16 kW
Battery capacity (kWh)			
0 kWh	964 $	1659 $	2540 $
30 kWh	198 $	667 $	1307 $
60 kWh	47 $	392 $	1045 $

As expected, in absence of storage or with a lower battery capacity, the net-metering program is more profitable for prosumers, delivering savings that are higher or comparable to the savings obtained by displacing energy use. The total energy savings are shown in Table 5.15.

Table 5.15 Total reduced amount of electricity cost (with net-metering)

PV power (kW)	0 kW	8 kW	12 kW	16 kW
Battery capacity (kWh)				
0 kWh	0 $	1726 $	2542 $	3526 $
30 kWh	751 $	1743 $	2396 $	3180 $
60 kWh	1502 $	1749 $	2350 $	3190 $

5.4.1.3 Net Present Value

The modest savings shown above must be assessed in comparison with the relatively high initial costs. Table 5.16 presents the Net Present Value (NPV) calculated using the economic parameters shown in Table 5.4 (inflation rate, discounted rate, time span, etc.).

Table 5.16 Net Present Value of PV+Battery systems – no grid exports

PV power (kW)	0 kW	8 kW	12 kW	16 kW
Battery capacity (kWh)				
0 kWh		-7.3 K $	-16.7K $	-26.2K $
30 kWh	-30.8K $	-31.7K $	-39.8K $	-48.4K $
60 kWh	-70.1K $	-69.6K $	-76.1K $	-83.8K $

The results show that employing a PV+Battery system for the representative household used in our simulations is not economically viable when there is no possibility to send the excess solar electricity to the grid.

The NPV results with grid exports are shown in Table 5.17. With net metering, the PV system without battery can be profitable, but all scenarios with batteries still deliver negative NPV values.

Table 5.17 Net Present Value of PV+Battery system with net-metering

PV power (kW)	0 kW	8 kW	12 kW	16 kW
Battery capacity (kWh)				
0 kWh		13.4K $	19K $	28.5K $
30 kWh	-25.15K $	-27.4K $	-25.4K V	-16.4K $
60 kWh	-50.2 K $	-68.6K $	-67.7K $	-61.3K $

It could be argued that the lifetime of PV panels (25 years) is usually longer than 20 years which is chosen as lifespan for the project. Table 5.18 presents the NPV results for PV-only systems considering the analysis period up to 25 years.

Table 5.18 Net Present Value of PV system without battery (25 years lifetime analysis)

PV size (kW)	8.1	12.2	16.2
NPV (Without net metering)	-2.7K $	-11.3K $	-20K $
NPV (With net metering)	23.9K $	34.4K $	49.9K $

Figure 5.8 and Figure 5.9 show cumulative discounted cash flows over the 20-year analysis period ("rolling NPV'). The year when the NPV becomes positive corresponds to the discounted payback time. The following figures are corresponding to the 8 kW PV system with and without the 30 kWh battery storage unit respectively.

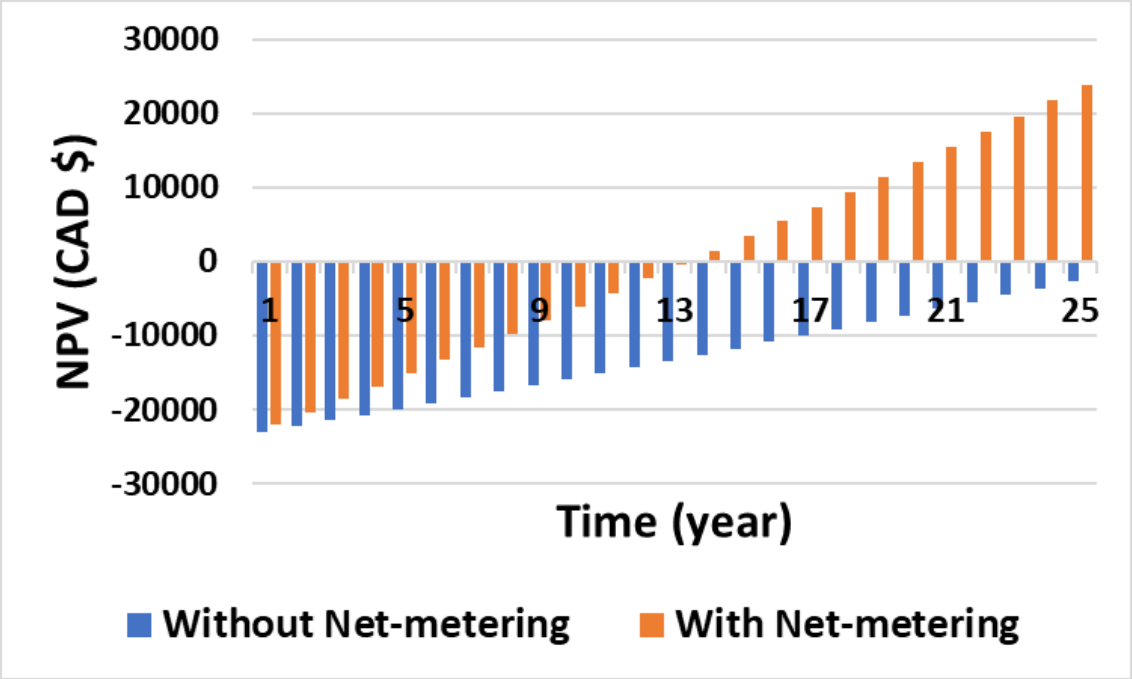

Figure 5.8 Net Present Value of 8 kW PV system without Battery

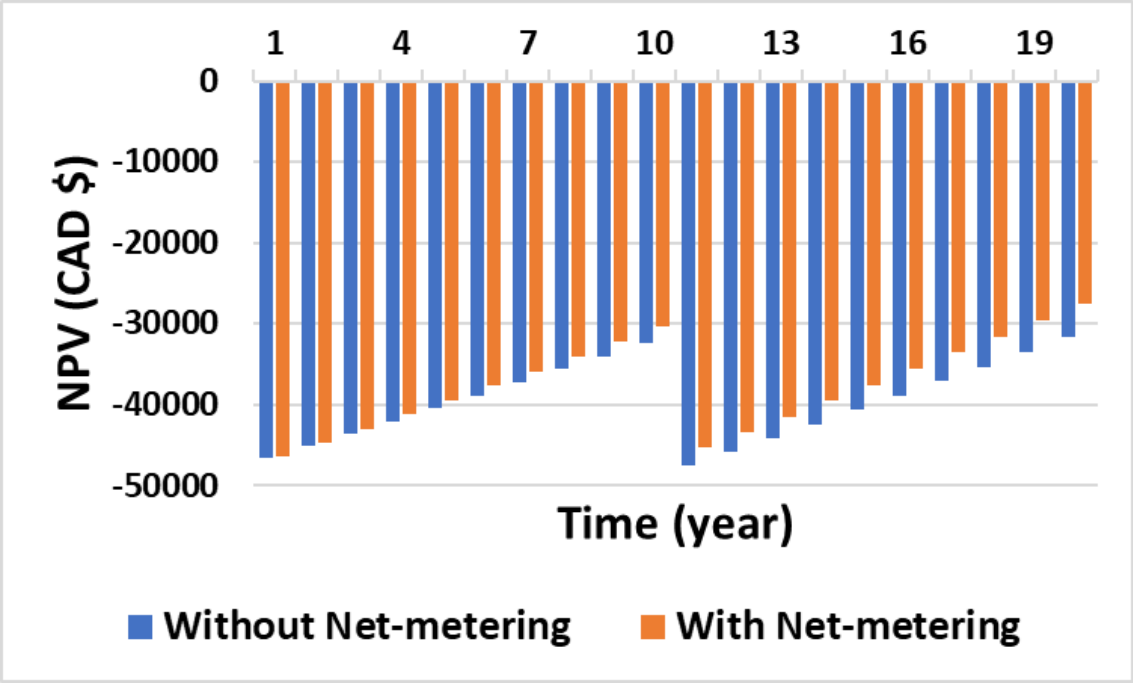

Figure 5.9 Net Present Value of 8 kW PV (8 kW) + Battery (30 kWh)

Figure 5.8 shows that, with the relatively high electricity rate as well as TOU pricing, a PV system without battery can be profitable after 13 years. As shown in Figure 5.9, the same PV capacity with battery has a much larger capital cost (turns the NPV value down), so the NPV still remains negative after 10 years, when the battery must be replaced, bringing the NPV value further down.

Figure 5.9 also shows that with the selected sizing, there is almost no difference between the scenarios with and without grid exports. The selected design brings self-consumption at a very high level, so that little energy is curtailed (without grid exports) or exported (with net metering).

5.4.2 Economic analysis with price signal

In the absence of PV panels and storage, the reference cost for the modelled house is 2423$ per year with the flat rate.

5.4.2.1 Annual cost savings

The yearly cost savings achievable with a PV+Battery system are shown in Table 5.19.

Table 5.19 Reduction on yearly electricity cost – PV+Battery system, flat rate

PV power (kW)	8 kW	12 kW	16 kW
Battery capacity (kWh)			
0 kWh	369 $	427 $	477 $
30 kWh	573 $	688 $	780 $
60 kWh	617 $	787 $	921 $
120 kWh	634 $	816 $	972 $

As expected, the cost savings delivered by self-consumption of PV energy and by avoiding to go over the 40 kWh/day threshold for the first-tier price are minimal, and the impact of having a battery quickly saturates over 30 kWh.

The results corresponding to the winter credit program are presented in Table 5.20 for various system size variants.

Table 5.20 Winter credits corresponding to system size variants

PV power (kW)	0 kW	8 kW	12 kW	16 kW
Battery capacity (kWh)				
0 kWh	-	12 $	19 $	22 $
30 kWh	233 $	239 $	242 $	244 $
60 kWh	302 $	310 $	313 $	314 $

It is interesting to compare the savings shown in the table above to the maximum achievable: if all electricity used during the DR events was displaced, 643 kWh could be credited, which is equivalent to 322 $. So for example, the battery bank with 60 kWh capacity reaches about 90 % of the maximum achievable savings even without PV.

The presented data in Table 5.20 only consider credits related to the demand response program, the total saving as result of reducing the overall grid usage are not included. Table 5.21, presents the combined savings.

Table 5.21 Total reduced amount on electricity bill (flat rate + winter credit)

PV power (kW)	0 kW	8 kW	12 kW	16 kW
Battery capacity (kWh)				
0 kWh	-	381 $	446 $	499 $
30 kWh	233 $	812 $	930 $	1024 $
60 kWh	303 $	927 $	1100 $	1235 $

If net-metering is assumed (even though it would not be possible currently in Québec), the extra savings presented in Table 5.22 can be achieved.

Table 5.22 Extra credits through net metering program (flat rate)

PV power (kW)	8 kW	12 kW	16 kW
Battery capacity (kWh)			
0 kWh	315 $	548 $	840 $
30 kWh	58$	197 $	395 $
60 kWh	14 $	114 $	313 $
120 kWh	2 $	91 $	274 $

For the systems with battery, the extra credits achievable from net metering are low, with a flat-rate tariff structure.

The analysis above assumes the "winter credit" program has been selected. Table 5.23 assumes the other option for DR events in Québec, the "Flex D" rate. For each result, the first value indicates the savings from reduced rate throughout the year, and the second value indicates the penalty for energy use during DR events. The latter is subtracted from the former to obtain net savings.

Table 5.23 Reduced electricity bill, Flex D rate (discounted rate benefit – penalty for grid usage during peak event)

PV power (kW)	0 kW	8 kW	12 kW	16 kW
Battery capacity (kWh)				
0 kWh	-	447 – 310 = 137 $	474 – 303 = 171 $	499 – 300 = 199 $
30 kWh	336 – 89 = 247 $	474 – 83 = 391 $	523 – 80 = 443 $	566 – 78 = 488 $
60 kWh	336 – 20 = 316 $	475 – 12 = 463 $	532-9 = 523 $	593 – 8 = 585 $

A comparison with Table 5.20 shows that the PV panels alone deliver more savings than with the winter credit program, which only delivers saving during the DR events. The savings in Table 5.23

only happen during the winter months, since the Flex D tariff only applies in winter. For rest of year, the PV+Battery system can deliver savings as well, as shown in Table 5.19. The results in Table 5.24 show savings for whole year. It is worth mentioning that the difference with Table 5.23 is not exactly what is reported in Table 5.19 since the latter is for the whole year, while the "flat rate" savings if the Flex D rate is selected should only be calculated for April through November.

Table 5.24 Total reduced amount on electricity bill (flat rate + flex rate D)

PV power (kW)	0 kW	8 kW	12 kW	16 kW
Battery capacity (kWh)				
0 kWh	-	352 $	413 $	463 $
30 kWh	247 $	777 $	887 $	973 $
60 kWh	316 $	892 $	1055 $	1179 $

A comparison between Table 5.21 and Table 5.24 (total savings with winter credits compared to total savings with Flex D rate) shows that the Flex D rate delivers slightly higher annual savings for the consumer (approximately 6 %).

5.4.2.2 Net Present Value

NPV values with and without net metering are shown in Table 5.25 and Table 5.26 respectively.

Table 5.25 Net Present Value of PV+Battery system without net metering

PV power (kW)	0 kW	8 kW	12 kW	16 kW
Battery capacity (kWh)				
0 kWh	-	-14.7k $	-25.2k $	-35.6k $
30 kWh	-35.5k $	-45.4k $	-54.7k $	-64.1k $
60 kWh	-74.8k $	-83.7k $	-91.6k $	-100.1k $

Table 5.26 Net Present Value of PV+Battery system with net metering

PV power (kW)	0 kW	8 kW	12 kW	16 kW
Battery capacity (kWh)				
0 kWh	0.0	-7.2k $	-12.2k $	-15.7k $
30 kWh	-35.5k $	-44.1k $	-50.0k $	-54.8k $
60 kWh	-74.8k $	-83.4k $	-88.9k $	-92.7k $

The possibility to inject the excess electricity generation into the grid through net metering results in better NPV values (or rather in less unfavourable NPV values), especially in absence of battery storage.

The results indicate that PV+Battery systems are not profitable in any scenario for any design. The achievable savings cannot compensate the high capital cost of PV+Battery systems, even with net-metering (which would not be possible currently in Québec).

Since the lifetime of PV panels (25 years) is longer than the assumed period in the calculations, the NPV analysis is repeated for 25 years for PV-only systems.

Table 5.27 Net Present Value of PV without battery (25 years time span)

PV size (kW)	**8.1**	**12.2**	**16.2**
NPV (Without net metering)	-11.8k $	-21.8k $	-31.8k $
NPV (With net metering)	-2k $	-4.7k $	-5.6k $

Figure 5.10 and Figure 5.11 show the cumulative discounted cash flows over the 20-year analysis period ("rolling NPV'). The year when the NPV becomes positive corresponds to the discounted payback time. The two following figures are corresponding to the 8 kW PV system with and without the 30 kWh battery storage unit respectively.

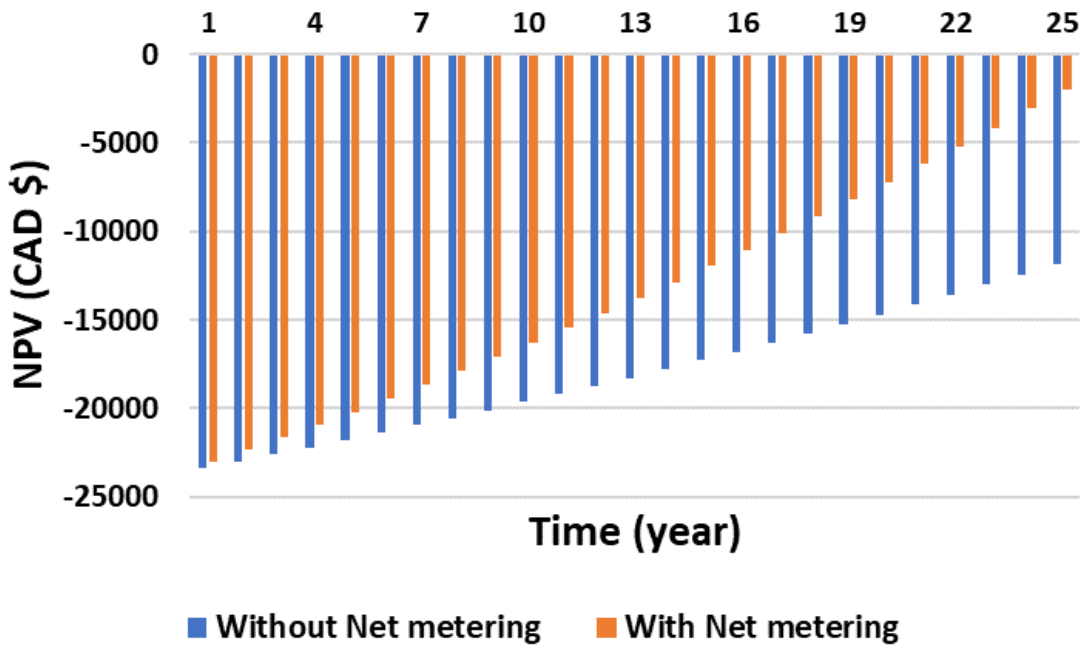

Figure 5.10 Net Present Value of 8 kW PV system without battery

Without batteries, net metering has a large impact on system's economic performance, even though the NPV remains negative.

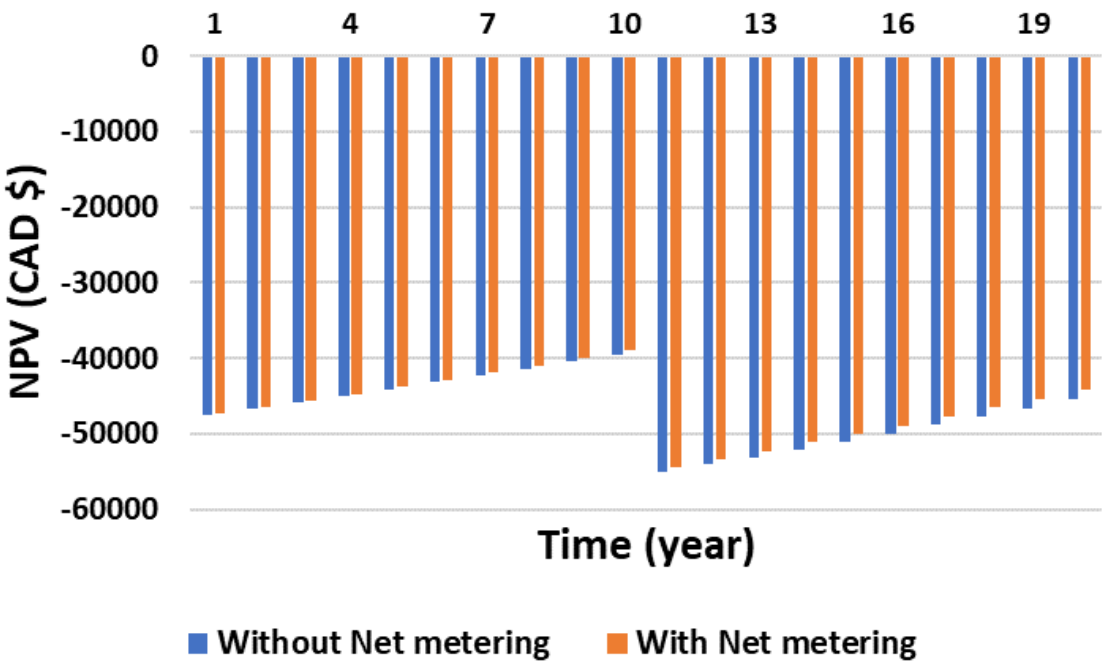

Figure 5.11 Net Present Value of PV (8 kW) + Battery (30.1 kWh)

With a 30-kWh battery, there is almost no difference between the scenarios with and without grid exports. The selected design brings self-consumption at a very high level, so that little energy is curtailed (without grid exports) or exported (with net metering).

5.4.3 Capital Expenditures of Flexibility

The previous sections have shown that the current flexibility incentives through TOU or price signals are not sufficient to make PV+Battery systems profitable in the selected contexts (representative of Ontario and Québec). Another way to look at the value of distributed generation and flexibility is to compare it to other generation technologies. A good indicator for electricity generation technologies is capital expenditures index, or CAPEX, which expresses the initial cost of each kW made available on the grid. The technology-specific baseline costs provide an opportunity for policymakers to analyse and compare various scenarios for extending the electricity grid potential to supply load. Interestingly, the concept of power CAPEX can be extended to flexibility, thereby considering as "generation" technologies that provide kW's of power during DR events rather than continuously. The following table provides a cost range for various technologies, which is published by the National Renewable Energy Laboratory in 2021 (NREL,

2021). Values were converted to CAD using an exchange rate of 1.25 CAD/USD and rounded. The table includes batteries, which are obviously not a "generator" as a coal power plant is, or as a wind turbine is, but can be considered as part of the means to provide power during DR events.

Table 5.28 Levelized capital expenditure of electricity generation technologies (NREL, 2021)

Electricity generation (or flexibility) technology	Power CAPEX (CAD/kW)	
	Min.	Max.
Onshore Wind	660	1800
Offshore Wind	1840	7050
Residential PV	700	3500
Geothermal	5500	----
Hydro power	2800	20300
Residential Battery	1550	5800
Biopower	4500	5500
Nuclear	7450	9400
Natural gas	950	3400
Coal	2900	7200

Due to the complexity of economic analysis for residential PV+Battery systems, those systems are not covered by the baseline technologies. PV systems and batteries are considered, but separately, with CAPEX cost of 700 to 3500 $/kW for PV and 1550 to 5800 $/kW for batteries.

To estimate the power CAPEX of PV+Battery systems, the modelled system needs to be capable of providing a steady supply to the grid over the entire peak hours period (usually 4 hours).

In our analyses above, the systems include 8 kW PV panels + a 30 kWh (7.5 kW peak power) battery storage, which is designed with self-consumption in mind. Based on our results, the CAPEX for electricity generation (or rather flexibility) from residential PV+Battery systems is ranging from 3600 to 5800 $/kW, therefore in a similar range as battery-only systems.

5.5 Chapter summary

The financial assessment presented in this chapter has compared various sizing for PV+Battery systems. The net present value (NPV) analysis shows that these systems are never economically viable under "price signal" rate structures, which consist of a flat rate with penalties or rewards for specific DR events (using current rates applicable in Québec). The flat rate would have to go over 15 ¢/kWh for PV-only systems to be profitable without net metering, and over 8 ¢/kWh with net metering. The results for a time of use (TOU) rate structure based on the current situation in Ontario are slightly better but lead to the same conclusion: no profitability can be achieved without net metering, and PV+Battery systems with 30 kWh storage capacity or more have a strongly negative NPV. Our results also show that in the most favorable scenarios, battery capital costs should decrease to a level of 220 $/kWh to reach profitability, which seems like an easily achievable target given the 100 $/kWh value often quoted in price forecasts.

Looking at residential PV+Battery systems from the utility perspective, they can be considered as "generators" (for DR events only) providing flexibility at a CAPEX which is not far from other renewable technologies

CHAPTER 6 CONCLUSIONS AND RECOMMENDATIONS

The residential sector represents a significant share of worldwide energy consumption and greenhouse gases emissions; it is targeted by numerous programs aiming at reducing these emissions. PV systems can play a role in decarbonizing the grid and the building sector, but the focus on maximizing the annual energy production has resulted in an exacerbation of the peak demand problems. Energy flexibility (the ability to adapt a building energy generation and demand) is a key aspect in decarbonizing the building sector: space and water heating can be effectively decarbonized by switching to electricity, but peak demands must be mitigated to maintain and increase the resilience of the grid. PV+Battery systems can rise to the challenge of addressing the decarbonization and the flexibility objectives, but they must be carefully designed, and their assessment is complex because of their interaction with occupied buildings and dynamic weather patterns. The overall goal of the work presented in this thesis was to assess the benefits of PV+Battery systems in typical residential buildings in the Canadian context.

6.1 Summary of key contributions

Chapter 2 presented a literature review of battery models in building performance simulation and energy system simulation tools. The review highlighted the need to develop models capable of representing the main battery technologies (lead-acid and lithium-ion) with a sufficient level of detail, taking into account performance degradation, the various elements having an impact on battery efficiency (e.g. self-discharge), and the impact of temperature on performance. TRNSYS was lacking these models, and none of the reviewed models was satisfying on all accounts. A library of component models was developed to respond to this need, and the developed models were compared to experimental data to assess their validity. The developed library was used in the simulation studies and is a contribution to other studies addressing PV+Battery systems (or battery systems coupled to other generation technologies) in TRNSYS.

Chapter 3 presented an archetypal model of a Canadian house with an all-electric heating, ventilation and air-conditioning (HVAC) system and a PV+Battery system. Occupant-driven load profiles for domestic hot water and non-HVAC loads (lighting, appliances, plug loads) are taken from Canadian empirical studies in the literature. The model has been used for the modelling studies in chapters 4 and 5. A preliminary assessment of PV+Battery systems is also presented in

that chapter, showing that increasing the battery size above 30 kWh leads to diminishing returns. The detailed archetypal model produced in this chapter can be used in other energy analyse studies.

Chapter 4 presents an analysis of the energy flexibility offered by PV+Battery system. Default control strategies in commercially available inverters are used: Grid support (or PV priority) and UPS-mode. No attempt is made to optimize these strategies in this study. Yearly KPIs such as self-generation and self-consumption show that adding batteries to a conventional grid-tied PV system can improve dramatically the available flexibility, with a saturation of the effects for battery capacity higher than 4 kWh/kWp under the selected assumptions. This is an interesting design rule for practitioners. Dynamic KPIs calculated for 1-h upward and downward flexibility events show that there is a large variability in available flexibility, depending on the day and time of the year and on the inverter control strategy. The UPS mode, which results in the lowest yearly self-generation and self-consumption, presents a significant downward flexibility potential, limited by the maximum battery discharge current, which resulted in a potential of up to 8 kWh per 1-h event, with a median value between 0 and 4 kWh depending on the time of the day (the downward flexibility is limited by the load itself, the PV+Battery system can not do better than removing the entire load). Its upward flexibility results from the ability to shut down PV generation and is entirely dependent on solar radiation. On the other hand, the grid-support (or PV priority) operation mode, which already minimizes grid imports, offers no potential for downward flexibility under the current assumptions. Its upward flexibility is variable between 0 and 12 kWh in this study, with a relatively constant median value around 5 kWh. The dynamic assessment of flexibility KPIs is a contribution to the literature, in addition to the design rules to maximize yearly KPIs.

Chapter 5 presented a financial assessment comparing various sizing for PV+Battery systems. The net present value (NPV) analysis shows that these systems are never economically viable under "price signal" rate structures, which consist of a flat rate with penalties or rewards for specific DR events (using current rates applicable in Québec). The flat rate would have to go over 15 ¢/kWh for PV-only systems to be profitable without net metering, and over 8 ¢/kWh with net metering. The result for a time of use (TOU) rate structure based on the current situation in Ontario are slightly better but lead to the same conclusion: no profitability can be achieved without net metering, and PV+Battery systems with 30 kWh storage capacity or more have a strongly negative NPV. Our results also show that in the most favorable scenarios, battery capital costs should decrease to a level of 220 $/kWh to reach profitability, which seems like an easily achievable target

given the 100 $/kWh value often quoted in price forecasts. Looking at residential PV+Battery systems from the utility perspective, they can be considered as "generators" (for DR events only) providing flexibility at a CAPEX which is not far from other renewable technologies. This economic analysis can guide policymakers an utilities wishing to develop incentive programs for PV+Battery systems, and help designers achieving an acceptable economic performance with given energy or resilience targets. The CAPEX comparison opens the door to a different assessment of distributed generation, considered not from the homeowner viewpoint but from the utility viewpoint.

6.1.1 Further research

The work on battery modelling has identified some remaining weaknesses in the proposed models: it is challenging to propose generic models applicable to a wide range of technologies, and another interesting option would be to consider automatic parameter identification based on widely available performance data, keeping the structure of the models but adapting the generic parameters to specific batteries without necessitating detailed test data. The same approach has been applied to identify parameters of the 5-parameter PV module model in TRNSYS (De Soto et al., 2006).

The work on flexibility has highlighted the importance of control strategies and the difficulty of assessing energy flexibility as "one number". Further research work is needed to develop KPIs that can communicate the potential of PV+Battery systems (or other building-integrated storage management systems) to utilities, and to develop optimized control strategies.

In this thesis, system sizing has been approached in a simplified way: a parametric analysis was conducted in Chapter 4, and only one system sizing was kept for Chapter 5. Sizing optimization for grid-tied PV+Battery systems is a multi-objective optimization problem which necessitates defining several pareto solutions regarding the criteria of interest (Mehrabankhomartash et al., 2017). Optimization criteria can include system reliability (resilience over grid failure), solar electricity generation cost, electricity bill saving, levelized expenditure for peak shaving and load shifting, as well as reducing greenhouse gas emissions (Ippolito et al., 2014). Doroudchi et al. (Doroudchi et al., 2016) employed mixed integer linear programming to optimize the energy cost of a single-family house considering four sizing configurations for grid-tied PV system installation and battery energy storage. They investigated the impact of various battery sizes on saving opportunity over monthly energy cost. Tan et al. (Tan et al., 2010) used the Monte Carlo simulation

technique (for simulating utility grid outage) to optimize the PV and back up battery system sizes regarding the loss of load probability index. Kaplani et al. (Kaplani & Kaplanis, 2012) considered the number of autonomy days as the main objective to investigate the optimum size of PV+Battery system. They implemented optimization through investigating the system success rate for accommodating the load during grid failure. Mehraban et al. (Mehrabankhomartash et al., 2017) optimized the size of a PV+battery system for commercial building based on yearly energy cost saving. In addition to the imported electricity from the grid, they also defined and considered the cost associated to grid failure. Accordingly, the optimum size was investigated through grid usage as well as compensated damage cost with supplying the load during power outage. Cervone et al. (Cervone et al., 2016) employed Markov-Chains approach to optimize the size of battery bank (lead-acid and Li-ion chemistry) for PV system using the payback period time as main objective. The methods proposed in these research works could be used with the models developed in this thesis to perform a more thorough system design optimization.

Finally, the economic analysis has delivered disappointing results form the homeowner point of view: the current rate structures in Ontario and Québec make PV+Battery systems not economically viable. Updating these results with the rapidly decreasing battery prices would be interesting on one hand, while taking into account the value of resilience would help, on the other hand. This is an active research area (Anderson et al., 2021) but little work has addressed the residential sector. It would also be interesting to further the analysis from the utility point of view, comparing the cost of subsidizing PV+Battery systems to the cost of upgrading power lines, transformers, and other components.

REFERENCES

Albright, G., Edie, J., & Al-Hallaj Jake, S. (2012). *A Comparison of Lead Acid to Lithium-ion in Stationary Storage Applications* .

Allard, Y., Kummert, M., Bernier, M., & Moreau, A. (2011). Intermodel comparison and experimental validation of electrical water heater models in TRNSYS. *Proceedings of Building Simulation 2011: 12th Conference of the International Building Performance Simulation Association, 14-16 Nov*, 688–695.

Anderson, K., Li, X., Dalvi, S., Ericson, S., Barrows, C., Murphy, C., & Hotchkiss, E. (2021). Integrating the Value of Electricity Resilience in Energy Planning and Operations Decisions. *IEEE Systems Journal*, *15*(1), 204–214. https://doi.org/10.1109/JSYST.2019.2961298

Barzegar Bafrouei, B. (2014). *Modeling and Optimization of Off-Grid solar street lighting system* [Dalhousie University]. https://dalspace.library.dal.ca//handle/10222/54075

Branker, K., Pathak, M. J. M., & Pearce, J. M. (2011). A review of solar photovoltaic levelized cost of electricity. In *Renewable and Sustainable Energy Reviews* (Vol. 15, Issue 9, pp. 4470–4482). https://doi.org/10.1016/j.rser.2011.07.104

Buchman, I. (2001). Batteries in a Portable World: A Handbook on Rechargeable Batteries for Non-Engineers. In *Chemistry & …*. Cadex Electronics Inc. https://batteryuniversity.com/

Buchmann, I. (2011). *Batteries in a Portable World - Chemistry Comparison*. 209–241.

Canadian Vehicle Survey: Annual. (2009). www.statcan.gc.ca,

Ceraolo, M., Lutzemberger, G., Poli, D., & Scarpelli, C. (2019). Model parameters evaluation for NMC cells. *Proceedings - 2019 IEEE International Conference on Environment and Electrical Engineering and 2019 IEEE Industrial and Commercial Power Systems Europe, EEEIC/I and CPS Europe 2019*. https://doi.org/10.1109/EEEIC.2019.8783503

Cervone, A., Carbone, G., Santini, E., & Teodori, S. (2016). Optimization of the battery size for PV systems under regulatory rules using a Markov-Chains approach. *Renewable Energy*, *85*, 657–665. https://doi.org/10.1016/J.RENENE.2015.07.007

Clauß, J., Finck, C., Vogler-Finck, P., & Beagon, P. (2017). Control strategies for building energy

systems to unlock demand side flexibility-A review. In *IBPSA Building Simulation 2017, San Francisco, 7-9 August 2017*. IBPSA. https://researchrepository.ucd.ie/handle/10197/9016

Copetti, J. B., Lorenzo, E., & Chenlo, F. (1993). A general battery model for PV system simulation. *Progress in Photovoltaics: Research and Applications*, *1*(4), 283–292. https://doi.org/10.1002/pip.4670010405

Croce, V., Lazzaro, M., Paternò, G., Ziu, D., Sanseverino, E. R., & Monti, A. (2017, July 12). Smart district energy optimization of flexible energy units for the integration of local energy storage. *Conference Proceedings - 2017 17th IEEE International Conference on Environment and Electrical Engineering and 2017 1st IEEE Industrial and Commercial Power Systems Europe, EEEIC / I and CPS Europe 2017*. https://doi.org/10.1109/EEEIC.2017.7977597

De Soto, W., Klein, S. A., & Beckman, W. A. (2006). Improvement and validation of a model for photovoltaic array performance. *Solar Energy*, *80*(1), 78–88. https://doi.org/10.1016/J.SOLENER.2005.06.010

Denholm, P., O'connell, M., Brinkman, G., & Jorgenson, J. (2013). *Overgeneration from Solar Energy in California: A Field Guide to the Duck Chart*. www.nrel.gov/publications.

DiOrio, N., Dobos, A., Janzou, S., Nelson, A., & Lunstrom, B. (2015). *Technoeconomic Modeling of Battery Energy Storage in SAM (NREL/TP-6A20-64641)*. National Renewable Energy Laboratory. http://www.nrel.gov/docs/fy15osti/64641.pdf

Doroudchi, E., Pal, S. K., Lehtonen, M., & Kyyra, J. (2016). Optimizing energy cost via battery sizing in residential PV/battery systems. *Proceedings of the 2015 IEEE Innovative Smart Grid Technologies - Asia, ISGT ASIA 2015*. https://doi.org/10.1109/ISGT-ASIA.2015.7387155

Downing, S. D., & Socie, D. F. (1982a). Simple rainflow counting algorithms. *International Journal of Fatigue*, *4*(1), 31–40. https://doi.org/10.1016/0142-1123(82)90018-4

Downing, S. D., & Socie, D. F. (1982b). Simple rainflow counting algorithms. *International Journal of Fatigue*, *4*(1), 31–40. https://doi.org/10.1016/0142-1123(82)90018-4

Duffie, J. A., & Beckman, W. A. (2013). Solar Engineering of Thermal Processes. In *Solar Engineering of Thermal Processes: Fourth Edition* (Fourth). John Wiley and Sons. https://doi.org/10.1002/9781118671603

E-Gear™ BESS. (n.d.). Retrieved October 11, 2021, from https://www.e-gear.us/egearBess-specifications.php

Edwards, S., Beausoleil-Morrison, I., & Laperrière, A. (2015). Representative hot water draw profiles at high temporal resolution for simulating the performance of solar thermal systems. *Solar Energy*, *111*, 43–52. https://doi.org/10.1016/j.solener.2014.10.026

Electric Vehicle (EV) – Battery University. (n.d.). Retrieved April 17, 2021, from https://batteryuniversity.com/learn/article/electric_vehicle_ev

Environment Canada. (2010). *Canadian Weather Energy and Engineering Data Sets (CWEEDS files) and Canadian Weather for Energy Calculations (CWEC files) updated user's manual*. Environment Canada. http://climate.weather.gc.ca/prods_servs/engineering_e.html

Facinelli, W. A., & A., W. (1983). Modeling and simulation of lead-acid batteries for photovoltaic systems. *PhDT*.

Fang, H., Zhao, X., Wang, Y., Sahinoglu, Z., Wada, T., Hara, S., & De Callafon, R. A. (2014). State-of-charge estimation for batteries: A multi-model approach. *Proceedings of the American Control Conference*, 2779–2785. https://doi.org/10.1109/ACC.2014.6858976

Feldman, D., Vignesh, R., Ran, F., Ashvia, R., Jal, D., & Robert, M. (2021). *U.S. Solar Photovoltaic System Cost Benchmark: Q1 2020*. https://www.nrel.gov/docs/fy21osti/77324.pdf

Fotouhi, A., Auger, D. J., Propp, K., & Longo, S. (2016). A Study on Battery Model Parametrisation Problem - Application-Oriented Trade-offs between Accuracy and Simplicity. *IFAC-PapersOnLine*, *49*(11), 48–53. https://doi.org/10.1016/J.IFACOL.2016.08.008

Guittet, D., Mirletz, B., & Prilliman, M. (2021). *What's New in the Battery Model for the System Advisor Model*. https://www.nrel.gov/docs/fy22osti/80862.pdf

Gundogdu, B., Gladwin, D. T., Gundogdu, B., & Gladwin, D. T. (2018). *A fast battery cycle counting method for grid-tied battery energy storage system subjected to microcycles*. 7–09. https://doi.org/10.1109/IEECON.2018.8712263

Hesse, H. C., Schimpe, M., Kucevic, D., & Jossen, A. (2017). Lithium-Ion Battery Storage for the

Grid—A Review of Stationary Battery Storage System Design Tailored for Applications in Modern Power Grids. *Energies 2017, Vol. 10, Page 2107*, *10*(12), 2107. https://doi.org/10.3390/EN10122107

Hyman, E. A. (1979). *Phenomenological Cell Modelling: A Tool for Planning and Analyzing Battery Testing at the BEST Facility*. https://www.osti.gov/servlets/purl/6051785

IEA. (2021). *IEA Statistical data*. https://www.iea.org/statistics

Ippolito, M. G., Di Silvestre, M. L., Riva Sanseverino, E., Zizzo, G., & Graditi, G. (2014). Multi-objective optimized management of electrical energy storage systems in an islanded network with renewable energy sources under different design scenarios. *Energy*, *64*, 648–662. https://doi.org/10.1016/J.ENERGY.2013.11.065

Jensen, S. Ø., Madsen, H., Lopes, R., Junker, R. G., Aelenei, D., Li, R., Metzger, S., Lindberg, B., Marszal, A. J., Kummert, M., Bayles, B., Mlecnik, E., Lollini, R., & Pasut, W. (2017). *Energy Flexibility as a key asset in a smart building future - Contribution of Annex 67 to the European Smart Buildings Initiative. Position paper of the IEA-EBC Annex 67 "Energy flexible Buildings."* International Energy Agency Energy in Buildings and Communities programme. http://www.annex67.org/publications/position-paper/

Jensen, S. Ø., Marszal-Pomianowska, A., Lollini, R., Pasut, W., Knotzer, A., Engelmann, P., Stafford, A., & Reynders, G. (2017). IEA EBC Annex 67 Energy Flexible Buildings. *Energy and Buildings*, *155*, 25–34. https://doi.org/10.1016/j.enbuild.2017.08.044

Johnson, G., & Beausoleil-Morrison, I. (2017). Electrical-end-use data from 23 houses sampled each minute for simulating micro-generation systems. *Applied Thermal Engineering*, *114*, 1449–1456. https://doi.org/10.1016/j.applthermaleng.2016.07.133

Kaplani, E., & Kaplanis, S. (2012). A stochastic simulation model for reliable PV system sizing providing for solar radiation fluctuations. *Applied Energy*, *97*, 970–981. https://doi.org/10.1016/J.APENERGY.2011.12.016

Kim, Y., Siegel, J. B., & Stefanopoulou, A. G. (n.d.). *A Computationally Efficient Thermal Model of Cylindrical Battery Cells for the Estimation of Radially Distributed Temperatures*.

Klein, S. A. et al. (2017). *TRNSYS*. Solar Energy Laboratory, University of Wisconsin. www.Trnsys.com

Kummert, M., Leduc, M.-A., & Moreau, A. (2011). Using MPC to reduce the peak demand associated with electric heating. *Model Predictive Control in Building Workshop*.

Lam, L., Bauer, P., & Kelder, E. (2011). A practical circuit-based model for Li-ion battery cells in electric vehicle applications. *INTELEC, International Telecommunications Energy Conference (Proceedings)*. https://doi.org/10.1109/INTLEC.2011.6099803

Li, K., Tseng, K. J., Wei, F., & Soong, B. H. (2018). A Practical Lithium-ion Battery Model Based on the Butler-Volmer Equation. *2018 International Power Electronics Conference, IPEC-Niigata - ECCE Asia 2018*, 1592–1597. https://doi.org/10.23919/IPEC.2018.8507765

Macklem, T., Lane, T., Schembri, L., Beaudry, P., Gravelle, T., & Kozicki, S. (2021). *Monetary Policy Report - October 2021*.

Manwell, F James. McGowan, J. G. (1994). Extension of the kinetic battery model for wind/hybrid power systems. *Proceedings of the 5th European Wind Energy Association Conference (EWEC '94), February*, 284–289.

Masson, G., & Kaziuka, I. (2020). *Trends in Photovoltaic applications 2020* . https://iea-pvps.org/trends_reports/trends/

Matsuichi, M., & Endo, T. (1968). Fatigue of metals subjected to varying stress. *Undefined*.

Mehrabankhomartash, M., Rayati, M., Sheikhi, A., & Ranjbar, A. M. (2017). Practical battery size optimization of a PV system by considering individual customer damage function. *Renewable and Sustainable Energy Reviews*, *67*, 36–50. https://doi.org/10.1016/J.RSER.2016.08.050

Mishra, P. P., Latif, A., Emmanuel, M., Shi, Y., McKenna, K., Smith, K., & Nagarajan, A. (2020). Analysis of degradation in residential battery energy storage systems for rate-based use-cases. *Applied Energy*, *264*, 114632. https://doi.org/10.1016/J.APENERGY.2020.114632

Newman, J., & Tiedemann, W. (1974). *Lawrence Berkeley National Laboratory Recent Work Title POROUS-ELECTRODE THEORY WITH BATTERY APPLICATIONS Publication Date*. https://cloudfront.escholarship.org/dist/prd/content/qt9vd6z2g7/qt9vd6z2g7.pdf

NRCan-OEE. (2021). *Comprehensive Energy Use Database*. Natural Resources Canada, Office for Energy Efficiency. https://oee.nrcan.gc.ca/corporate/statistics/neud/dpa/menus/trends/comprehensive_tables/list

.cfm

NRCan. (2021). *Energy Efficiency Trends in Canada to 2017*. https://oee.nrcan.gc.ca/publications/statistics/trends/2017/residential.cfm

NREL. (2021). *Annual Technology Baseline (ATB)*. https://atb.nrel.gov/

O'Connell, S., & Riverso, S. (2016, July). Flexibility analysis for smart grid demand side services incorporating 2nd life EV batteries. *IEEE PES Innovative Smart Grid Technologies Conference Europe*. https://doi.org/10.1109/ISGTEurope.2016.7856178

Pless, S., & Torcellini, P. (2010). *Net-Zero Energy Buildings: A Classification System Based on Renewable Energy Supply Options - NREL/TP-550-44586*. National Renewable Energy Laboratory. www.nrel.gov/sustainable_nrel/pdfs/44586.pdf

Powerwall | Tesla Canada. (n.d.). Retrieved October 11, 2021, from https://www.tesla.com/en_ca/powerwall

Rahman, M. M., Oni, A. O., Gemechu, E., & Kumar, A. (2020). Assessment of energy storage technologies: A review. *Energy Conversion and Management*, *223*, 113295. https://doi.org/10.1016/J.ENCONMAN.2020.113295

Rand, D. A. J., & Moseley, P. T. (2017). Lead–acid battery fundamentals. *Lead-Acid Batteries for Future Automobiles*, 97–132. https://doi.org/10.1016/B978-0-444-63700-0.00003-9

Reddy, T., & Linden, D. (2010). Linden's Handbook of Batteries. In T. Reddy (Ed.), *Amazon* (4th ed.). McGraw-Hill Professional Publishing.

Salom, J., Marszal, A. J., Widén, J., Candanedo, J., & Lindberg, K. B. (2014). Analysis of load match and grid interaction indicators in net zero energy buildings with simulated and monitored data. *Applied Energy*, *136*, 119–131. https://doi.org/10.1016/j.apenergy.2014.09.018

Samavatian, V., Iman-Eini, H., & Avenas, Y. (2018). An efficient online time-temperature-dependent creep-fatigue rainflow counting algorithm. *International Journal of Fatigue*, *116*, 284–292. https://doi.org/10.1016/J.IJFATIGUE.2018.06.037

Sears, J., Roberts, D., & Glitman, K. (2014). A comparison of electric vehicle Level 1 and Level 2 charging efficiency. *2014 IEEE Conference on Technologies for Sustainability, SusTech*

2014, 255–258. https://doi.org/10.1109/SusTech.2014.7046253

Shepherd, C. M. (1965a). Design of Primary and Secondary Cells. *Journal of The Electrochemical Society*, *112*(7), 657. https://doi.org/10.1149/1.2423659

Shepherd, C. M. (1965b). Design of Primary and Secondary Cells: II . An Equation Describing Battery Discharge. *Journal of The Electrochemical Society*, *112*(7), 657. https://doi.org/10.1149/1.2423659

Smith, P. K., Saxon, A., Keyser, M., Lundstrom, B., Cao, Z., Roc, A., & Corp, S. (2017). *Life Prediction Model for Grid-Connected Li-ion Battery Energy Storage System*. http:/www.osti.gov/scitech

Swinton, M. C., Moussa, H., & Marchand, R. G. (2001). Commissioning twin houses for assessing the performance of energy conserving technologies. *Proceedings of Performance of Exterior Envelopes of Whole Buildings VIII: Integration of Building Envelopes, Dec 2-7*, 1–10. http://nparc.cisti-icist.nrc-cnrc.gc.ca/npsi/ctrl?action=rtdoc&an=20378746&article

Tan, C. W., Green, T. C., & Hernandez-Aramburo, C. A. (2010). A stochastic method for battery sizing with uninterruptible-power and demand shift capabilities in PV (photovoltaic) systems. *Energy*, *35*(12), 5082–5092. https://doi.org/10.1016/J.ENERGY.2010.08.007

Thakkar, R. R. (2021). Electrical Equivalent Circuit Models of Lithium-ion Battery. In *IntechOpen*. IntechOpen. https://doi.org/10.5772/INTECHOPEN.99851

Tremblay, O., & Dessaint, L. A. (2009). Experimental validation of a battery dynamic model for EV applications. *24th International Battery, Hybrid and Fuel Cell Electric Vehicle Symposium and Exhibition 2009, EVS 24*, *2*, 930–939.

Tremblay, O., Dessaint, L. A., & Dekkiche, A. I. (2007). A generic battery model for the dynamic simulation of hybrid electric vehicles. *VPPC 2007 - Proceedings of the 2007 IEEE Vehicle Power and Propulsion Conference*, 284–289. https://doi.org/10.1109/VPPC.2007.4544139

WRI. (2020). *World Greenhouse Gas Emissions: 2016 | World Resources Institute*. https://www.wri.org/resources/data-visualizations/world-greenhouse-gas-emissions-2016

Xu, T., Wang, W., Gordin, M. L., Wang, D., & Choi, D. (2010). Lithium-ion batteries for stationary energy storage. *JOM 2010 62:9*, *62*(9), 24–30. https://doi.org/10.1007/S11837-010-0131-6

Zhang, C., Li, K., McLoone, S., & Yang, Z. (2014). Battery modelling methods for electric vehicles - A review. *2014 European Control Conference, ECC 2014*, 2673–2678. https://doi.org/10.1109/ECC.2014.6862541

Zhang, K. (2018). *Model Predictive Control of Building Systems for Energy Flexibility*.

Zheng, F., Xing, Y., Jiang, J., Sun, B., Kim, J., & Pecht, M. (2016). Influence of different open circuit voltage tests on state of charge online estimation for lithium-ion batteries. *Applied Energy*, *183*, 513–525. https://doi.org/10.1016/J.APENERGY.2016.09.010